Dielectric relaxation and structure of complex materials: supramolecular ensembles and hybrid adhesives.

PhD Thesis

Gerardo Martínez Rugerio

Materials Physics Centre
Basque Country University

December 2016

Dielectric relaxation and structure of complex materials: supramolecular ensembles and hybrid adhesives.

Manuscript presented to opt for Ph.D. degree in Physics of Nanostructures and Advanced Materials

by
Gerardo Martínez Rugerio

Thesis directed by
Ángel Alegría Loinaz

Materials Physics Centre
Basque Country University

December 2016

"To my family and my life partner,
my deepest thanks and gratitude
for your endless support"

Acknowledgements

"No duty is more urgent than that of returning thanks."

James Allen

I would like to express my gratitude toward my family and my love partner, for being an important part of this exiting adventure. Although the distance I always felt like you were by my side. Thank you Marta, my love, for your infinite caring and patience. Your guidance and love helped me through my hesitations and self-doubts, not just with moral support and valuable comments but you gave me the enthusiasm to pursue this goal.

I would also like to thank Prof. Juan Colmenero for giving me the opportunity to join the research group "Polymers and Soft Matter" at the Materials Physics Centre. My experience in this group has been the most satisfactory and fruitful.

Also, I would like to express my deepest gratitude to professor Ángel Alegría, which without his help this manuscript wouldn?t be possible. Thank you, for sharing your time, ideas, and experience and also for teaching me so enthusiastically and with unlimited patience about the wonders of Broadband Dielectric Spectroscopy. Your perpetual energy and interest in research motivated me like all other students. I really appreciate the confidence you had in my work and the incessant motivation he gave throughout my graduation.

Deep thanks to Prof. Arantxa Arbe for her help insights and patience while making this research.

My special thanks to Luis Botana, Isabel Asenjo, Silvia Arrese and Amaia Iturrospe for their time and patience while teaching me about the different instrumental equipment?s and also for their assistance in the fabrication of some of the investigated samples.

There are no words to express how grateful I am to my office co-workers and all members of the Polymers and Soft Matter group for making the work atmosphere ideal and also for all the help provided when I needed the most. For this, many thanks to you: Natalia, Izaskun, Lucia, Thomas, Dani, Paula, Ana, Alex, Marina, Fabienne and also to the ones that have

already continued with their journey: Luisa, Ana Sanchez, Irma, Manuel and Alejandro.

Also it was a great opportunity to be able to work with Dra. Maria Paulis and Dra. Vesna Daniloska from the Polymat group from San Sebastián. Thank you for your help with Acrylic-Polyurethane synthesis, and for being an excellent co-worker. It was great to work with you.

Many thanks to my friends, for listening and giving me support and advice. I also would like to acknowledge your patience during these stressful days. I always loved to have great times with you all. Thanks to Guido, Nosir, Petra, Ahmed, Leonardo, Manu, and Eric for all the precious moments that we shared.

Finally, I would like to thank the financial support obtained from the University of Basque Country (UPV/EHU) for the Master?s studies. And also the financial support given by the Materials Physics Centre (MPC) and the Basque country Government through the projects (IT-654-13 and nanoIKER2011-2013) and as well as the Ministerio de Economía y Competitividad (MAT2012-31088 and MAT2015-63704-P) for the fulfilment of the PhD program.

Resumen

"La literatura actual, en la que se usa la espectroscopia dieléctrica para el análisis de la dinámica segmental de materiales sujetos a restricciones debidas a efectos de auto-ensamblaje... reporta, que las características de los fenómenos de relajación dieléctrica segmental son notablemente influenciadas por las limitaciones de confinamiento impuestas por las estructuras emergentes."

Angel Alegria and Juan Colmenero,
Soft Matter, 2016

El estudiar "la relajación dieléctrica y la estructura de materiales complejos: en entidades supra-moleculares y materiales híbridos", se refiere a la interpretación de resultados obtenidos por medio del análisis cuantitativo de los fenómenos de relajación dieléctrica y su relación con los resultados de su caracterización estructural, en particular, para dos diferentes familias de materiales poliméricos. Este tipo de materiales presentan una dinámica compleja, y en muchos casos exhiben relajaciones jerárquicas, que se extienden en un amplio rango de tamaños y escalas de tiempo. En esta tesis, y como primer sistema considerado, investigamos la relajación dieléctrica de un oligómero funcionalizado. Su unidad molecular esta compuesta por dos partes de distinta composición; un primer "bloque" esta compuesto por unidades de dimetilsiloxano y el segundo esta compuesto por una cadena alifática cuya terminación es un grupo functional carboxilo. Hemos centraremos la atención en la interpretación molecular y el rol que juegan las interacciones específicas en la relación entre la estructura y dinámica del material. Para ello, ha sido necesario una investigación comparativa entre dos sistemas similares pero cuyas interacciones específicas son distintas, en particular el grupo functional terminal fue modificado reemplazando el grupo hidroxilo por el grupo metilo con el objetivo de bloquear las interacciones tipo puente de hidrógeno. Por otro lado hemos estudiado materiales complejos con relevancia en el desarrollo de nuevas aplicaciones industriales. En

particular hemos estudiado materiales adhesivos híbridos sintetizados mediante miniemulsion. Específicamente, investigamos la relación entre las condiciones de síntesis, el análisis de la relajación dieléctrica y la caracterización estructural de los componentes solubles e insolubles de un material adhesivo híbrido compuesto por grupos acrílicos y poliuretanos. Una vez determinado el origen molecular de los procesos de relajación dieléctrica en estos materiales, se han comparado distintos materiales híbridos obtenidos mediante distintas condiciones de síntesis. Las técnica experimental empleada de forma intensiva a lo largo de esta tesis fue la espectroscopia dieléctrica en un amplio rango de frecuencias (BDS, Broadband Dielectric Spectroscopy por sus siglas en inglés). Para estudiar las propiedades estructurales de los materiales también se han realizado experimentos de difracción de rayos-X, análisis térmico mediante calorimetría diferencial de barrido y espectroscopia Infrarroja.

Comenzamos este manuscrito con una breve introducción describiendo la motivación y sobretodo resaltando la importancia entre la relación estructura y dinámica en diferentes escalas de tiempo y de tamaño. Así mismo resaltamos los efectos de confinamiento que surgen a escala nano-métricas, que son de vital importancia para el desarrollo de nuevas tecnologías funcionales basadas en estos materiales.

En el segundo capítulo resumimos brevemente los conceptos fundamentales de materiales complejos y en particular los llamados "materiales blandos". También comentaremos sobre la existencia de distintas fases (sólidos y líquidos) y su relación con las fuerzas intermoleculáres que mantienen unidas las moléculas dentro del material. En este contexto, describiremos su posible organización estructural y sus transiciones de fase. Continuaremos con un breve resumen sobre los materiales poliméricos con los que vamos a trabajar, incluyendo el caso específico de co-polímeros de di-bloque. Concluiremos el capitulo con los aspectos dinámicos en materiales blandos, destacándose el variado comportamiento dinámico que presentan estos materiales. En este contexto se dan las características particulares de los sistemas formadores de vidrio y se discute específicamente la relación de la transición vítrea con la dinámica molecular del sistema en el contexto del Teorema de Disipación-Fluctuación.

En el tercer capítulo se describen las técnicas experimentales utilizadas en nuestros estudios. Comenzamos con una breve descripción de los conceptos físicos que hay detrás de las técnicas experimentales y posteriormente pasamos la descripción de los equipos utilizados. La primera sección comienza con una breve introducción a la difracción de rayos X en el contexto de la "ley de Bragg", introduciendo las herramientas matemáticas necesarias para interpretar los experimento de difracción y concluyendo esta parte con la descripción de las dos técnicas experimentales empleadas -SAXS y WAXS-. Para finalizar la sección, se describe la configuración instrumental

de los equipos. Las secciones siguientes, es decir, la espectroscopia infrarroja, el análisis térmico y la espectroscopia dieléctrica de banda ancha tienen un esquema de organización similar al primero.

En el cuarto capítulo y en la primera sección de este capítulo presentamos los resultados de la caracterización térmica y estructural del co-oligómero de dimetilsiloxano terminado en un grupo funcional carboxilo (ODMS-COOH) en comparación con un oligómero de dimetilsiloxano utilizado como referencia (ODMS). Para obtener información sobre las propiedades termodinámicas se realizaron mediciones de calorimetría diferencial de barrido (DSC). Además, mediante el uso de técnicas de difracción, tales como: la difracción de rayos X de ángulos pequeños (SAXS) y la difracción de rayos X de amplio espectro (WAXS), combinados con la espectroscopía infrarroja por transformada de Fourier ATR (FTIR), fue possible acceder a la principales características estructurales de estos materiales. Adicionalmente, se realizó la comparación con el co-oligomero de bloque en el que la terminación OH del grupo carboxilo de la cadena alifática fue reemplazada por un grupo metilo (ODMS-$COOCH_3$). En la segunda sección del capítulo exploramos cómo los distintos fenómenos dinámicos detectados por espectroscopía dieléctrica (DS) se ven afectados por las distintas restricciones estructurales.

En el quinto capítulo se presenta el análisis de relajación dieléctrica de materiales adhesivos híbridos cuyos constituyentes son grupos acrílicos-poliuretanos sintetizados mediante foto-polimerización en miniemulsion y también mediante polimerización térmica. En un principio consideraremos tres muestras diferentes: ambas partes del látex híbrido que resulta de un único protocolo de síntesis - la fracción soluble (Sol) y la fracción reticulada (Gel)- y también una muestra sintetizada con el mismo protocolo de síntesis y compuesta exclusivamente por grupos de acrilatos, usada como referencia. Posteriormente se estudian la fracción gel de tres muestras de látex sintetizadas siguiendo distintos protocolos a fin de establecer la influencia del proceso de síntesis en la estructura del Gel. Utilizando los resultados de espectroscopía dieléctrica de banda ancha (BDS) de los componentes del latex se estableció el origen molecular de las distintas relajaciones utilizando espectroscopía dieléctrica de banda ancha (BDS) observadas. Esto permitió el estudio comparativo, mediante BDS combinado con calorimetría diferencial de barrido (DSC), difracción de rayos X de Ángulo Pequeño (SAXS) y espectroscopía infrarroja (ATR-FTIR), de tres latex obtenidos con distintos protocolos de síntesis. En la parte final de capítulo se discuten las observaciones más importantes.

En el sexto y último capítulo de este manuscrito se presentan las conclusiones generales de los distintos estudios realizados, concluyendo que la aplicación subsiguiente de esta metodología a otros materiales complejos permitirá una mayor comprensión de la relación entre la movilidad de los componentes y la estructura del sistema.

Abstract

"In recent polymer literature where dielectric spectroscopy has been used to investigate the segmental dynamics of polymers under the constraints produced by self-structuring...the characteristics of the dielectric relaxation are markedly affected by the constraints imposed by the corresponding structural features."

Angel Alegria and Juan Colmenero,
Soft Matter, 2016

Dielectric relaxation and structure of complex materials: supramolecular ensembles and hybrid materials, refers to the interpretation of the results obtained by the dielectric relaxation analysis and the relation with the structural characterization of two different families of polymeric materials investigated, at different molecular levels. As the first system under study and due to practical reasons (well defined molecular-constituents materials) we studied the dielectric relaxation of small length carboxyl terminated dimethylsiloxane block-copolymers, centring the attention into understanding which was the role of specific interactions and their relation with the structure and dynamics. For this purpose, a comparative investigation of polymers with different specific interactions was necessary. A simple scenario of this problem was handled by the study of two different ODMS co-oligomer samples, which were expected to have distinct specific interactions. On the other hand and we have studied materials that are closer to technological applications. Particularly we investigate the relation of the synthetic conditions, dielectric relaxation analysis and structural characterization of different hybrid Acrylic-Polyurethane latex materials. The experimental techniques employed in both investigations were mostly dielectric spectroscopies in a broad range of frequencies have been combined to determine polymer dynamics. X-ray diffraction experiments have also been performed to study the structural properties of the materials. In addition, thermal calorimetric characterization has been used in the analysis.

We start this manuscript with a brief introduction describing our mo-

tivation into understanding these complex materials and highlighting the importance of the relation between structure and dynamics at different time and length scales, as well as the new confinement effects that emerge at the nano-scale that are of fundamental importance for the future development of functional novel technologies based on such materials.

In the second chapter we centre our attention into briefly outlining the fundamental concepts to understand these soft-matter materials. Also we comment on the existence of condensed phases, such as solids and liquids, and their relation with the intermolecular forces that held together the molecules within the material. In this context, we will describe their possible structural organization and their phase transitions. In the following section, a brief outline of the polymeric materials that we are going to be working with will be summarized, including the specific case of diblock copolymers. After the more structural aspects, the rich dynamical behavior of these materials will be highlighted. In that context the particular characteristics of glass forming systems will be given, specifically the relation of the glass transition with molecular dynamics of the system will be considered in the context of Fluctuation Dissipation Theorem.

In the third chapter we describe the experimental techniques used in our study. A brief description of the physics behind the techniques as well as the description of the equipment will be given. In this chapter we will focus on the description of the physical principles underlying different experimental techniques used in this work. The first section will start with a brief introduction to X-ray diffraction and the "Bragg's law", subsequently we will introduce the mathematical tools necessary to interpret the diffraction experiment. Later, the two employed experimental X-ray setups -SAXS and WAXS- will be briefly explained. To end this section, comments on the Instrumental Setup will be given. Subsequent sections, i.e., Infrared spectroscopy, Thermal analysis and Broadband dielectric spectroscopy will have similar outline as the first one.

In the fourth chapter and in the first section of this chapter, we present the results of thermal and structural characterisation of carboxyl terminated dimethylsiloxane co-oligomer (ODMS-COOH) in comparison with a reference dimethyl siloxane oligomer (ODMS). To get insight on the thermodynamic properties differential scanning calorimetry (DSC) measurements were performed. Moreover, by making use of scattering methods, such as: small angle X-ray scattering (SAXS) and wide angle X-ray scattering (WAXS), and combined with ATR Fourier transform infrared spectroscopy (FTIR) we were able to access to the main structural features of the samples. Additionally a different "end-chain" functionalization of the ODMS co-oligomer (ODMS-$COOCH_3$) was investigated to validate the structural interpretation. In the second section of the chapter we will explore how the DMS dynamics as detected by dielectric spectroscopy (DS) is affected by the distinct

structural constrains.

In the fifth chapter we present the dielectric relaxation analysis of Acrylic-Polyurethane hybrid adhesives synthesized via mini-emulsion photopolymerization. As a starting point, we consider three different samples - both parts of the synthesized hybrid latex (SoL and GeL fractions)- and also a reference sample synthesized with the same protocol as the previous ones but with only acrylic groups as their constituents. Afterwards, the gel fraction of three distinct latex samples will be studied in connection with their synthesis conditions. The dielectric analysis of the distinct samples was carried out using Broadband Dielectric Spectroscopy (BDS). Additionally, Differential Scanning Calorimetry (DSC), Small Angle X-ray Scattering (SAXS) and ATR-FTIR measurements were performed in order to access their thermodynamical and structural properties. The analysis of these Acrylic-Polyurethane gels by BDS -in combination with SAXS- provides access to characteristics of the network structure that would ultimately influence the properties of these materials. We will start the chapter with a brief introduction on Acrylic-Polyurethane hybrid adhesives, and continue with the description of the distinct samples and the experimental details. Then, we will present the results obtained by different experimental techniques, followed up by the discussion of important observations and summarizing it all in the conclusions.

As the sixth and last chapter of this manuscript we present the concluding remarks of our research. In the previous chapters we have described the results obtained for the dielectric relaxation phenomena and structure of two different polymeric complex materials; named ODMS-COOH carboxyl terminated co-oligomer and Acrylic-Polyurethane latexes. Additionally an interpretation of the molecular dipole assignments and the dynamic behaviour in different structured and unstructured environments has been given. The applied methodology, allowed us, to use different experimental techniques to elucidate and propose a molecular assignment that takes into account the dynamics and structure of the ODMS-COOH co-oligomer and the Acrylic-Polyurethane hybrid adhesives. Subsequent application of this methodology to other complex materials would permit a greater insight into the relation between mobility of the components and the structure of the system.

Contents

List of Figures

List of Tables

Chapter 1

Introduction

"Somewhere, something incredible is waiting to be known."

Carl Sagan

New materials used as fundamental components in modern scientific and technological research -particularly soft materials- are produced with an increasing complexity to satisfy different functionality requirements in order to be suitable for particular applications [1, 2]. Among the different materials that can be used to produce these complex-materials, polymers present several advantages that make them an excellent choice; due to their diversity in monomeric components and distinct possibilities of linkage they can be tuned and synthesized to exhibit a variety of complex architectures with different properties [3, 4, 5].

Furthermore, block copolymers offer an attractive route to develop new complex nano-structured materials. Recent efforts in controlled polymer synthesis enable the preparation of a wide range of block copolymer architectures including, linear, graft, dendritic, star-like, bottle-brush, hyperbranched, and cyclic block copolymers. All of these macromolecular architectures present an unique and interesting behaviour, they can spawn a large variety of structural arrangements by spontaneously self-assembling into a diversity of mesophases. Also, both the structure and the size of the mesophases-domains can be in principle carefully tuned by controlling the molecular weight, synthetic parameters or the specific interactions between the block components of the copolymer [6, 7].

Significant work has been carried out in the research of block copolymer systems that have specific interactions such a hydrogen-bonding, metal-binding, p-p stacking, etc., which leads to self-organizing structures with their own intricate features [8]. Not only the nature of secondary interactions but also the chemical structure of the units forming supramolecular aggregates can vary significantly, ranging from low molecular weight

molecules [9] in the so-called associating liquids [10] to sizable covalently bonded chains forming associating polymers [11]. Although an impressive progress was achieved regarding the synthesis of various associating polymers [9, 12, 13, 14] the studies of their dynamics especially on segmental level in melts and under confinement effects are rather limited, and most of the attention on block-copolymers has been focused on their structural features. However, the relation between the obtained structures, the confinement effects that arise and its environment-dynamic properties its of utmost importance and usually depends on the system under investigation.

In nano-structured materials confinement effects at molecular level emerge in a natural way, and they give rise to changes that will affect the structure and dynamics as well as the macroscopic properties of the material. These materials usually exhibit dynamic heterogeneities at the molecular level, i.e., different mobility's associated to the distinct components. Moreover, the "Polymers and Soft-Matter group" from the Material Physics Centre (MPC) of the Basque Country University (EHU/UPV), has developed a solid and leading methodology to study the structure and dynamics of these complex nano-structured materials. Members of the group have reported on the confinement-related effects of the segmental dynamics on block copolymers, in particular; the segmental dynamics of amorphous polydimethylsiloxane (PDMS) in a polystyrene-Polydimethylsiloxane PS-PDMS lamellar diblock copolymer [15]. Their results showed that the main relevant features governing the PDMS segmental motions within the lamellar layers originated from the chain anchorage to glassy PS blocks. This constraint imposed a specific dynamical behavior for the segments close to the interface as well as a gradient of mobility for other segments of the copolymer. On the contrary, confinement effects, imposed by geometric space restriction of PDMS chains did not seem to play a significant role at the length scale probed by the segmental relaxation process. However, Schönhals et al. previously reported on the segmental dynamics of confined PDMS oligomers within uncoated silica-based nanoporous glasses [16]. They observed a significant speeding up of the segmental dynamics when the pore size was lowered below 25 nm. Nevertheless, in these systems, the PDMS chains can diffuse freely within the pores, by contrast with the PDMS chains of the diblock studied in the PS-PDMS system.

Additionally, in a distinct article [17] from members of the PSMG, authors compare the dynamics of segregated cylindrical and spherical PDMS nanophases formed by self-assembly of asymmetric diblock PS-PDMS copolymers. They give evidence of both structural and dynamical anomalies when compared not only with bulk PDMS but also with PDMS in lamellar nanophases. However due to similar sizes of the PDMS lamellae with those of the cylindrical and spherical PDMS nanophases, the effect cannot be directly attributed to size effects by geometrical confinement.

In general, all these studies report a relatively minor but noticeable effect of the nanostructure on the component segmental dynamics. The effects are highlighted when the size of the segregated phase is reduced to about 10 nanometre, and in fact, most of the results have been interpreted as originated at the interface (a few nanometers thick). Therefore, in nanostructured materials of a few nanometers length these effects are expected to be large, leading to a bigger variation on the components dynamical properties. Usual confinement lengths in block copolymers are about a few tens nanometers. The structural lengths are determined by block sizes, whereas the segregation quality is controlled by the product χN, which imposes a limit to the smallest structural lengths that can be achieved. Thus it is desirable to look for materials that present phases with even smaller confinement length. Here we show that a way to obtain nano-structured materials of a few nanometers length is making use of functionalized oligomers. In this context, the aim of this Ph.D. thesis is to determine how the existence of different structures affects the dynamics of a polymer at different molecular levels. In particular, it is of fundamental interest to understand which is the role of specific interactions in their relation with the structure and dynamics. For this purpose, a comparative investigation of polymers with different -specific interactions and / or initial synthetic conditions- is necessary. A simple scenario of this problem is handled by the study of two different ODMS co-oligomer samples, which are expected to have distinct specific interactions.

On the other hand, and also with the intention of understanding the relation between the structure and dynamics of complex materials that have industrial-applications we have studied hybrid-polymer materials. Among these, polyurethane (PU) dispersions are widely used in different technological applications as coatings and adhesives due to their superior properties. Moreover, due to their low cost, processability, and tuneable properties these polymeric components are commonly used to develop the new and advanced materials.

Furthermore, the development of these new materials demands new methods of synthesis and preparation (e.g., those based on self-assembly or new polymerization procedures) as well as for new technologies of manipulation and characterization. In the literature we can find several comprehensive reports on the fabrication and chemical characterization of Acrylic-PU dispersions [18, 19, 20, 21, 22, 23], in particular of pressure sensitive adhesives (PSA's). One of the main conclusions obtained from these reports is that the adhesive properties of PSA's materials are mostly determined by their polymer architecture [24]. Therefore, understanding the polymer architecture is of great importance for synthesizing optimal tailored adhesives. Additionally, understanding these materials and being able to precisely tailor them imply great challenging problems to basic soft matter science that need to be

addressed: the relationship between structure and dynamics at different time and length scales, the dynamics at the interfacial level, the new confinement effects that emerge at the nano-scale, are, among others, fundamental problems but of fundamental importance for the future development of functional novel technologies based on such materials.

Moreover, in order to investigate the relation with the synthetic conditions we have and hybrid Acrylic-PU latex system. Dielectric spectroscopies in a broad range of frequencies have been combined to determine polymer dynamics. X-ray diffraction experiments have also been performed to study the structural properties of the materials. In addition, thermal calorimetric characterization has been used in the analysis. In the following chapter, we will describe the experimental techniques used to analyse our samples. A brief description of the physics behind the techniques as well as the description of the equipment will be given.

Chapter 2

Research framework

"What do we mean by soft matter? Americans prefer to call it "complex-fluids". This is a rather ugly name, which tends to discourage the young students. But it does indeed bring in two of the major features: complexity and flexibility."

Pierre-Gilles de Gennes, Nobel Lecture, December 9, 1991

Abstract: In this chapter, we will centre our attention into briefly outlining the fundamental concepts to understand Soft Matter materials. We will comment on the existence of condensed phases, such as solids and liquids, and their relation with the intermolecular forces that held together the molecules within the material. In this context, we will describe their possible structural organization and their phase transitions. In the next section, a brief outline of the polymeric materials that we are going to be working with will be also summarized, including the specific case of diblock copolymers. After the more structural aspects, the rich dynamical behavior of these materials will be highlighted. In that context the particular characteristics of glass forming systems will be given, specifically the relation of the glass transition with molecular dynamics of the system will be considered in the context of Fluctuation Dissipation Theorem (FDT).

2.1 Soft Matter

Soft matter is a suitable term for materials in states of matter that are neither simple liquids nor conventional crystalline solids (as understood by solid-state physics). The term soft matter originates from peculiar macroscopic mechanical properties exhibited by "soft materials" such as colloids,

surfactants, liquid crystals, certain biomaterials and polymers in the melt or solution. These soft materials share a number of common features that makes it worth considering them a class, among these characteristics we can highlight, the importance of the length scales of soft materials -which are intermediate between atomic sizes and macroscopic scales-, the importance of fluctuations and the Brownian motion (in the framework of FDT), and also the tendency of soft matter to self-assemble under appropriate circumstances. In this sense, the basic aim of soft matter physics is centered in understanding the collective properties of large assemblies of atoms and molecules "soft-materials" in terms of the interactions between their component parts. However this is a very difficult task and a great number of reviews and books have been published about the subject [25, 26, 27].

2.1.1 Intermolecular Interactions

If matter is made up of atoms and molecules, then the existence of condensed phases, such as solids and liquids, tell us something about the forces that act between the molecules that compose a material. We know that there must be and attractive force which is active between molecules when they are separated; it is this force that has to overcome the effect of thermal agitation to cause a gas to condense to a liquid. However, there must also be a repulsive force that prevents matter from complete collapsing, experimental observations have show that this repulsive force is rather short-ranged and strong. A typical representation of the potential responsible for this short/long range interactions is shown in Figure 2.1. The origin of the short-ranged repulsion is essentially quantum mechanical; at it arises as a result of Pauli's exclusion principle, which comes into operation when the electron orbitals of neighboring molecules begin to interact. It is not straightforward to derive a simple closed expression for the potential of short-range interactions, and usually functional forms are used. For many practical purposes a convenient model that captures much of the physics of liquids and solids is used, this idealizations is know as the "hard-sphere potential" with "long-ranged interactions".

The nature of long-range interactions depends on the system under investigation and they have a common origin in the electrostatic force, however it is convenient to distinguish between different types of long-range interactions. This distinction is made taking into consideration the order of magnitude of the bonds -between atoms and molecules of the material- compared to thermal energies. If the bond energy is very much bigger compared to thermal energy k_BT, then the probability of the bond breaking and reforming due to thermal agitation is small; these bonds can be thought as permanent or chemical bonds. In contrast, if the bond energy is comparable to, or only a few times bigger than, k_BT, then there is a finite probability that the bond may broke and subsequently reformed by thermal agitation;

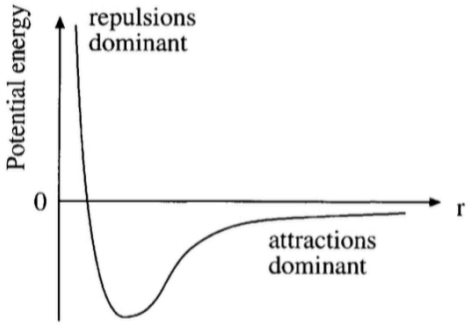

Figure 2.1: Typical potential energy curve as a function of the separation of two molecules or atoms

these bonds can be thought as temporary or physical bonds. Therefore, different long-range interactions arise by distinct effects of the: Van der Waals interactions, ionic interactions, covalent interactions, metallic interactions, hydrogen-bonding interactions and also by the hydrophobic interaction. Nevertheless, in general, it is difficult to make a quantitative statement about the precise form of the potential for any soft material, other than observing that it will be some combination of repulsive short-ranged contributions and attractive long-range contributions.

The clearest manifestation of the forces between molecules is the fact that upon cooling or heating a collection of molecules its physical state changes. Moreover, in systems where structure or ordering results from molecular self-assembly into aggregates, the forces between molecules (like Van der Waals and hydrogen-bonding interactions) are the ones responsible for the self-assembly process.

2.2 Structural Organization & Phase Transition

2.2.1 Structural Organization

One of the most important features that soft materials have in common is that the ordering in these materials is generally intermediate between that of a crystalline solid and that of a normal liquid. This lack of perfect crystalline order leads to the soft mechanical response of the materials. There may yet exist a partial translational and/or orientational order of molecules due to the formation of a mesophases. Polymer melts and solutions are also classified as "soft materials", although there is no long-range translational or orientational order. However, these phases are distinguished from conventional liquids due to their high viscosity and/or viscoelasticity behavior.

Another feature common to the ordering of soft materials is the peri-

odicity length of the structure formed, typically in the range $1 - 1000$ nm, which corresponds to "nanoscale" ordering. Another term often employed is "mesoscopic" ordering, due to the fact that the length-scale of the structures is intermediate between the microscopic (atomic) and macroscopic scales. Some examples of ordering in soft materials shown in Figure 2.2 taken from Ref. [27].

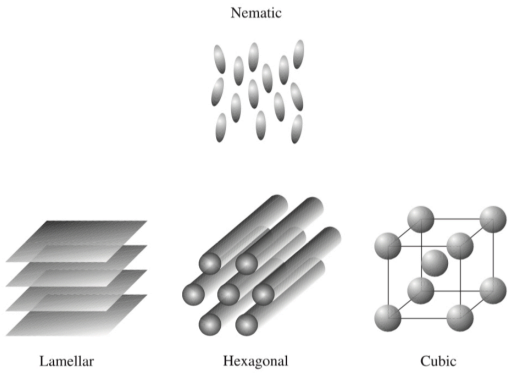

Figure 2.2: Examples of ordering in soft materials: a nematic liquid crystal, lamellar phase, hexagonal phase, and cubic phase

The simplest structure with translational order is a one-dimensional layered structure. In thermotropic liquid crystals, there are a number of such smectic phases formed by molecules in a weakly layered arrangement. Amphiphiles also form smectic phases, but they are usually called lamellar phases. Phases with two-dimensional transitional order are found for both thermotropic (in melt state) and lyotropic (in solution) liquid crystals, being termed columnar phases for thermotropic liquid crystals and hexagonal phases for lyotropic materials. There is only partial orientational and translational order of molecules within these aggregates. This lower level of molecular order produces a "softer" structure than for hexagonal phases formed by simple molecules or atoms. Structures with three-dimensional translational order include micelle cubic phases and bicontinuous cubic phases. These cubic phases are, on symmetry grounds, crystalline solids. However, unlike atomic or molecular crystals, they are built from supermolecular aggregates, i.e., micelles or surfactant membranes. Thus, as for hexagonal structures, these phases are softer than their atomic/molecular analogues, which are held together by shorter-range forces.

2.2.2 Phase Transitions

Phase transitions can be classified according to whether they are first or second order transitions; this classification was originally introduced by P. Ehrenfest based on the behavior of the thermodynamic free energy as a func-

tion of other thermodynamic variables [28]. Figure 2.3 show the temperature dependences of different thermodynamic quantities and the order parameter, the notation is as follows: μ, chemical potential; H, enthalpy; S, entropy; V, volume; C_p, heat capacity (at constant pressure); ψ, order parameter, the phase transition occurs at a temperature $T = T^*$ [27]. In this context a first-order transition is defined by discontinuities in its first derivative of the chemical potential with respect to the temperature. Enthalpy, entropy and volume can all be defined by appropriate first derivatives of the chemical potential and it is observed that all change discontinuously at a first order phase transition (see Figure 2.3a taken from Ref. [27]).

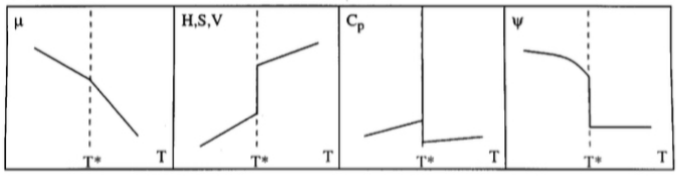

(a) first-order phase transition

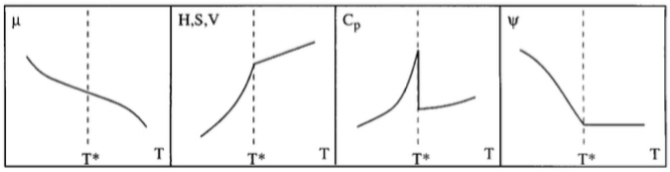

(b) second-order phase transition

Figure 2.3: Temperature dependences of different thermodynamic quantities and order parameter

To understand second order transitions is useful to recall the thermodynamic definition of the heat capacity, that is, the derivative of the enthalpy with respect to temperature. In Figure 2.3a, we observe that for materials where the chemical potential change discontinuously the heat capacity becomes infinite for temperatures where the first order transition is observed. The physical meaning of this becomes evident when considering the boiling of water, for a system that exhibits a first order transition, any heat absorbed by the system will drive the transition rather than increasing the temperature, i.e., there will be an infinite capacity for absorption of heat. On the other hand, a second-order phase transition is characterized by a continuous first derivative of the chemical potential, but with a discontinuous second derivative. Thus for systems that exhibit a second order transition and in which enthalpy, entropy and volume all change continuously -although their slopes are different above and below transitions- the heat capacity associated to the phase transition will change abruptly but remaining finite, as seen in Figure 2.3b.

2.3 Glass-forming Liquids

Liquids that can be cooled down to very low temperatures avoiding crystallization are glass- forming system. In general, when a glass-forming system is cooled down from the melt to a given temperature, its viscosity will increase and affect the molecular structural rearrangements necessary to find the thermodynamic equilibrium of the system at that specific temperature. When through a continuous cooling these molecular rearrangements cannot follow the cooling rate, the system will fall out of equilibrium and a glass system will be formed. The structure of this glassy system is the one of a disordered material, and it appears to be "frozen" within the experimental observation time. The temperature at which vitrification -"the freezing of the molecules of the material"- occurs is characterized by a temperature range called the glass transition temperature. The transition temperature can be defined in a thermodynamic perspective by the temperature at which changes in the temperature-dependence of the volume or enthalpy will occur in the material, see Figure 2.3b. A particular feature of the glass transition temperature is that it is not unique since it is not a true thermodynamic transition and has a kinetic origin. It will span a small temperature range that depends on the cooling rate applied to the material: The smaller the cooling rate is, the larger the time is given to the system to reach its equilibrium and lower the glass transition would be. However, this dependence on the cooling rate is relatively weak, and a order of magnitude change in the cooling rate may affect T_g by only $3-5$ K. Below T_g the glassy state is unstable with respect to the supercooled liquid states and the crystalline solid state. A glass is continuously relaxing towards a more stable state. Nevertheless, from an experimental point of view, the molecular motions involved in the structural relaxations in a glass some ten degrees below the T_g are in general too slow compared to the laboratory time-scale and its physical properties do not appreciably change over time scales of several years. Hence, the glassy system is mechanically stable for practical purposes, even though is thermodynamically unstable [29] and its main macroscopic properties are strongly related to the dynamics of processes occurring at the molecular level.

2.4 Polymeric Materials

Polymers are long string-like molecules made of repeating chemical units called monomers connected by covalent bonds as it is schematized in Figure 2.4. The number of monomers in a polymer is typically several thousand, and can be as large as tens of millions. Polymers are crucial materials in modern technology; they are encounter as plastics, rubbers, films, textiles and we can see their influence in products of our every day life.

Regarding their thermodynamic properties, they are an important sub-

Figure 2.4: Schematic representation of polyethylene polymer

family of the glass-forming materials since a fully crystalline polymer is hardly obtained even using careful preparation procedures. They consist of large molecular entities with more or less complex atomic structure that makes it difficult to obtain a pure crystalline arrangement and in many cases avoid completely crystallization. Polymers can be classified according to the type of polymerization from which they have been synthesized, either by: step growth polymerization, which is a stepwise reaction between functional groups of polymeric monomers. Polymers prepared in such way increase their molecular weight at a very slow rate at low conversion rates, an only they reach moderately high molecular weights at very high conversions. And chain growth or addition polymerization involves the linking of monomers incorporating double or triple chemical bonds. Chain-growth polymerization requires an active centre, which may be a free radical (in the radical polymerization), cation (in the cationic polymerization) or anion (in the anionic polymerization). Once an active centre is created, a polymer chain grows extremely rapidly, and when it is deactivated by an irreversible termination reaction, the polymer chain is "dead" and no longer takes part as a reactant. Thus, this type of polymerization is divided in three steps: initiation, propagation and termination. Initiation is the first step of the polymerization process that includes two sub-steps being the first one the production of free radicals. The second part of the initiation involves the addition of the created radicals into a first monomer to produce the chain initiating radical. In the propagation, each addition creates a new radical having the same identity as the previous one, but being larger by one monomer unit. At some point, the propagating polymer chain stops growing and terminates. Termination occurs by bimolecular reaction between radicals by combination (coupling) or, more rarely, by disproportion. In addition polymerization high molecular weight chains are formed rapidly as oppose to the step-growth polymers.

As a consequence of the polymerization conditions, the chains in a given polymer can have different molecular weights, and molecular weight distribution functions are used to describe this situation. The number-average molecular weight M_n and the weight-average molecular weight M_w are respectively defined as

$$M_n = \frac{\sum N_i M_i}{\sum N_i} \tag{2.1}$$

and

$$M_w = \frac{\sum N_i M_i^2}{\sum N_i M_i} \tag{2.2}$$

with N_i the number of molecules of molecular weight M_i. The polydispersity index is defined as the ratio $M_w/M_n \geq 1$ and provides a characterization of the width of the molecular weight distribution. Same kind of polymers with different average molecular weights and/ or polydispersity can exhibit very different properties related to the chain structure and dynamics. However, these are not the only characteristics affecting the polymeric features. In fact, polymers can exist in various conformations, that is the spatial arrangements of the molecular groups of the polymer chain established by rotations about single bonds (i.e. planar zigzag, folded chain and random coils), and in different configurations, that is the organization of the atoms along the chain. There are also many different architectures in which polymers can be found. The most basic polymer architecture is a linear chain, but polymers can present more complex architectures, for example closed ring, chain branching, or a set of polymers can be connected by bonds to form a polymer network. All these characteristics influence the mechanical and dynamical properties of each specific system, mainly at high temperature.

Polymeric materials usually present complex thermodynamic transition processes. Previously, phase transitions have been defined thermodynamically. However, to model these transitions we must turn to theories that describe the ordering in the system like the Flory-Huggins theory, which is a powerful model used to describe polymer-solvent or polymer-polymer mixtures. Furthermore, and as mentioned before, in complex systems like polymeric materials the conventional phase behavior scheme of gas, liquid or solid presented by other materials it usually does not fit their behavior. They do not form gas phases, and it is unusual for them to behave as simple liquids; usually they are much more viscous, even in solution. Additionally, in the solid state, polymers never completely crystallize and adopt a richer range of structural arrangements, many of which can be distinguished on the basis of the flow behavior (rheology) rather than by their molecular organization. Moreover, solid polymers can also adopt glassy states, in which case their structure can be either amorphous or semicrystalline. Furthermore, when polymers melt they exhibit a viscoelastic behavior, which refers to the existence of a combination of viscous and elastic behavior, depending on the time-scale of observation. Therefore, the structure and dynamics of these complex materials are closely related, and the structural arrangements

that the materials can access will depend on the liquid-like behavior of the material.

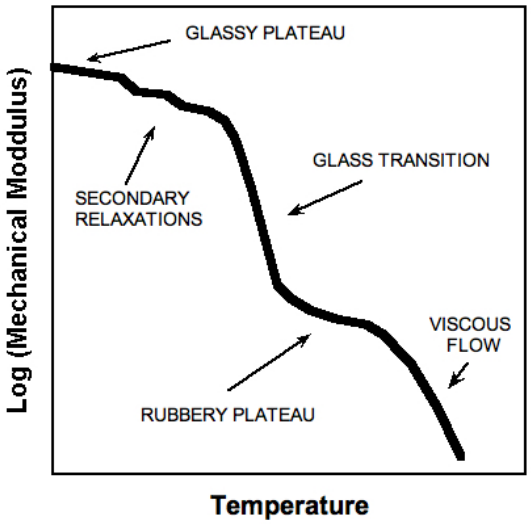

Figure 2.5: Schematic illustration of the temperature variation of the mechanical modulus for typical amorphous polymers

A qualitative representation of the variation of the mechanical properties in a polymer is shown in Figure 2.5. When cooled from high temperature where they behaves as viscous liquids, polymers with high enough molecular weight behave rubber-like, i.e they can not flow easily but they can be largely deformed. In this regime the different polymer chains are physically entangled and only after long time the entanglements can be removed. At even lower temperatures, i.e., approaching the glass transition temperature, the dynamics associated to the polymer chain becomes too slow. In this temperature range, only motions with characteristic length-scales of the order of inter and intra molecular distances (segmental motions) control the main properties of the polymer. At these relatively small length scales, the atomic disorder is the key factor and the dynamical and structural features of the polymers are close to those typical of glass-forming systems in general. On further cooling and reaching T_g the segmental motions of a polymer involve times in the range of a few seconds, and the mechanical modulus reaches values typical of solids. However, at this temperature other faster molecular motions also take place, particularly, those responsible of the local changes in the backbone chain conformations and/or side chain groups. When cooled down at very low temperatures these local motions are too slow and the mechanical modulus of the polymer increases gradually reaching a low temperature plateau typical of a rigid solid.

2.5 Block Copolymers

When one links together two or more homopolymers -i.e., polymers consisting of identical repeating units- of different species, the obtained polymer is called a copolymer. In particular block copolymers are a class of polymer materials where the individual chains are composed by large portions each formed by a specific monomeric unit. Different configurations of these components can be observed as shown in Figure 2.6 taken from Ref. [30].

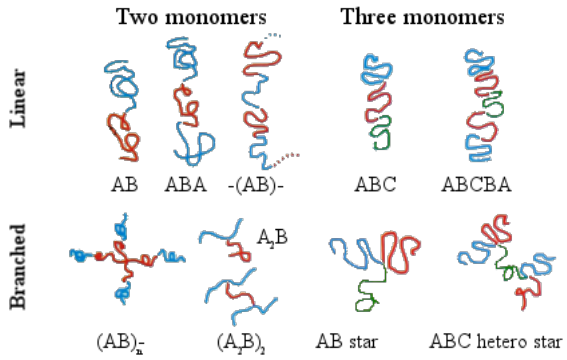

Figure 2.6: Block copolymers in different molecular architectures according to two, three or more monomer types

In the simplest case, a linear diblock copolymer is a polymer constructed by attaching one end of a linear homopolymer of one species to the end of another linear homopolymer of a distinct species creating a longer but still linear molecule. Symbolically, this is written as a $A-B$ copolymer where A and B denote the distinct species. The portion of the chain, which is of species A, is referred to as the A block, and likewise the portion of the chain, which is of species B, is referred to as the B block. Hence, diblock copolymer refers to a copolymer comprised of two blocks of distinct species.

Ensembles of diblock copolymers exhibit some well-known and interesting thermodynamic behavior [31]. Typically, when one has two distinct species of monomer, there exists a net repulsive interaction between the monomers. That is, their dissimilar molecular properties result in immiscibility, in analogy to oil and water.This repulsive interaction is traditionally quantified by the Flory parameter [32], χ_F. To first order, this energy is independent of T. However, the free energy of the system is generally expressed as a dimensionless free energy, F/k_BT, and so, to first order, this energy behaves as H/T where H is a constant. Experimentally, χ_F is found to behave as:

$$\chi_F = K + \frac{H}{T} \tag{2.3}$$

where K is a corrective term, which contains entropic effects that are not included in the Flory- Huggins entropy of mixing. The temperature de-

pendence in χ_F gives experimentalists a way to vary χ_F dynamically, and thus a way to probe the impact the magnitude of χ_F has on the system. So, with a diblock copolymer, one has a molecule in which the monomers in block A will be repulsed by the monomers in block B. The chemical bonds in the polymer are sufficiently strong that the molecule will not break up and dissociate. However, the flexibility of the molecule is such that the repulsion between A and B blocks will bias the molecule's random walk so as to minimize contact between dissimilar species. In a system of many copolymer molecules, copolymer molecules will also attempt to orient so as to minimize the contact between their block A and their neighbor's block A, and vice versa. When this tendency is strong enough to overcome natural entropy and diffusion effects in the system, this drive toward alignment induces a spontaneous ordering of the system. This ordering is called microphase separation. Several ordered structures are possible which minimize exposure of dissimilar blocks to each other. The most common of these are the lamellar, cylindrical, and spherical morphologies [33, 34]. In the lamellar structure, the copolymers tend to orient so that block A lies to one side of a dividing plane while block B lies to the other. The dividing plane is called the interphase. The chemical joint between block A and block B typically lies roughly within this dividing plane. Symbolically, one might write this as $A \mid B$ with A indicating a region dominated by species$A$, B a region dominated by species B, and $\mid$ the interphase where the $A-B$ joints would reside. In a typical three-dimensional system, this layering would repeat several times in the mirroring pattern $A \mid BB \mid AA \mid BB \mid A$. The space between two consecutive interphase planes is called a subdomain. Each subdomain is either dominated by species A or species B. The perpendicular distance between two interphase planes is called the subdomain thickness. The thickness of species $A's$ subdomain may be different than that of species B, depending on the relative sizes of the A and B blocks in the copolymer as well as other geometric factors. The total domain thickness is the sum of the A and B subdomain thicknesses. The cylindrical and spherical morphologies are similar in concept, except that instead of the interface being a plane, the $A-B$ junction centres on a cylindrical or spherical surface with block A penetrating inside and block B extending outside, or vice versa. (The smaller block will be the species on the inside of the cylinder or sphere. As with the lamellar case, in an extended three-dimensional system several such domains will form. In the case of cylinders, they will organize on a hexagonal lattice. In the spherical case, the spherical domains will repeat on a body-centered cubic lattice for instance. Other, more exotic structures are also possible such as the gyroid.

The phase behavior of a $A-B$ diblock copolymer is controlled by some experimental parameters: the degree of polymerization N, the composition f, the temperature T and the $A-B$ Flory-Huggins interaction parame-

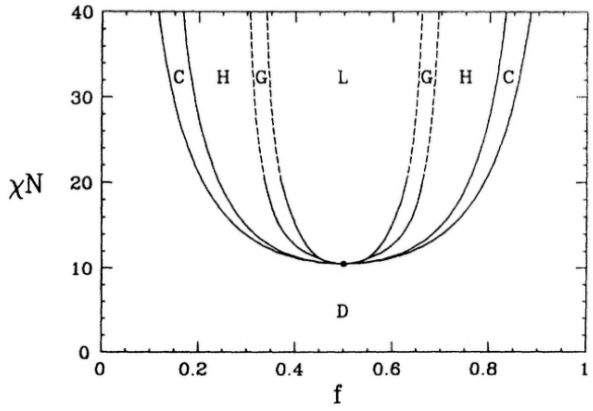

(a) phase diagram predicted by self-consistent mean field theory

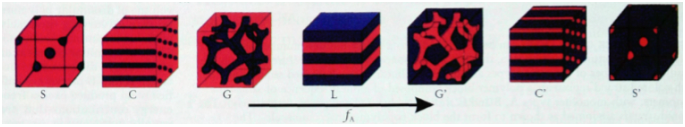

(b) pictorial representation of the theoretical phase diagram

Figure 2.7: Diblock copolymer -self consistent mean field theoretical- phase diagram

ter χ_F. A typical phase diagram, Ref. [35], predicted by the self-consistent mean field theory and is shown in Figure 2.7a. As it can be seen, in general, repulsion between two different segments (high values of χ) and a large degree of polymerization favor phase separation, while higher temperatures promote mixing. When the volume fraction of block $A(f_A)$ is small, it forms spheres surrounded by a matrix of B. As f_A increases towards 0.5, the minority nanodomains will form first cylinders in a hexagonal lattice, then a bicontinuous gyroid structure, and finally lamellas. The size and periodicity of the nanodomains depend on the chain sizes (N); larger chains will form larger domains. When we have a low degree of polymerization, as is the case of the co-oligomers, we could expect that no phase separation would be shown. However, the situation can change if other energetic terms come into play. This is the case of systems with extra interactions (as the presence of H-bonds) or when at least one of the blocks has a strong tendency to crystallize. In these cases the segregation of the block could be favored.

2.6 Molecular Dynamics

As has been commented above, one of the fundamental aspects of soft-matter is the relevance of the molecular motions, which take place at different length-

/time scales and are possible in general due to remaining structural disorder. In contrast, in addition of the ubiquitous molecular and lattice vibrations, the dynamics of crystalline solids is basically restricted to crystal lattice defects. A convenient way to investigate the molecular motions is by means of relaxation techniques. These relaxation techniques make use of the response of the material properties to an applied external perturbation. Depending on the nature of the perturbing field one speaks of mechanical relaxation, dielectric relaxation, and so on.

2.6.1 Fluctuation Dissipation Theorem

Thermodynamic quantities that characterize a macroscopic sample are in general average values. Moreover, due to the stochastic motions of the molecules (or particles) these quantities fluctuate around their mean value [36]. An example for that is the Brownian motion. If we consider $x(t)$ to be a quantity of a well-defined subsystem of a sample with a macroscopic significance and $\langle x \rangle$ its average value -for instance, x can be the volume, the energy or also the polarization of the subsystem[1], then the relation $\Delta x(t) = x(t) - \langle x \rangle$ will define the stochastic process of the fluctuations of $x(t)$. For a stationary process the average value $\langle \Delta x(t) \rangle$ vanishes, however its mean quadratic fluctuation $\langle \Delta x(t)^2 \rangle = \langle \Delta x^2 \rangle$ takes a value different from zero. The correlation function is defined as the average of the product of two values Δx separated by a time ζ .

$$\Psi(\zeta) = \langle \Delta x(t) \cdot \Delta x(t+\zeta) \rangle \tag{2.4}$$

The correlation function describes the dependence of $\Delta x(t+\zeta)$ on $\Delta x(t)$. In the stationary state the time t does not play a role

$$\Psi(\zeta) = \langle \Delta x(0) \cdot \Delta x(\zeta) \rangle \tag{2.5}$$

with $\Psi(-\zeta) = \Psi(\zeta)$. That means Ψ is a symmetrical function with regard to ζ. For $\zeta \to \infty$, $\Psi = 0$ holds. The relationship of the correlation function to $\langle \Delta x^2 \rangle$ is given by $\langle \Delta x^2 \rangle = \psi(0)$. And usually the normalized correlation function is considered;

$$\phi(\zeta) = \frac{\langle \Delta x(0) \cdot \Delta x(\zeta) \rangle}{\langle \Delta x^2 \rangle} \tag{2.6}$$

The inverse Fourier transformation of the correlation function $\Psi(\zeta)$ is called spectral density $\langle \Delta x^2 \rangle_\omega$ and is a measure for the frequency distribution of the fluctuation Δx. In the theories of stochastic processes $\langle \Delta x^2 \rangle_\omega$ is often called power spectrum [37].

[1] According to Ref. [36] a subsystem is defined as a small but macroscopic part of the sample having all its natural interaction with the surrounding

$$\left\langle \Delta x^2 \right\rangle_\omega = \frac{1}{2\pi} \int_{-\infty}^{\infty} \Psi(\zeta)\, exp(i\omega\zeta)\, d\zeta \tag{2.7}$$

and it holds $\left(\Delta x^2\right)_\omega = \left\langle \Delta x^2 \right\rangle_{-\omega}$. The relationship to the mean square fluctuation is given by

$$\left\langle \Delta x^2 \right\rangle = \Psi(0) = \int_{-\infty}^{\infty} \left\langle \Delta x^2 \right\rangle_\omega d\omega \tag{2.8}$$

The Fluctuation Dissipation Theorem (FDT) of Callen and Welton [38], relates the response of a system to an outer disturbance to the spontaneous fluctuations of the system and therefore is the basis of using relaxation techniques for investigating the molecular dynamics.

2.6.2 Linear Response Theory

When a system suffers a small perturbation its response is related with the perturbation in a linear way. For example for an electrical perturbation by means on an electric field $\mathbf{E}$ the system polarization $\mathbf{P}$ is given by:

$$\mathbf{P} = \chi \mathbf{E} \tag{2.9}$$

where χ is the electrical susceptibility, which in the simplest case of homogeneous and isotropic response is a constant scalar. The electric polarization of a material arises by different microscopic mechanisms, ones are very fast since involve the motion of electrons and atoms (electronic and atomic polarization) whereas others can be relatively slow as those arising form the reorientation of permanent molecular dipole moments or the migration of charge carries. Thus in general χ will take time dependent values, which can be expressed as:

$$\chi(t) = \chi_\infty + \Delta\chi\,[1 - \varphi(t)] \tag{2.10}$$

Where $\varphi(t)$ is a normalized function that represents the relaxation of the system towards the final equilibrium state, after the perturbation. In the very simple case $\varphi(t)$ is given by an exponential function characterized exclusively by the so called relaxation time τ, i.e.

$$\varphi(t) = exp\left(\frac{-t}{\tau}\right) \tag{2.11}$$

A convenient way of determining the dielectric relaxation of a given system is by measuring the frequency dependent dielectric permittivity [39]. In the framework of the linear response theory the frequency dependent permittivity is connected with the time relaxation function $\varphi(t)$ by a Fourier transformation as:

$$\varepsilon^{*}(\omega) = \varepsilon_{\infty} + \Delta\varepsilon \int_{0}^{\infty} \frac{\mathrm{d}\varphi(t)}{\mathrm{d}t} exp(-i\omega t)\, dt \tag{2.12}$$

where the fact that ε^{*} is a complex number $\left[\varepsilon^{*}(\omega) = \varepsilon^{'}(\omega) - i\varepsilon^{''}(\omega)\right]$ is related with the existence of a phase shift between the oscillation of the perturbing electric field and that of the system polarization, shift provoked by the finite value of the relaxation time. $\varepsilon^{'}(t)$ and $\varepsilon^{''}(t)$ are connected to each other by the Kramers-Kroning relations and consequently each brings all the dynamical information.

Particularly the relaxation strength

$$\Delta\varepsilon = \frac{2}{\pi} \int_{0}^{\infty} \varepsilon^{''}(\omega) \frac{d\omega}{\omega} \tag{2.13}$$

When the FDT theorem applies the following relation between the spontaneous fluctuations of the polarization and the complex permittivity exists:

$$\left\langle \Delta P^{2} \right\rangle_{\omega} \propto \frac{\varepsilon^{''}(\omega)}{\pi\omega} \tag{2.14}$$

which evidences that the main fluctuations occurs at a frequency where the imaginary part of the permittivity is large. In the simplest case of an exponential relaxation function, the complex permittivity is expressed as:

$$\varepsilon^{*} = \varepsilon_{\infty} + \Delta\varepsilon\,(1 + i\omega\tau)^{-1} \tag{2.15}$$

2.6.3 Molecular dynamics in glass-forming systems

The dynamics of glass-forming systems are very complex and normally several relaxation processes are observed in such systems. The characteristic lengths of the molecular motions involved vary from one process to another and, some of them are highly sensitive to temperature and external pressure. Furthermore, the characteristic times span over many decades (from 10^{-13} s to 10^{5} s). The most prominent relaxation process in glass-forming materials in general is that related to the molecular dynamics controlling the glass transition, i.e., the segmental dynamics in the polymer case. This main relaxation process is often referred to as the α-relaxation, whereas those faster relaxations are named with other Greek letters β-, γ-, ... , and, as a whole, they are referred to as secondary relaxations. In the particular case of polymer materials, there are slower motions which involve the polymer chains and that are responsible of the mechanical relaxation processes reflecting the viscoelasticity of polymeric materials. This slowest relaxation process is usually named terminal relaxation. A schematic representation of different mechanical relaxation process was already shown in Figure 2.5. Many of these molecular motions also result in corresponding dielectric relaxation

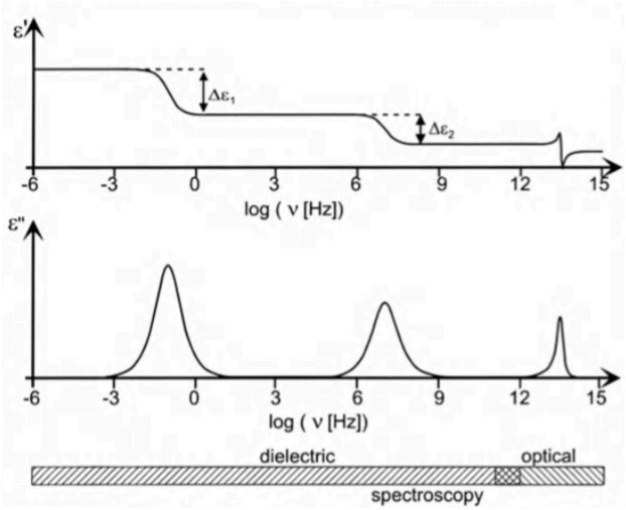

Figure 2.8: Dielectric relaxation processes usually observed

process (see Figure 2.8 taken from Ref. [40]). The requirement in this case is that the molecular motion involves fluctuations in the molecular dipole moments. This is generally the case for most of the local and segmental motions but no so common for the terminal relaxation, since the molecular dipole associated to the whole chain is in general very low due to the usual random orientation of the monomeric dipole moments. Nevertheless, in the case of polymers with highly regular monomeric structures a resulting dipole moment sensitive to chain motions can exist and consequently a corresponding dielectric relaxation process be observed.

In the following, a brief description of the general features of the relaxation processes occurring in typical glass-forming systems is given [40]. As mentioned above, the molecular motions involved in the α-relaxation are related to the glass transition and they strongly depend on temperature: approaching T_g from the melt state, the molecular motions will drastically slow down and the system will appear "frozen". The temperature dependence of the characteristic relaxation time τ_α associated to the primary relaxation is non-Arrhenius and it can usually be described by a Vogel-Fulcher-Tamman function:

$$\tau_\alpha = \tau_\infty exp\left(\frac{B}{T - T_0}\right) \tag{2.16}$$

Here τ_∞ and B are temperature independent parameters, while the Vogel temperature T_0 represents the singularity at which the characteristic relaxation time tend to diverge. This empirical temperature dependence of the structural relaxation can be justified by two main phenomelogical theoretical approaches: the free volume theory developed by Doolittle [41]

and Cohen [42, 43], and the Adam-Gibbs theory [44]. The first theory is based on the assumption of a local volume V attributed to molecules -i.e. low molecular weight glass-formers or liquids- or segments of the polymer chain. Defining the free volume V_f as $V_f = V - V_c$ where V_c is a critical volume and assuming that the mechanism of the molecular transport is a jump over a distance, the relaxation can occur only if $V_f > V^{'}$, where $V^{'}$ is the minimal free volume required for the jump. In this framework, T_0 in the VFT equation is the temperature at which the free volume vanishes. The latter theory is based on the cooperativity approach to the glass transition. Adam and Gibbs introduced the concept of cooperatively rearranging region (CRR) defined as a subsystem, which upon a sufficient thermal fluctuation, can rearrange into another configuration independently of its environments. In this scenario, the Vogel temperature T_0 corresponds to a divergence of the size of the CRR.

It is possible to find some peculiar and universal features of the α-relaxation occurring in all glass-forming systems. The first is related to the non-Arrhenius behavior of the temperature dependence of the primary relaxation above mentioned. In connection to this feature, the fragility parameter m defined as:

$$m = \left. \frac{\partial log\tau}{\partial \left(\frac{T_g}{T}\right)} \right|_{T_g} = T \tag{2.17}$$

allow us to classify the system as fragile or strong according to the well-known Angell's criteria [45]. According to the way the characteristic relaxation time τ_α approaches the glass-transition temperature, systems showing prominent non-Arrhenius behavior are called fragile (large values of m), while those manifesting an Arrhenius-like dependence on temperature are classified as strong (small values of m). In this classification, glass-forming polymers are usually fragile.

Another feature of glass forming systems is the non-exponential nature of the response of the system to various perturbations. This particular behavior can be explained taking into account two different scenarios. One is supposing a heterogeneous set of environments in the system. In this framework, each environment will be characterized by its own exponential-relaxation but with different relaxation times among them. Therefore, the non-exponential relaxation would be due to the superposition of the exponential functions with different relaxation times. Alternatively, a homogeneous scenario has been proposed where all the environments relax almost identically in an intrinsically non-exponential way. Generally, it is accepted that heterogeneities are an important key in the dynamics of glass-forming systems, although the question whether the relaxation function is intrinsically exponential is still a subject of debate. Usually, a stretched exponential function is used to

characterize response functions in the time domain:

$$\phi_{KWW}(t) = exp\left[-\left(\frac{t}{\tau}\right)^{\beta}\right] \tag{2.18}$$

with τ setting the time scale and $\beta < 1$ determining the stretching of the decay. From a mathematical point of view, the KWW function can be expressed as a superposition of exponential functions:

$$\phi_{KWW}(t) = \int_0^{\infty} g(\tau)\, exp\left(\frac{-t}{\tau}\right) d\tau \tag{2.19}$$

with $g(\tau)$ representing a distribution function of the relaxation times. This would correspond to the physical picture of the heterogeneous scenario above mentioned. We note that distributions of relaxation times are commonly found behind the broad features of the relaxations in the glassy state. Usually, these distributions can be attributed to heterogeneous environments in the glassy materials.

Before describing the phenomenological features of other dynamic processes in glass-formers, it is worth mentioning the mode coupling theory (MCT) that represents a microscopic approach to the structural glass transition. MCT considers the density fluctuations as the most important low-frequency process and describes the glass transition as an essentially dynamic phenomenon [46]. The main physical interpretation behind is the structural arrest that occurs because particles can no longer leave their cage at finite time. Exhaustive reviews on MCT can be found in Refs. [47, 48, 49, 50, 51].

Below the glass transition temperature, only short-range molecular motions can take place. In general, these local motions are at origin of the so-called secondary relaxations. Such local motions can be of different nature depending on the glass forming material. In polymers, secondary relaxations are often associated to local motions of molecular groups in the main chain or in the side group -i.e., methyl group rotations, twisting motions or motions of the side group about the bonds linking them to the main chain-. In low molecular weight glass formers such relaxations might involve the motions of essentially all parts of the basic structural unit [52]. However, some secondary relaxations may not involve just intra-molecular motions. In fact, Johari and Goldstein [53] showed the presence of these relaxations even in glass formers composed of completely rigid molecules and therefore the relaxation should be originated from some motion of the entire molecule. The temperature dependence of the relaxation times associated to relaxations in the glassy state is that expected for the thermally activated processes, that is the Arrhenius Law:

$$\tau = \tau_{\infty} exp\left(\frac{E_a}{k_B T}\right) \tag{2.20}$$

where E_a represents the activation energy of the process, k_BT is the Boltzmann's constant and τ_∞ is a parameter that represents the relaxation time at $T \to \infty$.

In summary, glassy materials show a subtle dynamics, which at moment is not completely understood. However, among the different relaxation techniques used for the investigation of glassy materials and in particular the polymer dynamics, those detecting the dielectric relaxation are very suitable since most of the polymers have permanent molecular dipole moments in the monomeric unit. In this case, the segmental dynamics of a polymer will be detected through the spontaneous fluctuations of the dipole moments in the monomeric units. Moreover and in particular by using Broadband Dielectric spectroscopy, BDS, a range of 10 decades in frequency can be explored in a single set up and up to 16 decades by combining different equipment. In addition, BDS techniques are extremely sensitive and allow detecting very weak relaxation processes. Thus, BDS is a powerful relaxation technique that will allow us to investigating either, materials having very small dipole moments, or a given polar system as a minority component in a mixture or composite material.

Chapter 3

Experimental Techniques

"The interaction of electromagnetic waves with matter in the frequency regime between 10^{-6} and 10^{12} Hz is the domain of broad band dielectric spectroscopy. In this extraordinary dynamic range, molecular and collective dipolar fluctuations, charge transport and polarisation effects at inner and outer boundaries take place, and determine the dielectric properties of the material."

F. Kremer and A. Schönhals, 2002

Abstract: In this chapter we will focus on the description of the physical principles underlying different experimental techniques used in this work. The first section will start with a brief introduction to X-ray diffraction and the "Bragg's law", subsequently we will introduce the mathematical tools necessary to interpret the diffraction experiment. Later, the two employed experimental X-ray setups -SAXS and WAXS- will be briefly explained. To end this section, comments on the Instrumental Setup will be given. Subsequent sections, i.e., Infrared spectroscopy, Thermal analysis and Broadband dielectric spectroscopy will have similar outline as the first one.

3.1 X-ray Diffraction

X-Ray crystallography is an analytical tool used to identify the atomic and molecular structure of a crystalline material. The physical principle underlying the structural analysis originates from the scattering of incident X-rays by the atoms in a crystalline lattice, in turn, this will create a diffraction pattern which is possible to analyze. In simple terms, by measuring the angles and intensities of the diffracted X-rays, one can produce a three-dimensional

picture of the density of electrons within the material. From this electron density, the mean positions of the atoms in the material can be determined, as well as their disorder and other relevant information.

3.1.1 Bragg's Law

When X-rays are incident on an atom, they make the electronic cloud move as does any electromagnetic wave. The movement of these charges re-radiate waves with the same frequency, blurred slightly due to a variety of effects; this phenomenon is known as Rayleigh scattering (or elastic scattering). These re-emitted wave fields can interfere with each other either constructively or destructively, producing a diffraction pattern on a detector. The resulting wave interference pattern is the basis of diffraction analysis. In order for waves to interfere they must fulfill the Bragg condition. Bragg diffraction occurs when radiation, with wavelength comparable to atomic spacing, is scattered in a specular way by the atoms of a crystalline system, and undergoes constructive interference. For a crystalline solid, the waves are scattered form lattice planes separated by the inter-planar distance, d. The path difference between two waves undergoing constructive interference is given by, $2dsin\theta$, where, θ, is the scattering angle. The effect of the constructive or destructive interference intensifies due to the cumulative effect of reflections in successive crystallographic planes of the crystalline lattice. This leads to Bragg's law, which describe the condition on θ_B for the constructive interference to be at its strongest when:

$$2dsin\theta_B = n\lambda \tag{3.1}$$

where, n, is a positive integer and, λ, is the wavelength of the incident wave.

A diffraction patter is obtained by measuring the intensity of scattered waves as a function of the scattering angle. Very strong intensities known as Bragg peaks are obtained in the diffraction pattern at the points where the scattering angle satisfies the Bragg condition.

3.1.2 Diffraction Experiment

The physical principle underlying a diffraction experiment resides in the scattering of incident radiation onto a sample. A schematic representation of the process is depicted in Figure 3.1. In the figure we have an incident beam of monochromatic radiation with wavelength, λ, and intensity, I_0. The radiation becomes scattered by a sample and the intensity, $I(\mathbf{q})$, of the scattered waves is registered by a detector, D, at a distance, A, subject to variation of the direction of observation. Making use of the scattering vector, $\mathbf{q}$, defined as:

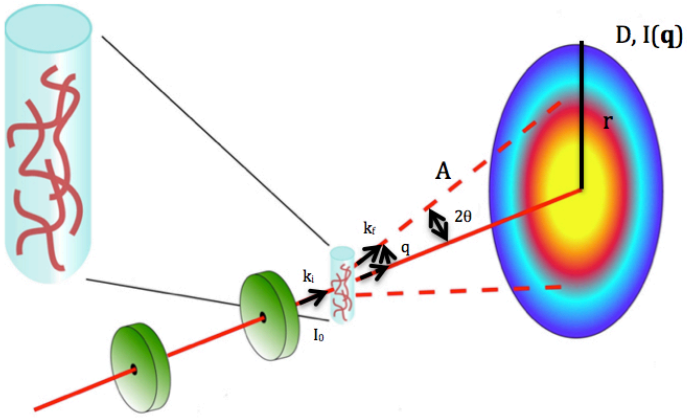

Figure 3.1: Schematic representation of the physic's behind X-ray diffraction patterns, in particular for small angle X-ray scattering

$$\mathbf{q} = \mathbf{k}_f - \mathbf{k}_i \tag{3.2}$$

where $\mathbf{k}_f$ and $\mathbf{k}_i$ denote the wave vectors of the incident and the scattered plane waves respectively. The result of a scattering experiment is usually expressed by giving the intensity distribution in the $\mathbf{q}$-space, $I(\mathbf{q})$. In the majority of scattering experiments on polymers the radiation frequency remains practically unchanged. This implies that the magnitude of the incident and scattered wave vectors are:

$$|\mathbf{k}_f| \approx |\mathbf{k}_i| = \frac{2\pi}{\lambda} \tag{3.3}$$

Moreover, the magnitude of the scattering vector, $|\mathbf{q}|$, is related to the scattering angle, θ, by:

$$|\mathbf{q}| = \frac{4\pi}{\lambda} sin\theta \tag{3.4}$$

where θ is identical to half of the angle enclosed by $\mathbf{k}_i$ and $\mathbf{k}_f$. Mathematically we can represent and model scattering data in reduced forms by means of two different functions. The first one, denoted by $\Sigma(\mathbf{q})$, is the differential scattering cross-section per unit volume:

$$\Sigma(\mathbf{q}) = \frac{1}{V}\frac{\mathrm{d}\sigma}{\mathrm{d}\Omega} = \frac{1}{V}\frac{I(\mathbf{q})\,A^2}{I_0} \tag{3.5}$$

In light scattering experiments this function is called the Rayleigh ratio. While the effect of the volume is removed, $\Sigma(\mathbf{q})$ remains dependent on the scattering power of the particles in the sample, which varies with the applied radiation. For X-rays, the scattering power is related to the electron

densities. The dependence on the applied radiation (X-ray) of the measured intensity is eliminated using the interference function, $S(\mathbf{q})$, also called scattering function or scattering law, which for materials containing equivalent particles is defined as:

$$S(\mathbf{q}) = \frac{I(\mathbf{q})}{I_m N_m} \tag{3.6}$$

Here N_m represents the total number of particles in the sample and I_m is the scattering intensity produced by one particle, if placed in the same incident beam. The Scattering function can be expressed in terms of the particle's positions as:

$$S(\mathbf{q}) = \frac{1}{N_m} \sum_{i,j}^{N_m} \langle exp\left[-i\mathbf{q} \cdot (\mathbf{r}_i - \mathbf{r}_j)\right] \rangle \tag{3.7}$$

Instead of specifying the discrete positions ($\mathbf{r}_i$) of all particles, one can also use a continuum description and introduce the particle density distribution, $c_m(\mathbf{r})$. In this case the function is expressed as:

$$S(\mathbf{q}) = \frac{1}{\langle c_m \rangle} \int exp(-i\mathbf{qr}) \left(\langle c_m(\mathbf{r}) c_m(0) \rangle - \langle c_m \rangle^2 \right) d^3\mathbf{r} \tag{3.8}$$

Equation 3.8 expresses, $S(\mathbf{q})$, as the Fourier transform of the space dependent correlation function of the particle density. A third form of the basic scattering equation is obtained if structures are characterized with the aid of the pair distribution function, $g(\mathbf{r})$:

$$S(\mathbf{q}) = \frac{1}{\langle c_m \rangle} \int exp(-i\mathbf{qr}) \left(g(\mathbf{r}) - \langle c_m \rangle \right) d^3\mathbf{r} \tag{3.9}$$

Per definition, the product $g(\mathbf{r}) d^3\mathbf{r}$ gives the probability that, starting from a given particle, the particle itself or some other particle is found in the volume element $d^3\mathbf{r}$ at a distance $\mathbf{r}$. Three equivalent relations have been presented: equations (3.7), (3.8) and (3.9), can all be conveniently used in the evaluation of scattering data. All three equations express a Fourier relation between, $S(\mathbf{q})$, and functions that describe properties of the microscopic structure in statistical terms. To put special emphasis on this well-defined structural background, $S(\mathbf{q})$, firstly introduced as the "scattering function", is often also addressed as the structure function or structure factor, for more information see Ref. [54].

3.1.3 Small Angle X-ray Scattering

Small Angle X-ray Scattering (SAXS) is a fundamental method for structure analysis of soft condensed matter. It has emerged as an essential tool used to unravel the structure details with characteristic dimensions at length scales

up to 100 nm and beyond. It is used at all fronts in material science for development porpoises. The SAXS method yields information on the sizes or shapes of particles and also on the internal structure of disordered and partially ordered systems. The applications of the technique cover various fields, from metal alloys to synthetic polymers in solutions and as bulk material, biological macromolecules, emulsions, porous materials, and nano-particles, etc. Moreover, SAXS also makes it possible to investigate in real-time intermolecular interactions such as self-assembly and large conformation changes.

In a diffraction experiment the atoms within the material will scatter the incident radiation into all directions. This produces a background radiation almost constant for small-angle measurement. Furthermore, particles (i.e., cluster of atoms) inside the sample will produce an additional scattering (excess scattering), given the fact that particles are made of different components of the material with distinct density. By measuring the angle-dependent distribution of the scattered radiation (intensity) it is possible to draw conclusions about the average particle structure. The result is a 2D interference pattern, where the intensity varies from position to position in the detection plane. The interference pattern is characteristic to the internal structure of the material, i.e., to the orientation and distances of the atoms or cluster to each other. The interference pattern will therefore contain contributions of neighboring particles as well. This additional interference pattern multiplies with the form factor of the single particle and it is the structure factor. The structure factor becomes more evident, when the particle positions turn into increasingly ordered. When the domain size of ordered particles increases (i.e., formation of long-range order), the system is said to crystallize.

The structure factor of a crystalline substance is normally called Lattice factor. It is a set of narrow and intensive peaks well-defined angles indicative for crystal symmetry according to the Bragg's Law. It can be shown that the ratios of the peak positions on the q-scale have typical values, which reveal the crystal symmetry. For example, for lamellar symmetry, $q = 1, 2, 3$, for cubic symmetry, $q = 1, \sqrt{2}, \sqrt{3}$, for hexagonal symmetry, $q = 1, \sqrt{3}, 2$, etc.

3.1.4 Wide Angle X-ray Scattering

Wide Angle X-ray Scattering (WAXS) is an X-ray measurement technique, which is often used to determine the crystalline structure in materials and polymers. This technique specifically refers to the analysis of Bragg peaks scattered at wide angles, which implies sub-nanometre-sized structures, essentially interatomic distances. According to this method the sample is mounted in a wide-angle X-ray goniometer, and the scattering intensity is plotted as a function of the angle. The physical principle of wide angle X-ray scattering is the same as the one for small-angle X-ray scattering (and all diffraction techniques), however the main difference between WAXS and

SAXS is given by the relative distance from the sample to the detector. In the first case this distance is shorter and thus diffraction maxima at larger angles are observed.

3.1.5 X-ray diffraction Instruments setup

In this thesis SAXS and WAXS diffraction measurements were carried out on different equipment's. Below we will describe the different instrument setups for both types of experiments, starting with SAXS measurements we have:

SAXS experiments were conducted in Rigaku 3-pinhole PSAXS-L equipment (see Figure 3.2), operating at 45 kV and 0.88 mA. The Micromax-002+ X-Ray Generator System is composed by microfocus which sealed tube source module and integrated X-Ray generator unit which produces Cu K_α transition photons of wavelength $\lambda = 0.1542$ nm. The flight path and the sample chamber in this equipment are under vacuum. The scattered X-Rays are detected on a two-dimensional multiwire X-Ray Detector (Gabriel design, 2D-200X). This gas-filled proportional type detector offers a 200 mm diameter active area with ca. 200 micron resolution. After radial integration, the scattered intensities were obtained as a function of momentum transfer q. Reciprocal space calibration was done using silver behenate as standard. The sample to detector distance was 0.5 m, covering a Q-range between 0.05 $Å^{-1}$ and 0.80 $Å^{-1}$. The measurements as a function of temperature were performed by means of a Linkam Scientific Instruments THMS600 temperature controller. This setup allows measurements in the range from 77 K to 873 K with temperature stability 0.1 K.

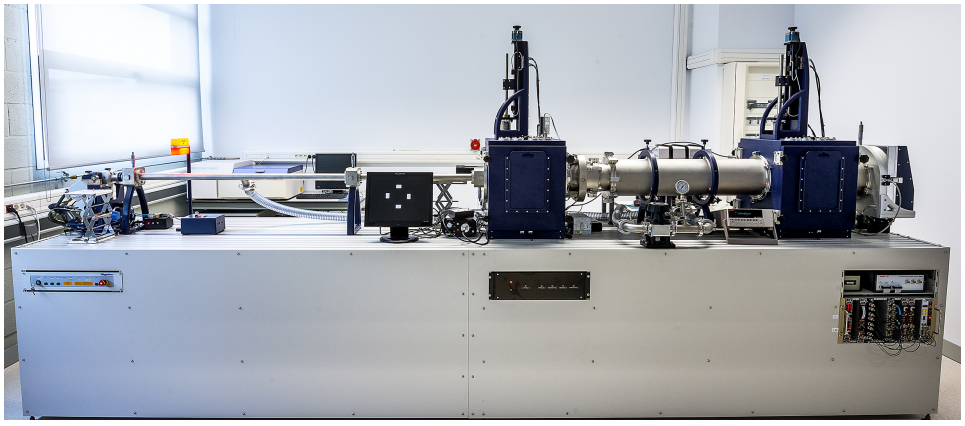

Figure 3.2: Rigaku 3-pinhole PSAXS-L equipment

WAXS measurements were performed on a Bruker D8 Advance diffractometer (see Figure 3.3a) working in parallel beam geometry. With the help of a Göbel mirror, the originally divergent incident X-ray beam from line

focus X-ray tube (Cu, operating at 40 kV and 40 mA) is transformed into an intense and parallel beam that is free of K_β radiation. The parallel beam optic required in the secondary beam path is achieved by an equatorial axial Soller slit of 0.2°. The linear detector LYNXEYE used presents an active area of 14.4 mm x 16 mm.

(a) Bruker D8 Discover diffractometer (b) Instrument optics

Figure 3.3: WAXS Instrument setup

3.2 Infrared spectroscopy

Infrared spectroscopy is a technique based on the absorption of light due to vibrations of the atoms of a molecule. Essentially, an infrared spectrum is commonly obtained by passing infrared radiation through a sample and quantifying what fraction of incident radiation is absorbed at a particular energy. The energy at which any peak in absorption spectrum appears corresponds to the frequency of vibration of a part of a sample molecule.

3.2.1 Infrared Absorption

In the infrared range, the light absorption mechanism is dominated by transitions between vibration energy levels in the ground state, which arise from the various modes of vibration of the molecule (i.e., stretching and bending of various covalent bonds). Two main quantities relevant to determine the frequency of vibrational modes are the stiffness of the bond and the masses of the atoms at each end of the bond. The stiffness of the bond can be characterized by the proportionality constant between force and displacement, k (derived from Hooke's law). The reduced mass, $m_{1,2}$, provides the equivalent mass oscillating during the vibration and is given by:

$$m_{1,2} = \frac{m_1 m_2}{m_1 + m_1} \tag{3.10}$$

where m_1 and m_2 correspond to the masses of the atoms at the ends of the bond. The equation relating the force constant, the reduced mass and the frequency of absorption is:

$$\nu = \left(\frac{1}{2\pi}\right)\sqrt{\frac{k}{m_{1,2}}} \tag{3.11}$$

This equation may be modified so that direct use of the wavenumber values for bond vibrational frequencies can be made, namely:

$$\frac{1}{\lambda} = \tilde{\nu} = \frac{\nu}{c} = \left(\frac{1}{2\pi c}\right)\sqrt{\frac{k}{m_{1,2}}} \tag{3.12}$$

where c correspond to the speed of light in vacuum. A molecule can only absorb radiation when incoming infrared radiation is of the same frequency as one of the fundamental modes of vibration of the molecule. Vibrations can involve either a change in bond length (stretching) or bond angle (bending). Some bonds can stretch in-phase (symmetrical stretching) or out of phase (asymmetric stretching). There will be many different vibrations for even fairly simple molecules. The complexity of an infrared spectrum arises from the coupling of vibrations over a large part of or over the complete molecule. Such vibrations are called skeletal vibrations. Bands associated with skeletal vibrations are likely to conform to a patter or fingerprint of the molecule as a whole, rather than a specific group within the molecule.

3.2.2 Dipolar selection Rules

For a molecule to show infrared absorptions it must possess a specific feature, that is, an electric dipole moment of the molecule must change during the vibration. In a simple approach this is the selection rule for infrared spectroscopy. In Figure 3.4 an illustration of an "infrared-active" molecule is given, it shows a diatomic molecule with different nucleus. The dipole moment of such molecules will change as the bond expands and contracts. In contrast, also an example of a "none infrared-active" molecule will be a diatomic molecule with the same nuclei; due to the fact that its dipole moment remains zero no matter how long the bond contracts or expand [55].

3.2.3 Fourier Transform Infrared Spectroscopy

Fourier transform infrared spectroscopy (FTIR) is an alternative measurement technique where, instead of recording the amount of energy absorbed at each frequency, this infrared light is guided through an interferometer.

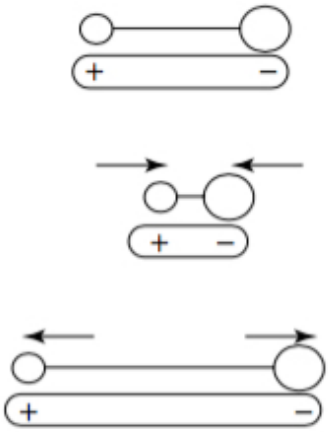

Figure 3.4: Illustration of an "infrared-active" molecule, a diatomic molecule with different nucleus

The operating principle of the FT-IR instrument is described as follows. To collect an IR spectrum the instrument uses a system called an interferometer. The interferometer arrangement consists of a source, a beam-splitter, two mirrors, a laser and a detector. Briefly, the energy goes from the broadband source to the beam-splitter which splits the beam into two parts. One part is transmitted to a moving mirror; one part is reflected to a fixed mirror. The moving mirror moves back and forth at a constant velocity. This velocity is timed according to the very precise laser wavelength in the system, which also acts as an internal wavelength calibration. The two beams are reflected from the mirrors and recombined at the beam-splitter. The beam from the moving mirror has travelled a different distance than the beam from the fixed mirror. When the beams are combined an interference patter is created, since some of the wavelengths recombine constructively. This interference pattern is called an interferogram. This interferogram then goes from the beam-splitter to the sample, where some energy is absorbed and some is transmitted. The transmitted portion reaches the detector. The detector reads information about all wavelengths in the infrared range simultaneously as a function of the position of the moving mirror producing the interferogram. To obtain the infrared spectrum, the signals are sent to the computer and by means of Fourier transformation of the interferogram it is converted into the so-called "single beam spectrum". A reference or background single beam is also collected without a sample, and the sample IR spectrum is obtained by taking the ratio with its background. The output signal will give sample transmittance (or % T spectrum). This transmittance spectrum can be converted to absorbance by taking the negative $log10$ of the data points.

3.2.4 Attenuated Total Reflection Infrared Spectroscopy

Attenuated total reflection infrared spectroscopy (IR-ATR) is a technique used in conjunction with infrared spectroscopy that enables samples to be examined directly in the solid or liquid state without further preparation. ATR uses the optical property of total internal reflection. Most modern infrared spectrometers can be converted to characterize samples via ATR by mounting the ATR accessory in the spectrometer sample compartment. Infrared spectroscopy by ATR is applicable to the same chemical or biological systems as the transmission method. One advantage of ATR-IR over transmission-IR, is the limited path length into the sample. This avoids the problem of strong attenuation of the IR signal in highly absorbing media, such as aqueous solutions or polymeric materials.

3.2.5 Infrared spectroscopy Instrument setup

The Jasco FT/IR-6300 instrument (see Figure 3.5) offers a high level of resolution and a high signal-to-noise ratio. It is designed for a wide range of important research and development applications. Depending on its accessories it is capable of measuring from the Near IR (15000 cm^{-1}) to the Far IR (50 cm^{-1}). Particularly, the wave number working range can be extended to cover Near to Far-IR applications by switching various optical components, i.e., light source, beam splitters, and detector. The resolution limit is 0.07 cm^{-1} and the signal to noise ratio is 50000 : 1 (1 min with 4 cm^{-1} resolution at around 2200 cm^{-1} wavenumber).

Moreover, the FT/IR-6300 includes the "Rapid Scan" (20 Hz) feature as standard. The Rapid Scan system enables the instrument to perform up to 20 scans per second providing real-time analysis of reaction kinetics. Also Step scan and full vacuum options are also available. Step Scan FT-IR spectroscopy offers the capability to obtain rapid time-resolved infrared measurements. The time-resolved Step Scan FT-IR technique involves displacing the moveable mirror of the interferometer in a step-wise manner.

(a) Jasco FT/IR-6000 series spectrometer (b) Optical scheme

Figure 3.5: FTIR Instrument setup

In this thesis, infrared spectra were measured with a FTIR Jasco 6300

spectrometer. An ATR accessory equipped with a diamond crystal (Specac golden-gate technologies) was used for sampling. The spectra were recorded in the region of $4000 - 400$ cm^{-1}, detector TGS, apodization Cosine. The spectral data were processed with JASCO SpectraManager II software. Samples were scanned at 4 cm^{-1} resolution, accumulation: 100 scans.

3.3 Thermal Analysis

Thermal methods of investigation normally referred to as thermo- or thermal analysis or thermo-analytical techniques, are techniques extensively used in research of polymeric materials. In such techniques the properties of materials are studied as they change with temperature. Several methods are commonly used and these are distinguished from one another by the property that is measured. Two principal methods commonly used are; Thermogravimetric Analysis (TGA), in which changes in weight are measured as a function of increasing temperature, and Differential Scanning Calorimetry (DSC), in which changes in "heat content" are measured as a function of increasing or decreasing temperature. Other methods that come within this definition involve the use of changes in sample dimensions (dilatometry); changes in electrical resistance; changes in mechanical properties, etc [56].

3.3.1 Differential Scanning Calorimetry

Normally "Calorimetry" is referred as the measurement of heat changes in a substance as the temperature is varied. In a calorimeter in which the sample is held at constant volume, changes in internal energy are detected. If the pressure is constant, then enthalpy changes are measured. In the latter experiment phase transitions are characterized by finite enthalpy changes -if they are first order- or by changes in the gradient of enthalpy with temperature -if they are second order (see Figure 3.6)-. Differential Scanning Calorimetry is a thermo-analytical technique in which the necessary amount of heat required to establish a nearly zero temperature difference between a substance and an inert reference material is measured, as the two specimens are subjected to identical temperature regimes at a controlled cooling or heating rate. The reference sample has a well-defined heat capacity over the range of temperatures of scanning. The main application of DSC is the study of phase transitions because they involve energy changes or heat capacity changes that can be detected by this technique. Thus, DSC provides insight into the different degrees of freedom as well of the general thermodynamical behavior of the materials under study. As previously mentioned, in particular for polymeric materials two main types of transitions are present, with a characteristic temperature associated to the distinct processes: the melting / crystallization and the glass liquid transformation. The melting

temperature is the temperature where the crystalline domains of a sample melt.The glass transition temperature is the temperature at which the material goes from a glassy state (disordered solid) to a rubbery/viscous-liquid state, and it can be associated to the ability of the polymer segments to move. Changes in properties such as specific volume and heat capacity occur as a polymer undergoes each of the thermal transitions. Figure 3.6 taken from Ref. [57], shows the changes in specific volume with temperature for a simple liquid (SL) and a glass forming liquid (GFL).

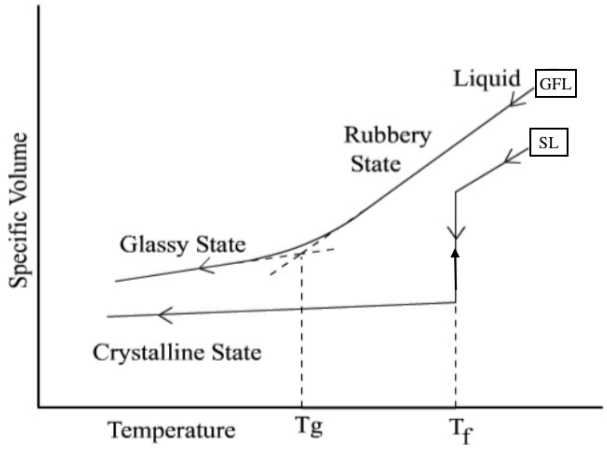

Figure 3.6: Schematic representations of glass transition and melting processes

The melting process is a first-order transition with a discontinuous change in the specific volume at the transition temperature. The glass transition temperature involves only a change in the temperature coefficient (a plot of the temperature coefficient of the specific volume vs. temperature shows a step).

3.3.2 Modulated Differential Scanning Calorimetry

In a standard DSC experiment, measurements of the difference in the heat-flow rate, between a sample and an inert reference are performed as the sample is heated, cooled or held at an isothermal temperature making use of a heating/cooling linear profile. Modulated differential scanning calorimetry (MDSC) is an improved technique in which an oscillating heat profile is applied to the sample superimposed with the traditional linear heat profile. The linear heating rate will give us similar information as the one obtained by standard DSC, and the sinusoidal (modulated) heating rate will allow the simultaneous measurement of the sample's heat capacity giving us extra information about the thermal processes in the sample. In MDSC temperature varies non-linear and is given by the following equation:

$$T(t) = T_0 + \beta t + A_t sin(\omega t) \tag{3.13}$$

where T_0 is the starting temperature, t is the time,β is the linear heating rate, A_t is the amplitude of temperature modulation and ω is the modulation frequency. Thus, the heating rate in equation, will be:

$$\frac{\mathrm{d}T}{\mathrm{d}t} = \beta + A_t \omega cos(\omega t) \tag{3.14}$$

which is not constant. Thus MDSC combines high resolution and sensitivity in the same experiment. Due to this additional alternating heat profile applied to the sample MDSC can separate the reversing and non-reversing components of the heat flow signal. In other words MDSC separates at least partially the thermodynamic component of the total heat flow signal (reversing component) from its kinetic component (non-reversing component). To perform this separation the heat flow signal is given by:

$$\frac{dH}{dt} = C_p \frac{dT}{dt} + f(T,t) \tag{3.15}$$

where $\frac{dH}{dt}$ is the Total (average) Heat Flow due to the linear heating rate. It is equivalent to standard DSC at the same average heating rate. C_p is the heat capacity component of the Total Heat Flow and is calculated from just the heat flow that responds to the modulated heating rate, i.e., $C_p = \frac{A_{HF}}{A_{HR}}$, where A_{HF} and A_{HR} are the amplitudes of the Heat Flow oscillations and Heating Rate oscillations respectively. $\frac{dT}{dt}$ corresponds to the measured heating rate, which has both a linear and a sinusoidal (modulated) components. The function $f(T,t)$ corresponds to the Kinetic component of the Total Heat Flow and is calculated from the difference between the Total signal and the Heat capacity component. In this sense $C_p \frac{dT}{dt}$ gives the Reversing Heat flow Component of the Total Heat Flow. The quality of the modulated experiment depends on the selected parameters defining the modulated temperature profile (A_t, ω, β)

MDSC measures neither reversibility nor non-reversibility of transitions. The term "Reversing" was chosen because true heat capacity (heat associated with increasing or decreasing a materials temperature) is reversible. However, a heat capacity change during a transition is almost never reversible. While a transition in the Reversing signal is associated with a heat capacity change, it may or may not be reversible. Traditional DSC provides a single signal $\left(\frac{dH}{dt}\right)$ that is the sum of all thermal events occurring at a specific temperature or time during the experiment. This often causes difficulty in detection of small transitions or in data interpretation. MDSC improves upon traditional DSC since it measures the Total Heat Flow plus its Heat Capacity Component and obtains the Kinetic Component from their dif-

ference. Its ability to resolve complex transitions into specific components improves data interpretation [58].

3.3.3 DSC Instrument setup

The TA Instruments Q2000 (see Figure 3.7a) is a research-grade differential scanning calorimeter with great performance in baseline flatness, precision, sensitivity, and resolution. The Advanced Tzero technology and multiple exclusive hardware and software features make the instrument powerful, flexible, and easy-to-use. Moreover, modulated DSC technology and a reliable 50-position auto sampler are also available.

The Tzero cell (see Figure 3.7b) provides fast signal response, flat and reproducible baselines, and high sensitivity-resolution, and data precision. A chromel/constant an Tzero thermocouple is located symmetrically between the sample and reference sensor platforms, and acts as an independent measurement and furnace control sensor. Matched chromel area thermocouples are welded to the underside of each sensor platform, providing independent sample and reference heat flow measurements. Sample cell thermal characteristics are determined by means of a calibration process involving measurements of the empty cell and standard sapphire samples.

High quality DSC experiments require precise purge gas flow rates. Mass flow controllers, along with integrated gas switching, provide flexible control as part of individual methods. Purge gas flow rates can be set from $0 - 240$ mL/min in increments of 1 mL/min. The system is precalibrated for common gases. A Liquid Nitrogen Cooling System (LNCS) provides high performance and great flexibility. It has the lowest operational temperature (to -180 °C), greatest cooling rate capacity (to 140 °C/min), and an upper temperature limit of 550 °C.

(a) TA instruments Q2000 calorimeter (b) Instrument Tzero cell

Figure 3.7: DSC Instrument setup

In this thesis, DSC calorimetric measurements were carried out using a Q2000 from TA Instruments (a gas flow (He) of 25 mL/min was used for

thermalization). The samples were prepared by encapsulating $5-10$ mg of the different polymeric materials in an aluminium pan. The sample pan was inserted in the instrument holder.

3.4 Broadband Dielectric Spectroscopy

As already described for IR absorption, the interaction of Electromagnetic waves (EM) radiation with molecular systems give rise to quantized transitions between the electronic, vibrational and rotational molecular energy states usually at frequencies above and about 1 THz (10^{12} Hz). If we wish to understand what happens when EM radiation in the range of 10^{-6} to 10^{12} Hz interacts with molecular systems, we must consider the concept of dielectric relaxation. In this vast frequency range several phenomena occurs related with; first dipole relaxation arising from the translational-rotational motions of molecular dipoles, and second the electrical conduction arising from translational motions of charges carriers. Exploring this range is what is known as Broadband Dielectric Spectroscopy. In this section we give a general overview on the theoretical background of electric polarization summarizing some relevant phenomena, for detailed information see Ref. [40].

3.4.1 Interaction of electromagnetic waves with matter

The interaction of electromagnetic fields with matter is described by Maxwell's equations

$$rot\mathbf{E} = -\frac{\partial}{\partial t}\mathbf{B} \tag{3.16}$$

$$rot\mathbf{H} = \mathbf{j} - \frac{\partial}{\partial t}\mathbf{D} \tag{3.17}$$

$$div\mathbf{D} = \rho_e \tag{3.18}$$

$$div\mathbf{B} = 0 \tag{3.19}$$

In this set of equations $\mathbf{E}$ and $\mathbf{H}$ describe the electric and magnetic field, $\mathbf{D}$ the electric displacement, $\mathbf{B}$ the magnetic induction, $\mathbf{j}$ the current density and ρ_e, the density of charges. For small electric field strengths (linear response) $\mathbf{D}$ can be expressed by

$$\mathbf{D} = \varepsilon_0 \varepsilon^* \mathbf{E} \tag{3.20}$$

where ε_0 is the dielectric permittivity of vacuum. ε^* is the complex dielectric function or dielectric permittivity. According to Maxwell's equations ε^* is time (or frequency) dependent if time dependent processes take place within the sample.

3.4.2 Electric polarization and Relaxation phenomena

Electric polarization phenomena refer to the relative displacement of electrical charges caused by an external electric field. It includes very fast displacements of negative and positive charges of atom or molecules, much slower orientation of permanent dipoles toward the direction of the field, and trapping of mobile charge carriers at the interfaces of impurities or other defect boundaries. Relaxation phenomena are related to these slower polarization processes. In general, time dependent processes within a material lead to a difference of the time dependencies of the outer electrical field $\mathbf{E}(t)$ and the resulting dielectric displacement $\mathbf{D}(t)$. For a simple periodic electrical field $\mathbf{E}(t) = \mathbf{E}_0\ exp(-i\omega t)$, (where ω is the angular frequency, $i = \sqrt{-1}$) the complex dielectric function is expressed as:

$$\varepsilon^*(\omega) = \varepsilon^{'}(\omega) - i\varepsilon^{''}(\omega) \tag{3.21}$$

where $\varepsilon^{'}(\omega)$ is the real part and $\varepsilon^{''}(\omega)$ the imaginary part of the complex dielectric function. In the stationary case, which will only be considered here, the difference of the time dependencies of $\mathbf{E}(t)$ and $\mathbf{D}(t)$ is a phase shift, $\mathbf{E}(t) = \mathbf{E}_0\ exp(-i\omega t + \delta)$. The ratio $\left(\frac{\varepsilon^{''}}{\varepsilon^{'}}\right) = tan\delta$, where δ is the phase shift between $\mathbf{D}$ and $\mathbf{E}$. The corresponding function to $\varepsilon^*(\omega)$ in the time domain is the time dependent dielectric function $\varepsilon(t)$.

The polarization $\mathbf{P}$ describes only the electric displacement vector ($\mathbf{D}$) that originates from the response of a material to the external field. Hence it is defined as

$$\mathbf{P} = (\varepsilon^* - 1)\,\varepsilon_0\mathbf{E} = \chi^*\varepsilon_0\mathbf{E} \tag{3.22}$$

where χ^* is the dielectric susceptibility of the material; $\chi^* = (\varepsilon^* - 1)$. Similar to Ohms law the following relation can be established between the current density $\mathbf{j}$ and the electric field:

$$\mathbf{j} = \sigma^*\mathbf{E} \tag{3.23}$$

where $\sigma^* = \sigma^{'}(\omega) + i\sigma^{''}(\omega)$ is the complex conductivity. $\sigma^{'}$ and $\sigma^{''}$ are the corresponding real and imaginary parts. Because the current density and the time derivative of the electric displacement vector are equivalent quantities according to eq. 3.17 and eq. 3.20 it holds

$$\sigma^* = i\omega\varepsilon_0\varepsilon^* \tag{3.24}$$

In general a macroscopic polarization $\mathbf{P}$ can be related to microscopic dipole moments $\mathbf{p}_i$ of the molecules or particles within a volume V by

$$\mathbf{P} = \frac{1}{V}\sum \mathbf{p}_i \tag{3.25}$$

where, i, counts all dipole moments in the system. Molecules or particles have a dipole moment if the electric centres of gravity of positive and negative charges do not match. The simplest case is given by a positive charge $+q$ and a negative one $-q$ being separated by a distance d with dipole moment $\mathbf{p} = q\mathbf{d}$. The microscopic dipole moments can have a permanent or induced character. The latter is caused by the local electrical field $\mathbf{E}_{loc}$, which distorts a neutral distribution of charges. In the linear case $\mathbf{p} = \alpha\mathbf{E}_{loc}$ holds where the polarizability α is a measure of the mobility of negative and positive charges. One example of induced polarization is the electronic polarization where the negative electron cloud of an atom (molecules) is shifted with respect to the positive nucleus. Electronic polarization takes place on a time scale of 10^{-12} s because of the low mass of the electron. Atomic polarization can take place at a slightly longer time scale (infrared frequencies). All these contributions can be summarized by an induced polarization $\mathbf{P}_\infty$ that responds nearly instantaneously to the applied electric field variations. Many molecules have a permanent dipole moment $\boldsymbol{\mu}$ that can be oriented by an electrical field. Hence for a system containing only one kind of dipoles we obtain that;

$$\mathbf{P} = \frac{1}{V}\sum \mathbf{p}_i + \mathbf{P}_\infty = \frac{N}{V}\langle\boldsymbol{\mu}\rangle + \mathbf{P}_\infty \tag{3.26}$$

where N denotes the whole number of dipoles in the system and $\langle\boldsymbol{\mu}\rangle$ the mean dipole moment. In general the mean value of the dipole moments is determined by different factors, the contributions to polarization from this part are called orientational polarization. Assuming that inertia effects contribute only to $\mathbf{P}_\infty$ the main factors are the interaction of dipoles and the strength of the electric field at the location of the dipole.

3.4.3 Theoretical models

For an alternating voltage of very high frequency, permanent molecular dipoles cannot follow the variation of the electric field and the measured dielectric permittivity will be essentially determined by the induced atomic and electronic material polarization $\mathbf{P}_\infty$. When the frequency decreases, molecular dipoles try to follow the direction of the electric field. The degree of orientation increases when the frequency decreases, so the dielectric permittivity will increase. At low enough frequencies, molecular dipoles can follow the electric field and a plateau of the dielectric permittivity (static value) will be observed. Neglecting inertia effect the simplest ansatz to calculate the time dependence of the dielectric behavior is the assumption that the change of the polarization is proportional to its actual value (first order differential equation). This model is named Debye relaxation, and the equations that describe the model are written as follow

$$\frac{\mathrm{d}\mathbf{P}(t)}{\mathrm{d}t} = -\frac{1}{\tau_D}\mathbf{P}(t) \tag{3.27}$$

where τ_D is a characteristic relaxation time. Equation (3.27) leads to an exponential decay for the correlation function $\phi(t)$

$$\phi(t) = exp\left(-\frac{1}{\tau_D}\right) \tag{3.28}$$

In section **??**, it was already shown that the corresponding complex dielectric function $\varepsilon^*(\omega)$ is given by:

$$\varepsilon^*(\omega) = \varepsilon_\infty + \frac{\Delta\varepsilon}{1+i\omega\tau_D} = \varepsilon_\infty + \Delta\varepsilon\left[\frac{1}{1+i\omega^2\tau_D^2} - \frac{i\omega\tau_D}{1+i\omega^2\tau_D^2}\right] \tag{3.29}$$

where the real part of the dielectric function is related to the stored energy, and the imaginary part is the imaginary part of the dielectric function (also named dielectric losses) is related to the dissipation of energy. In the Debye case the dielectric losses are characterized by a symmetric peak (in $log(\omega)$ scale) with the maximum centered at $\omega = 1/\tau_D$, with a full with at half maximum of about 1.14 decades, and a ε'' peak value of $\Delta\varepsilon/2$. On the other hand the real part of the dielectric function is characterized by a step like function with an inflection point at $\omega = 1/\tau_D$. Only in rare cases Debye-like relaxation behavior according to above equations is observed. Usually the measured dielectric functions are much broader than predicted by the Debye function. Moreover, in many cases the dielectric function is asymmetric. That means that short time (high frequency) tail is more pronounced than the long time (low frequency) one. This type of non-Debye relaxation in the time domain is empirically described by the Kohlraush/Williams/Watts-function (KWW-function), which reads

$$\phi(\tau) = exp\left[-\left(\frac{t}{\tau_{KWW}}\right)^{\beta_{KWW}}\right] \tag{3.30}$$

In the frequency domain the data are often described by the empirical function of Havriliak and Negami

$$\varepsilon^*_{HN}(\omega) = \varepsilon_\infty + \frac{\Delta\varepsilon}{(1+(i\omega\tau_{HN})^\alpha)^\gamma} \tag{3.31}$$

The fractional shape parameters α and γ, with $0 < \alpha, \alpha\cdot\gamma \leq 1$, describe the symmetric and asymmetric broadening of the complex dielectric function. In general de non-Debye character of the experimental curves can be described (at least mathematically) as a continuous superposition of Debye components with different relaxation times.

3.4.4 Measurements in the Frequency Domain

Dielectric spectroscopy is one of the so-called relaxation techniques. In a simple way, dielectric relaxation technique consists of applying an external field to the system perturbing slightly the equilibrium. Once the field is removed the system will turn back to the previous equilibrium providing information about the dynamics of the system. Specifically, BDS technique consists on the study of the frequency dependent complex dielectric permittivity of insulator materials. In this way, the reorientation of the permanent molecular dipoles is detected. For a capacitor C^* filled with a material under research the complex dielectric function is calculated by

$$\varepsilon^*(\omega) = \varepsilon^{'}(\omega) - i\varepsilon^{''}(\omega) = \frac{C^*(\omega)}{C_0} \tag{3.32}$$

where C_0 is the vacuum capacitance of the arrangement and C^* the complex capacitance of the filled capacitor. Using a sinusoidal electric field $E^*(\omega) = E_0 exp(i\omega\tau)$ with the angular frequency ω and at field strengths within linear response the dielectric function, $\varepsilon^{''}(\omega)$(omega) can be derived by measuring the complex impedance $Z^*(\omega)$ of the sample capacitor, which is directly related with the sample capacitance

$$\varepsilon^*(\omega) = \frac{C^*(\omega)}{C_0} = \frac{1}{i\omega Z^*(\omega) C_0} = \frac{J^*(\omega)}{i\omega\varepsilon_0 E^*(\omega)} \tag{3.33}$$

where $J^*(\omega)$ is the complex current density and ε_0 the permittivity of free space. Therefore, by measuring the electric field (voltage applied to the capacitor) and the complex current density (current across the capacitor) one can obtain the dielectric function.

3.4.5 Dielectric Spectroscopy Instrument setup

Novocontrol Alpha-A modular measurement system (see Figure 3.8) features high performance dielectric, conductivity, electrochemical, impedance and gain phase measurements in the frequency domain. The system is modular and based on an Alpha-A mainframe unit, it is usually combined with one or more test interfaces optimized for special functionality. Test interfaces for impedance measurement offer in addition high general-purpose performance like highest accuracy and ultra wide impedance and frequency range. Furthermore, the Alpha-A family covers 18 orders of magnitude impedance range (16 orders for each impedance test interface), 12.5 orders of magnitude frequency range and 2 m° basic phase accuracy. As a result, permittivity, conductivity and impedance of nearly all materials can be measured broadband and over a wide temperature range without changing sample geometry or sample cells.

Due to its extremely wide frequency range, the ALPHA-A is ideally suited to analyze both slow and fast relaxation and charge transport phenomena in materials. The DC resistance of a material, e.g., is usually extracted from the low frequency data, while molecular relaxations with relaxation times in the nanosecond regime require high frequency measurements. Glasses or polymers frequently show multiple relaxations that typically differ in their relaxation times. Coverage of a broad frequency bandwidth is thus a crucial feature of instruments used for the characterization of such phenomena. In a single instrument, the ALPHA-A covers frequencies from 1 mHz up to 10 MHz with an unlimited number of frequency points per sweep.

Temperature control is achieved by Quatro Cryosystem, which is a high quality temperature control system for applications in materials research. The system aims to set or change the temperature of the sample under test with high accuracy (±0.01 K) and reproducibility. The Quatro Cryosystem is designed to provide easy, safe and fully automatic operation, enabling computer-controlled long time experiments over several days without supervision. The principle of operation can be seen in Figure 3.8b and it is described as follows: A heating element builds up and controls a specified pressure in the liquid nitrogen Dewar vessel in order to create a highly constant nitrogen stream. The pressure and temperature in the Dewar vessel are measured by two channels of the Quatro controller. The nitrogen stream, heated to a temperature appropriate for the desired sample temperature, flows directly through the sample cell mounted in the cryostat. The gas and sample temperatures are measured by the two remaining channels of the Quatro controller. The four-channel design allows highly stable, fast and safe system operation.

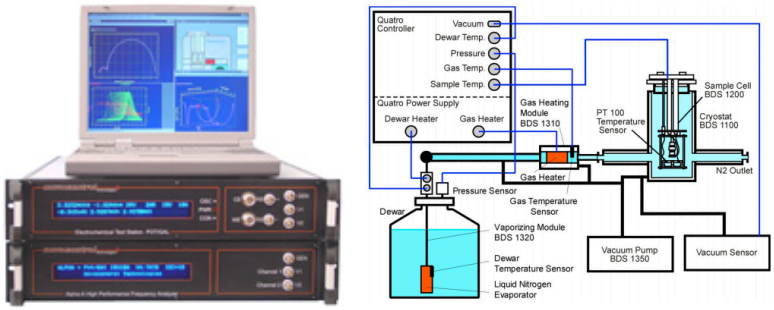

(a) Novocontrol Alpha-A modular instrument (b) Novocontrol Quatro modular instrument

Figure 3.8: BDS Instrument setup

Measurements of the complex dielectric permittivity vs. frequency were performed typically in the range $10^{-2} - 10^{7}$ Hz, using a Novocontrol high-resolution dielectric analyzer (Alpha-A). Moreover, specific measurements

ranging from $10^6 - 10^9$ Hz using a sample capacitor connected at the end of a coaxial line were also performed using an impedance analyzer (Agilent 4291B). The sample cells were set in the cryostat, and its temperature were controlled using the Quatro cryosystem.

Chapter 4

Self-assembly of a carboxyl-terminated DMS oligomer

"Block copolymers are all around us, found in such products as upholstery foam, adhesive tape and asphalt additives. This class of macromolecules is produced by joining two or more chemically distinct polymer blocks, each a linear series of identical monomers, that may be thermodynamically incompatible (like oil and vinegar)."

Frank S. Bates and Glenn H. Fredrickson

Abstract: In the first section of this chapter we will present the results of thermal and structural characterisation of carboxyl terminated dimethylsiloxane co-oligomer (ODMS-COOH) in comparison with a reference dimethyl siloxane oligomer (ODMS). To get insight on the thermodynamic properties differential scanning calorimetry (DSC) measurements were performed. Moreover, by making use of scattering methods, such as: small angle X-ray scattering (SAXS) and wide angle X-ray scattering (WAXS), and combined with ATR Fourier transform infrared spectroscopy (FTIR) we were able to access to the main structural features of the samples. Additionally a different "end-chain" functionalization of the ODMS co-oligomer (ODMS-$COOCH_3$) was investigated to validate the structural interpretation. In the second section of the chapter we will explore how the DMS dynamics as detected by dielectric spectroscopy (DS) is affected by the distinct structural constrains.

4.1 ODMS-R Introduction

Most of advanced materials used now days in state of the art technological applications are multi-component or/and nano-structured systems [59, 60]. Due to their technological relevance considerable efforts are being done in the quest for obtaining methods that enable the preparation of such materials with tuneable physical and chemical properties.

In this direction, a simple approach to obtain these desired materials, is by making use of physical blends of polymer constituents. Among the different polymer constituents that can be used, block copolymers are well-known by their ability to self-assemble into a wide variety of morphologies either in bulk (lamellas, gyriods, cylinders, spheres, etc.) or in solution (spherical micelles, vesicles, cylinders, etc.). Additionally, the shape and size of self-organized morphologies can be suitably controlled through a number of factors, such as the relative block lengths, the chemical nature of the blocks, and the type of solvent for the solution preparation [61]. Furthermore, they form a collection of elementary building blocks for the precise construction of advanced materials via bottom-up, atom- and energy-efficient approaches [62]. Moreover, certain type of block copolymers can be considered as associating polymers. They consists of a relatively new class of materials generically defined as "arrays of monomeric units that are held together by highly directional and reversible non covalent interactions" [63]. The structural reversibility caused by transient nature of secondary interactions renders supramolecular polymers as promising materials with unique properties.

In nanostructured materials, "confinement effects" at molecular level (topological constrains, interface interactions, etc.) emerge in a natural way, giving rise to changes that will affect both the structure and dynamics as well as the macroscopic properties of the material. These materials usually exhibit dynamic heterogeneities at the molecular level, i.e., different mobility's associated to the distinct components. Particularly, several studies found in the literature [64, 65, 66, 67, 68, 15, 69, 70, 17] report confinement-related effects on the segmental dynamics of the block copolymers. In general, all these studies report a relatively minor but noticeable effect of the nanostructure on the component segmental dynamics. The effects are highlighted when the size of the segregated phase is reduced to about 10 nanometre, and in fact, most of the results have been interpreted as originated at the interface (a few nanometers thick) [15, 69]. Therefore, in nano-structured materials of a few nanometers length these effects are expected to be large, leading to a bigger variation on the components dynamical properties. Usual confinement lengths in block copolymers are about a few tens nanometers. The structural lengths are determined by block sizes, whereas the segregation quality is controlled by the the product, χN see Figure 2.7a, which imposes a limit to the smallest structural lengths that can be achieved. Thus it is

desirable to look for materials that present phases with even smaller confinement length. Here we show that a way to obtain nano-structured materials of a few nanometers length is making use of functionalized oligomers (a functionalized oligomer can be thought as a block co-polymer with small length components, and therefore they will be referred as block co-oligomers). In this way it has been possible to obtain such well segregated nanostructure with structural lengths below 10 nanometers. Therefore, this approach allowed us to explore the confinement effects on the dynamics for this very small length scales.

4.2 Samples and Experimental Details

4.2.1 Samples

In this part of the thesis we will study the structural and dynamical properties of three different oligomer samples with distinct end-chain terminations. The first one, monocarboxydecyl terminated polydimethylsiloxane was prepared by living anionic polymerization of hexamethyl cyclotrisiloxane (supplied by Polymer Source, Inc.) and was used as delivered. The resulting co-oligomer structure is:

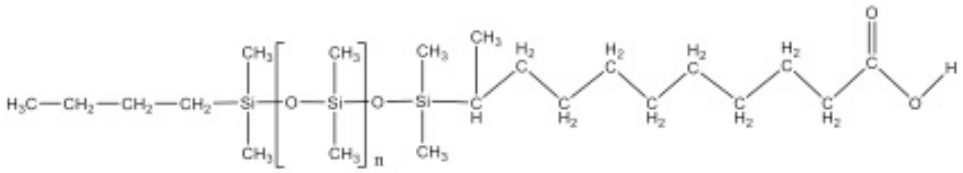

Figure 4.1: ODMS-COOH chemical formula

Having weight average molecular weight (Mw) of 1300 g/mol and polydispersity ratio (Mw/Mn) of 1.3; implying values of n about 13 ± 3. The material is a viscous liquid at room temperature.

This compound can be seen as a block-copolymer with a relatively large DMS block and a smaller aliphatic component with a carboxylic acid ending group. For simplicity, the distinct dimethylsiloxane co-oligomer samples used in this thesis will be referred as ODMS-R co-oligomers (where R corresponds to the different end-group termination). In particular monocarboxydecyl terminated oligodimethylsiloxane will be referred as ODMS-COOH.

For comparison, a low molecular weight oligodimethylsiloxane (ODMS) reference sample (also supplied by Polymer Source, Inc.) with weight average molecular weight (Mw) of 1500 g/mol and polydispersity ratio (Mw/Mn) of 1.25 ,(n about 18 ± 4), was also characterized. The structure of this sample is:

The third oligomer sample, referred as ODMS-$COOCH_3$, was obtained in

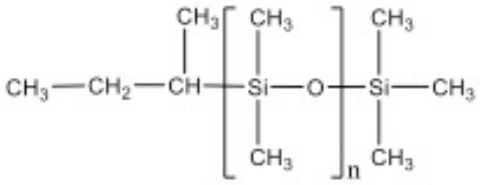

Figure 4.2: ODMS chemical formula

our laboratories by modifying the monocarboxyl terminated polydimethylsiloxane following the procedure described in Ref. [71] obtaining the following structure:

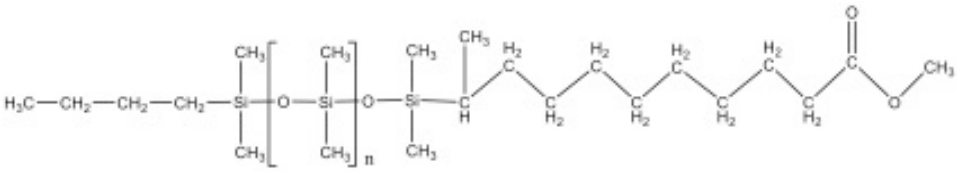

Figure 4.3: ODMS-$COOCH_3$ chemical formula

In short, the procedure started dissolving 1.33 g (1.04 mmoles) of ODMS-COOH win 64 ml of a mixture toluene:methanol (9 : 1 volume:volume) and 2.56 ml of a 2.0 M solution of trimethylsilyldiazomethane (5.12 mmoles) was added. The mixture was allowed to react in a loosely capped vial for 30 minutes at room temperature, allowing the nitrogen gas formed during the reaction to scape. Excess reagent was eliminated by adding approximately 320 microliters ($\approx$ 5.6 mmoles) of acetic acid and allowing the mixture to stand for 30 minutes at room temperature. The sample compound was purified by rotary evaporation of the solvents at 330 K. As the other DMS based samples, the system is a viscous liquid at room temperature.

4.2.2 Experimental Details

4.2.2.1 Differential Scanning Calorimetry (DSC)

Modulated differential scanning calorimetric measurements were carried out using the Q2000 calorimeter form TA instruments, previously described. The samples were prepared by encapsulating $5 - 10$ mg of the liquid material in hermetic aluminium pans. The sample pan was inserted in the instrument holder and let it cool at a fast rate down to 100 K. The calorimetric results were obtained by temperature modulated experiments while heating from 100 K to 300 K, and cooling back to 100 K at the same rate and finally heating back to 300 K. In the experimental protocol we used an average heating/cooling rate of 3 K/min, with 60 s period oscillation and 0.5 K temperature amplitude.

4.2.2.2 Small Angle X-ray Scattering (SAXS)

SAXS diffraction experiments were performed on the Rigaku PSAXS-L equipment described above. The scattered intensities are represented as a function of the momentum transfer q. Reciprocal space calibration was done using silver behenate as a standard. The sample to detector distance was 2 m, covering a q range from $0.008 - 0.2$ Å^{-1}. The measurements as a function of temperature were performed by means of a Linkam Scientific Instruments THMS600 temperature controller from 150 K up to 300 K, in steps of every 10 K. The measuring time was 1 hr each temperature. The measurements were corrected (subtraction) for the very low-q scattering tail ($\approx q^{-4}$) likely due to voids and impurities in the samples.

4.2.2.3 Wide Angle X-ray Scattering (WAXS)

WAXS diffraction experiments were performed on a Bruker D8 discover diffractometer, described above, and the measurements were done in reflection mode varying the scattering angle 2θ from $5 - 30^\circ$ with a step of 0.05°. The counting time was 5 s/point. The sample were placed on a flat Si-111 waffer in an Anton Paar TTK 450 low-temperature chamber under vacuum conditions in the temperature range from 130 K to 300 K

4.2.2.4 Infrared Spectroscopy (ATR-FTIR)

ATR-FTIR measurements were carried out by means of the Jasco 6300 spectrometer, described above. IR spectra measurements were performed at room temperature, at about 220 K and at about 180 K. The spectra were obtained after 120 accumulations with 4 cm^{-1} resolution.

4.2.2.5 Broadband Dielectric Spectroscopy (BDS)

Broadband Dielectric Spectroscopy experiments were performed using a broad range of frequencies and temperatures. Data were acquired using two different instruments. For the lower frequency data a Broadband Dielectric Spectrometer (BDS) Alpha A Novocontrol was used, covering the range from 10^{-2} up to 10^7 Hz, over temperatures from 120 K up to 300 K (with stability better than $\pm$ 0.1 K). Higher frequency data were collected using a Agilent 4291B Impedance analyzer exploring a frequency range from 10^6 up to 10^9 Hz over a temperature range from 120 K up to 300 K.

In all cases the sample preparation was carried out by adding (by drop) about $50 - 100$ mg of sample over a gold plated electrode disk of 10 (high frequencies) and 30 (low frequencies) mm diameter. Moreover, an upper electrode of 10 and 20 mm (high/low frequencies) was placed on the previous prepared film over the gold-coated disk, and the separation of 0.1 mm between both electrodes was maintained by using a cross-shaped teflon spacer

of small area. The sample cell was set in a cryostat, and its temperature was controlled via nitrogen gas jet stream coupled with the Novocontrol quatro controller. The dielectric measurements of the samples were obtained, after a first fast cooling, isothermally from 120 K to 140 K in steps of 5 K, from 140 K to 170 K in steps of 2.5 K, from 170 K to 230 K in steps of 5 K. Then the sample was cooled back to 120 K at a rate of 3 K/min and finally heated again to 230 K with the same steps previously mentioned.

4.3 Results and Interpretation

In this section we will present the different results obtained in our experiments. To get insight on the thermodynamic properties of our samples we will start with modulated differential scanning calorimetry (DSC) results. We will continue the description of the results with those obtained by Scattering methods (small angle X-ray scattering and wide angle X-ray scattering), which are used to access the structural features of the samples. By FTIR we pursued a molecular level description of the entities involved in the main structural features. Finally, by dielectric relaxation techniques we will investigate the segmental dynamics of the ODMS nanosegregated phases.

4.3.1 Differential Scanning Calorimetry

DSC measurements allow us to study the thermodynamical behavior of the distinct samples under investigation. Our analysis starts with the identification and interpretation of different thermodynamic features of monocarboxyl terminated dimethylsiloxane co-oligomer (ODMS-COOH) present in the differential scanning calorimetric scans. In Figure 4.4 we show the total Heat flow as a function of temperature for ODMS-COOH sample compared with that of dimethylsiloxane oligomer (ODMS) reference. The temperature range explored, $130 - 300$ K, allowed us to have a complete description of the thermodynamic process occurring in the sample.

In Figure 4.4a we illustrate the heat flow curves corresponding to the first heating run and the subsequent cooling run at 3 K/min for the ODMS-COOH co-oligomer. When comparing heating and cooling runs a quite symmetric behavior is found. Figure 4.4b presents the heat flow curves obtained on quenched ODMS oligomer during two heating runs and one intermediate cooling run with a rate of 3 K/min. Here the different traces show clearly distinct behaviors. The first heating run (dark line) presents the most important thermodynamic processes taking place within the system, starting from low temperatures along the first heating curve we notice the characteristic glass transition step observed about 150 K. Higher in temperature along the curve we can observe a cold crystallization peak in the range of $170 - 180$ K, we also identify a complex melting process in the temperature

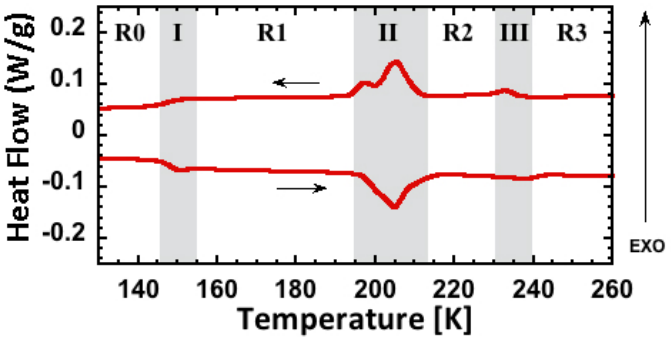

(a) DSC curves for the carboxyl terminated dimethylsiloxane co-oligomer (ODMS-COOH)

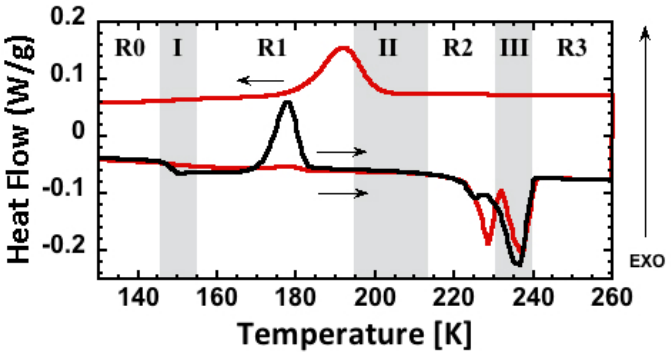

(b) DSC curves for pure dimethylsiloxane oligomer (ODMS). Black line corresponds to the heating curve of the material after quenching

Figure 4.4: DSC scans for two ODMS samples showing the heat flow as a function of temperature

range about 235 K. Moving on the description of the process happening on the cooling curve we see that it presents an exothermic peak about 190 K corresponding to the melt crystallization of the ODMS. The second heating curve obtained after the slow cooling rate mainly presents a new complex melting process taking place on the same region (235 K) as the melting process in the first heating run, now with a clear double-peak melting feature. The differences in the melting region should be associated to the different ways the crystalline material is obtained. In the first heating run crystallization occurs when heating a fully amorphous material (cold crystallization) before melting. Contrary, in the second heating run a previously crystallized material during cooling (melt-crystallization) is analyzed. In the former, the nucleation is favored and grow of the crystalline nucleus is limited. Contrary, during melt-crystallization fewer crystalline nuclei growing easily are formed.

If now we look back to Figure 4.4a in the heating curve, we can observe

that within the temperature range of I grey area (about 150 K) a step like jump in the heat flow takes place. We should notice that this step match well with that observed in the same area on the first heating run curve of Figure 4.4b, implying that the step correspond to the ODMS block glass transition in the co-oligomer. If we quantify the heat flow jump in ODMS-COOH we obtain a value (18 mW/g), which is not far from that calculated from the jump observed in ODMS (23 mW/g) affected by the weight fraction of DMS ($\approx$ 87%) in ODMS-COOH. These results suggest that only DMS, and essentially all the DMS segments, are involved in the process.

Moving to higher temperatures, in the II grey area ($195 - 210$ K) a melting-like process is observed. This process is directly related to the crystallization-like peak shown in the same temperature range on the cooling curve. Comparing the cooling curves of both Figure 4.4a and 4.4b, in the II grey area we notice that in the ODMS sample the crystallization takes place in a lower temperature range, which in addition of the above result on the glass transition region, provides evidence that in ODMS-COOH the observed crystallization-melting processes are hardly involving DMS units. The melting energetic contribution obtained for ODMS-COOH was about 11 J/g which taking into account the weight fraction of the functional part (13 %) would imply 85 J/g of the functional group. This value is about half of the melting energy of decanoic acid, which should be indicative of a partial crystallization of the aliphatic part and or a different crystalline form. The later is suggested by the much higher melting temperature of decanioc acid (305 K).

Increasing the temperature further we detect a small peak feature at $230 - 240$ K, identified as the III grey area. The small exothermic peak on the cooling curve and the corresponding weak melting process on the heating curve would indicate some sort of additional structural rearrangement. Comparing what is seen in this area to the one during cooling for the pure ODMS we notice that there is no evidence of any similar process. However, although reference ODMS melting occurs in this same temperature range the connection between both behaviors would be a coincidence, since no signs of DMS crystallization in ODMS-COOH exists (as will be confirmed below). The energy involved in these melting-like features was calculated to be of about 0.85 J/g or equivalently to 1.1 kJ/mol, which could suggest the possible relevance of hydrogen bonding in this transition (usual hydrogen bond energies are about $5 - 30$ kJ/mol).

The above results suggest that conventional ODMS crystallization is completely inhibited in ODMS-COOH co-oligomer but other different structural transitions take place, hardly involving DMS units. Moreover, Figure 4.4b gives us evidence that in the range between area I and area II there is a wide temperature interval where ODMS segments will move in an ordered environment, which would prevent DMS crystallization, which is actually

occurring in the reference ODMS sample.

To obtain detailed information about the structures responsible of the thermal features that are detected by means of DSC, X-ray scattering experiments will be helpful.

4.3.2 X-ray diffraction (SAXS and WAXS)

As noticed above, DSC results evidence three different temperature intervals where distinct thermodynamic processes occur in ODMS-COOH sample, which probably implies four different structural states corresponding to regions R0, R1, R2, and R3 respectively as identified in Figure 4.4. We start the structural analysis with the X-ray scattering data sensitive to short-range correlations, i.e., Wide Angle X-ray Scattering (WAXS).

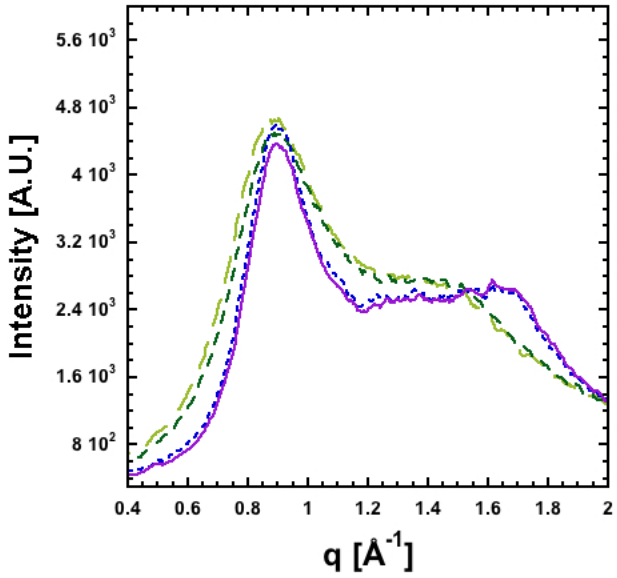

Figure 4.5: Wide angle X-ray scattering diffractograms for ODMS-COOH co-oligomer sample at four relevant temperatures: long-dashed line corresponds to measurements at 250 K, short-dashed to 220 K, doted line to 160 K and solid line to 130 K

The results obtained for the ODMS-COOH are shown in Figure 4.5. The diffractograms in the Figure show the scattered intensity, I [A.U.], as a function of the momentum transfer q, at four relevant temperatures, long-dashed line corresponds to measurements at 250 K, short-dashed to 220 K, doted line to 160 K and solid line to 130 K, each located within one of the regions defined above (R3, R2, R1, R0 respectively). These temperatures were selected in order to detect possible changes in the local order structure of the co-oligomer as we decrease temperature as we pass from one temperature re-

gion to another. Considering the diffractogram in Figure 4.5 at 250 K (long-dashed line characteristic of R3), the most visible feature is the presence of an amorphous halo centered about q= 0.93 $Å^{-1}$ as could be expected for a short-range disordered structure of a liquid sample. Accordingly a secondary broad halo at higher values of q is also present in the diffractogram. Decreasing the temperature down to region R2 (220 K, short dashed line) does not affect significantly the curve. On the contrary, when entering in region R1 (160 K, dotted line) we notice that the main halo becomes better resolved, and a shoulder-like feature for q-values of about 1.7 $Å^{-1}$ develops-overlaid on the secondary broad halo. This give us evidence that ODMS-COOH is no longer fully amorphous but it presents some ordered short-range structure. With no much developed crystals since no sharp peaks are visible. Decreasing further the temperature down to region R0 (130 K, solid line) we do not observe any significant additional change in the diffractogram. We can conclude that the local structure of the ODMS-COOH changes from a well disorder structure above 220 K (R2 and R3) to a more ordered structure below 220 K (R1 and R0). Consequently the changes in local order structure should be attributed to those molecular entities responsible for the thermodynamic transition observed by DSC curves in the temperature range $195 - 215$ K. The other phenomena detected by DSC have not much impact in the local structure.

When comparing the obtained patterns on ODMS-COOH with those of the reference ODMS sample, for two distinct structural-environments, i.e. amorphous phase and ordered phase, clear differences are apparent (in Figure 4.6; dotted and solid lines correspond to ODMS-COOH diffractograms and large and small dashed lines correspond to ODMS diffractograms. Moreover, dotted and large dashed lines corresponds to samples in the amorphous phase while solid and short dashed lines corresponds to distinct structural environments). We can see that the ODMS crystallization manifests clearly in WAXS patterns, however the emerging shoulder-like feature in ODMS-COOH at about q= 1.7 $Å^{-1}$ is not related to conventional ODMS crystalline phase. The q-values of the shoulder-like and peak-maxima differs from those exhibited by the reference ODMS crystalline phase and the ones reported in literature [17]. These results confirm that the short-range order in ODMS-COOH is more likely associated to some kind of crystallization involving the aliphatic part. However, no reflection from the crystalline form of decanoic acid (main peaks at q= $0.5, 0.8, 1.3, 1.6$ $Å^{-1}$) is detectable which would confirm that it is a different crystalline form or other imperfect structure (mesophase).

In Figure 4.7, we plot the small angle X-ray scattering intensity, I [A.U.], as a function of the momentum transfer, q [$Å^{-1}$], for the ODMS-COOH co-oligomer. Empty circles correspond to the diffractogram of the co-oligomer as measured at different temperatures representative of the regions defined

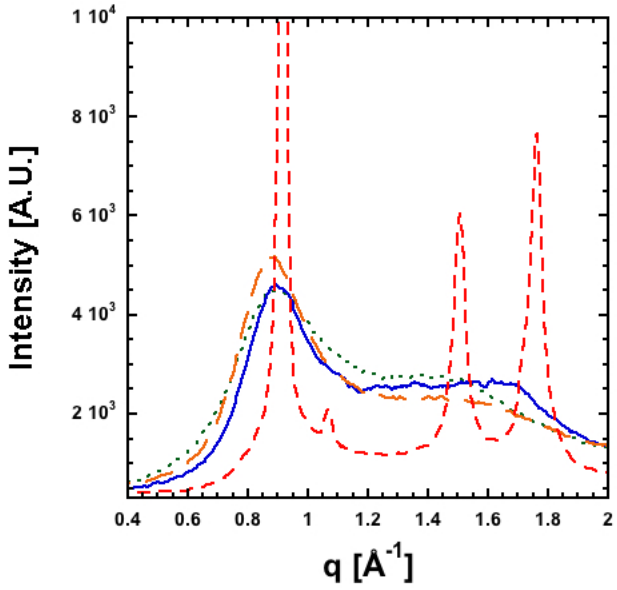

Figure 4.6: Wide angle X-ray scattering diffractograms for ODMS-COOH co-oligomer and reference ODMS oligomer samples for two distinct structural-environments (doted / solid lines correspond to fully amorphous/amorphous with some structuration ODMS-COOH co-oligomer and long / short dashed lines to amorphous / crystallized ODMS respectively)

above. At about of 250 K (R3) the SAXS patter shows no distinctive features as corresponds to a system in a conventional liquid state. This corroborates the absence of any thermal transition by DSC above this temperature.

The data in Figure 4.7a show the SAXS results at about 230 K corresponding to R2 below the weak thermal transition but above the strongest one. Here, we can notice that the sample present an ordered structure characterized by visible peaks at about q= 0.1, 0.2, 0.3 and 0.4 $Å^{-1}$. These would correspond to a lamella like structure with 6.2 nm lamellar periodicity, as the characteristic peaks appearing every integer multiple of the momentum transfer. The dotted line in Figure 4.7a correspond to the description of the SAXS diffractogram by a lamella model using the "Scatter" software [72]. Taking into account that no short-range crystalline structure were detected by WAXS in region R2, the SAXS diffractograms evidence that ODMS-COOH becomes a structured liquid in such region.

The data in Figure 4.7b correspond to region R1, i.e., below the strongest thermal transition but above the glass transition of ODMS. We observe that the lamellar structure persists through the cooling but a second structure appear over-imposed as a very prominent peak at q = 0.12 $Å^{-1}$. This corresponds to a structural periodicity of 5.2 nm. No clear signatures of corresponding higher-q reflexions are detected, although a weak contribution

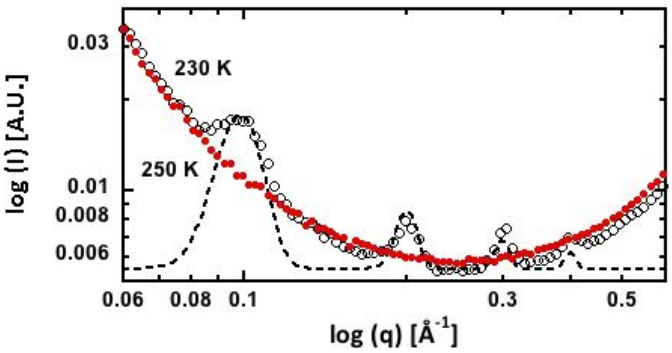

(a) ODMS-COOH difractograms at experimental-temperatures set to 230 K (empty circles) and 250 K (filled circles)

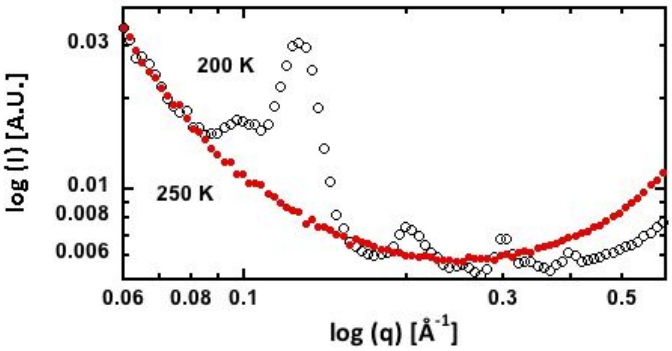

(b) ODMS-COOH difractograms at experimental-temperatures set to 200 K (empty circles) and 250 K (filled circles)

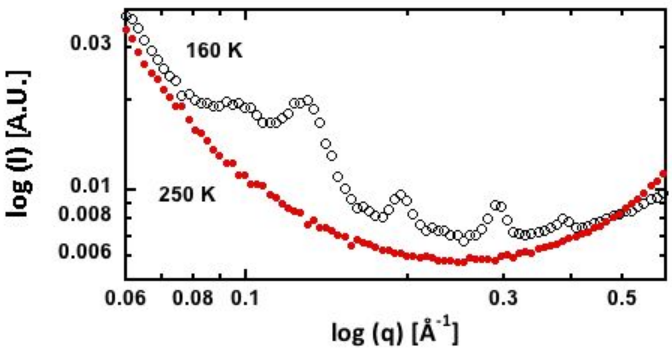

(c) ODMS-COOH difractograms at experimental-temperatures set to 160 K (empty circles) and 250 K (filled circles)

Figure 4.7: Small angle X-ray scattering diffractograms for ODMS-COOH co-oligomer sample at four relevant temperatures

could be envisaged at q$\approx$ 0.25 Å^{-1}. This suggests that the new structure is

not well developed (small domain size) as is usually found in semi-crystalline polymers. The results imply a coexistence of two structures, probably with a semi-crystalline arrangement (detected in the WAXS) inside the lamellar inter-spacing without involving DMS units. This means that DMS would remain in the liquid state and only becomes frozen below the glass transition.

Finally, the data in Figure 4.7c, collected at a temperature close to the glass transition of ODMS, show that the lamellar periodicity persists and the diffraction peak of the new structuration becomes less defined. This is likely due to distortions of the structures occurring when the glass transition of the DMS phase takes place.

4.3.3 Fourier Transform Infrared Spectroscopy

The results obtained above evidence that the ODMS-COOH undergoes different structural transitions, one related with long range ordering only, and the other manifested also as short range ordering. The energetic evaluation of these transitions suggested that hydrogen bonding could be involved in the former whereas the aliphatic part would be responsible of the later, DMS units being not involved directly in any of those transitions. A way to address whether this picture is valid is by exploring the effects of the thermal/structural transitions in the FTIR spectra. In this way we have access to specific molecular-group vibrations and how these vibrations are related to changes in the molecular environment.

Figure 4.8 shows the complete ATR-FTIR spectra for ODMS-COOH co-oligomer and reference ODMS sample. The principal bands have been assigned according to similar $((CH_3)_2SiO)_x$ compounds reported in the literature [73]. In the figure we can notice differences in some specific absorption bands. In particular ODMS-COOH presents a pronounced absorption peak around 1700 cm^{-1} that corresponds exclusively to the C=O of the carboxyl ending group (nothing is detectable on the ODMS reference in this range). In addition, the ODMS-COOH spectra show a broad band in the range $3400 - 2800$ cm^{-1} characteristic of the O-H vibrations. Also the ODMS-COOH present prominent peaks at 2930 and 2850 cm^{-1} a range where C-H stretching from aliphatic compounds usually occurs. Therefore these three features are very much specific of the functional group of ODMS-COOH. Contrary, the strong absorption bands below 1600 cm^{-1} appearing in both samples would correspond to specific vibrations involving DMS bonds.

Taking these results into account, together with the above discussed molecular origin of the structural changes in ODMS-COOH we have first analyzed the effect of temperature changes in the C=O band. In Figure 4.9 we notice that decreasing temperature bellow 250 K, entering in R2, the band changes its profile and a second component around 1690 cm^{-1} becomes apparent (blue curve in figure). This change suggests that the local environment has changed as would be the case if hydrogen-bond like inter-

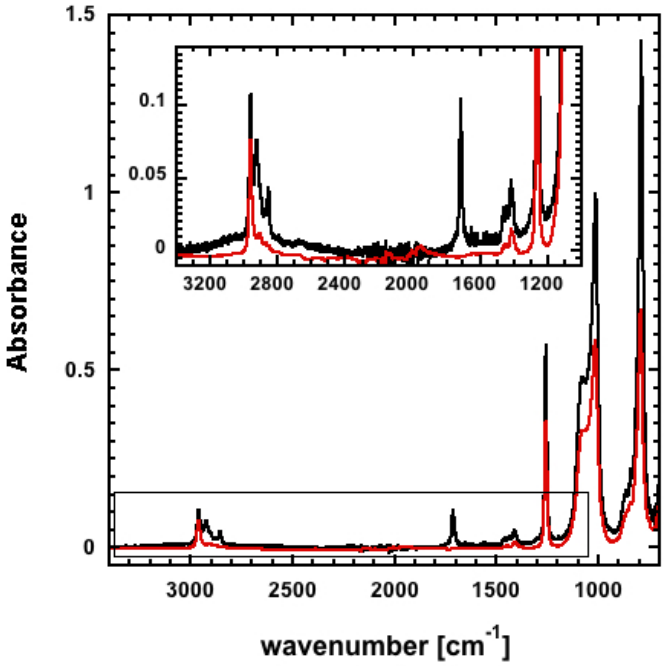

Figure 4.8: Complete Infrared data spectra ($3400 - 700$ cm^{-1}) for ODMS-COOH (black curve) and ODMS (red curve) samples at the melt temperature. Inset show the blow up of the square area int he high wavenumber region

actions develop. The reduction of the strength of the C=O bond given by the hydrogen bond interaction would explain a decreasing of the vibrational frequencies resulting in the second component of the C=O absorption band. Decreasing temperature further to R1 we notice an overall shift of the double-peak band with a better-resolved low frequency component (green curve in figure).

As mentioned above fundamental vibrations in the $3400 - 2800$ cm^{-1} region are generally due to O-H and C-H stretching vibrations. In Figure 4.10 we can observe a broad band corresponding to the O-H vibration, clearly noticeable for wavenumber's above 3000 cm^{-1}. It is also observed three well-defined and distinctive bands at lower wavenumbers. The prominent peak at about 2960 is related to the C-H stretching of the Si methyl groups, as it also appears in the ODMS reference. Moreover and in particular for this band, decreasing the temperature and measuring within R2 and R3, it do not show significant changes in the peak position as expected from the analysis of DSC and X-ray results. The second and third bands at about 2940 and 2860 respectively, also appear in decanoic acid infrared spectra and are most likely related to C-H stretching of the aliphatic part. In the figure we can not detect any change while decreasing the temperature down to R2. However

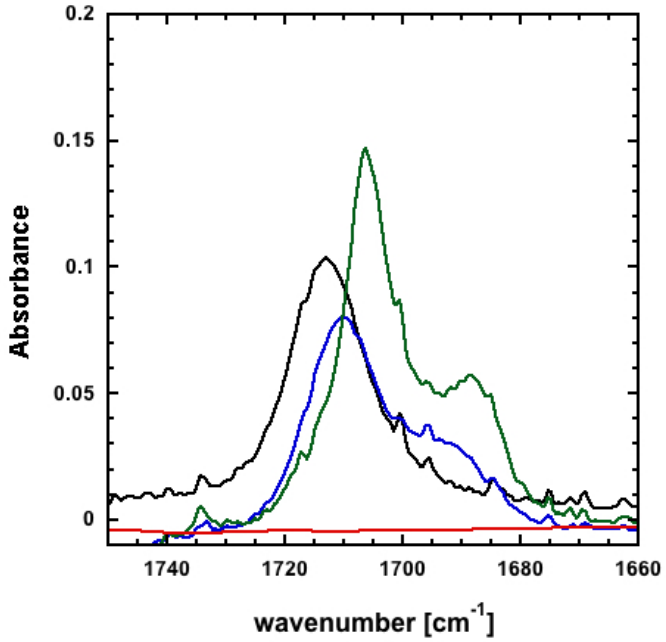

Figure 4.9: Infrared data spectra ($1800 - 2650$ cm^{-1}) for ODMS-COOH at three different temperatures within regions: R3 (black curve), R2 (blue curve) and R1 (green curve) and ODMS in R1 (red curve)

a shift of the second band maxima towards lower frequencies and a slight increase of the O-H band intensity occurs as we decrease the temperature down to R1. This again would be indicative of some change in the local environment of the aliphatic chains.

Now related to the DMS segments in our samples, in Figure 4.11 the peak that appears at 1260 corresponds to the characteristic vibration of the Si-CH_3 symmetric bending, distinguished by the very strong and sharp band. The two very strong and distinctive bands that appear at 1090 and 1020 cm^{-1} correspond to the vibration of the O-Si-O asymmetric stretching. The bands that appear at 790, 840 and 860 cm^{-1} corresponds to a mixture of the the stretching vibration of the Si-CH_3 band and the rocking of $Si(CH_3)_2$. The monotonous evolution of the infrared spectral bands is in agreement with the fact that we do not detect appreciable changes within the DMS related bands while decreasing the temperature and undergoing the two thermodynamic transitions detected by differential scanning calorimetry.

4.3.4 Structural assignments and its origin

So far we have identified distinct thermodynamic and structural features of the ODMS-COOH co-oligomer sample, we will summarize our findings as follows. DSC scans of the co-oligomer exhibits three different thermodynamic

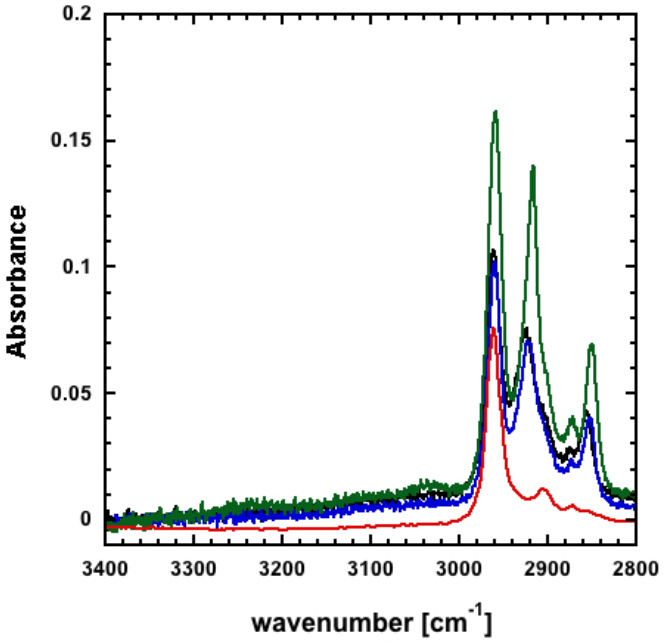

Figure 4.10: Infrared data spectra ($3400 - 2800$ cm^{-1}) for ODMS-COOH at three different temperatures within regions: R3 (black curve), R2 (blue curve) and R1 (green curve) and ODMS in R1 (red curve)

features at distinct temperature intervals (see I, II and III in Figure 4.4), which probably implies four different structural regions (see R0, R1, R2 and R3 in Figure 4.4). DSC, SAXS, WAXS and FTIR measurements at different temperatures were performed, in particular -at high temperatures within R3- measurements do not show evidence of any thermal or structural features occurring. Furthermore, the co-oligomer thermal behavior is as in the melt state and it presents the structure of an amorphous liquid. In DSC scans -around 230 K (III)- a small exothermic peak is noticed, it has been related to the formation of long-range ordering of supramolecular co-oligomer networks given by the creation of hydrogen-bonds between distinct end-chain carboxyl groups. Measuring at temperatures below the small exothermic peak, i.e. in R2, WAXS diffractograms show no short range-structure formation, however SAXS diffractograms evidence long-range structures with characteristics of a lamella phase. Additionally, the IR bands that are most affected by this process are those attributed to -COOH group. In particular, FTIR measurements within R2, show that the C=O band changes its profile which suggests that the local environment is different would be expected in the case of hydrogen-bond formation. At lower temperatures around 210 K (II in DSC scans), a noticeable exothermal peak is observed indicating a rather complex crystallization process. After comparing it with ODMS ref-

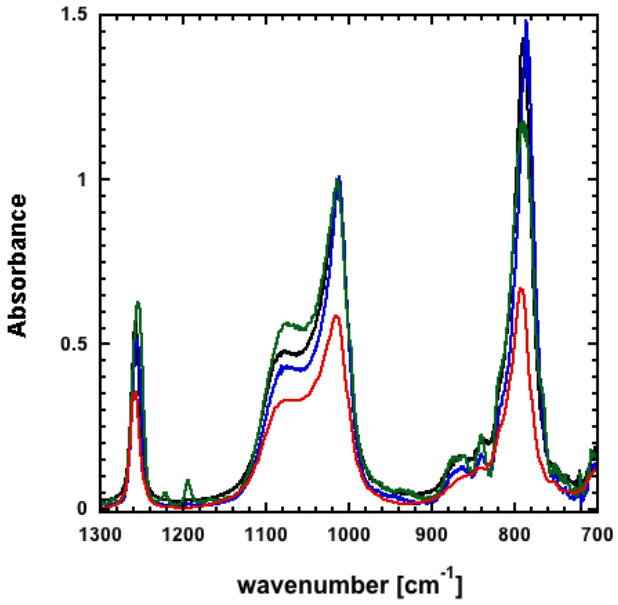

Figure 4.11: Infrared data spectra ($1150 - 700$ cm^{-1}) for ODMS-COOH at three different temperatures within regions: R3 (black curve), R2 (blue curve) and R1 (green curve) and ODMS in R1 (red curve)

erence, we concluded that this thermal process is related to the ordering of the aliphatic part of the ODMS-COOH co-oligomer. WAXS diffractograms confirm this picture since no DMS crystallization occurs. SAXS measurements within temperatures in R1, shows that ODMS-COOH lamellar structure persists, however a second structure appears over-imposed. This imply a coexistence of two structures, probably with an ordered arrangement (detected by WAXS) inside the lamellar inter-spacing without involving DMS units. Additionally, DSC measurements at lower temperatures around 150 K (I), detect a characteristic step-like thermal feature that corresponds to the glass transition of the DMS part of the co-oligomer without any detectable trace of DMS crystallization (see Figure 4.4).

As a way of validating the proposed structural assignments and their origin, parallel measurements of ODMS-$COOCH_3$ -a sample in which the molecular unit is essentially the same as ODMS-COOH, except that the methyl end group substitution prevents the formation of hydrogen-bonds. In the above picture this minor molecular change would inhibit the high temperature structuration occurring at 230 K.

The DSC results for ODMS-$COOCH_3$ sample (Figure 4.12) confirms that in region III no thermal features are detectable. WAXS (Figure 4.13) and SAXS (Figure 4.14) measurements neither detect the development of strutuctual features a few degrees below 230 K. Moreover, no significant features

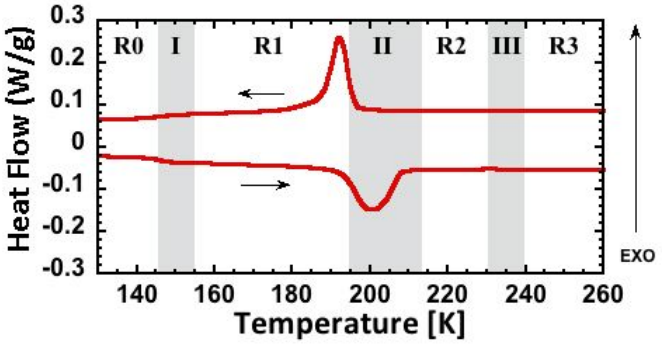

Figure 4.12: Differential Scanning Calorimetry measurements for the methyl terminated dimethylsiloxane co-oligomer (ODMS-$COOCH_3$)

are observed down to temperatures of about 190 K. Below this temperature (≈R2) an exothermic peak in DSC scans is observed. This peak can be attributed to the crystallization of ODMS as seen when compared with Figure 4.4b. Moreover, for temperatures in the region of 150 K we can detect a step-like feature corresponding to the glass transition of DMS entities. Comparing the ODMS-$COOCH_3$ glass-transition with the reference sample it is observe that in the latter the energetic difference in the step-like feature is less than in the reference one, this is related to the fact partial crystallization of DMS in the ODMS$COOCH_3$ co-oligomer has not been avoided.

WAXS diffraction patterns give us evidence of some complex structure arising. When comparing the obtained methyl terminated diffraction patterns with the one of crystallized ODMS (dashed line in Figure 4.13) we observe that many of the arising peaks can be related to the partial crystallization of the DMS. The other peaks should be related with crystallization of the aliphatic part that in this co-oligomer seems to be better developed due to the presence of well resolved peaks.

On the other hand, SAXS diffraction patterns also exhibit structural-features of this DMS crystallization, it is important to notice that this structure only arise after the crystallization of DMS has occurred.

The results obtained by DSC exhibit thermodynamic differences between the two functionalized oligomers. This outcome is related with the different structures obtained by X-ray diffraction. One interesting feature is that although both functionalizations are chemically similar the resulting structures are quite different. In the first case, where well-ordered lamellae about 5 nm thick are formed, the DMS crystallization is inhibited, whereas in the ODMS-$COOCH_3$ it is not possible to avoid DMS crystallization. Contrary to ODMS oligomer where crystallization can be avoided by quenching into liquid nitrogen the quenching of ODMS-$COOCH_3$ can not prevent the crystallization process involving both DMS and aliphatic parts.

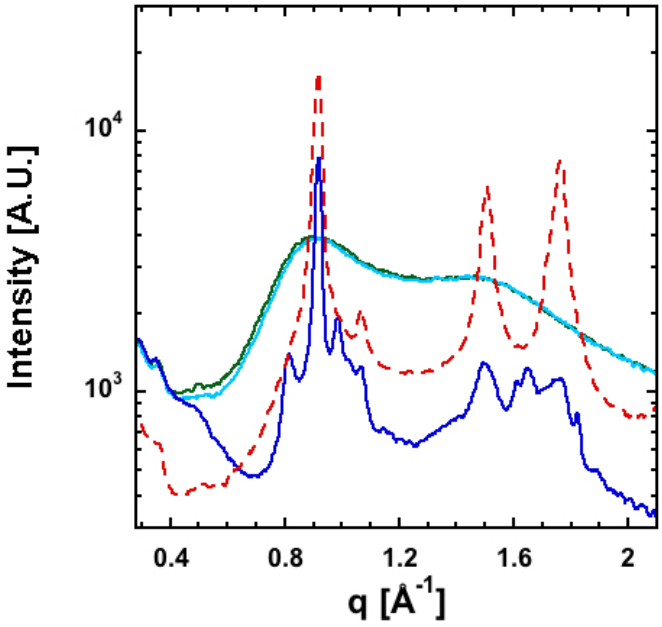

Figure 4.13: Wide angle X-ray scattering diffractograms for ODMS-$COOCH_3$ co-oligomer sample at R3, R2 and R1. Also crystallized ODMS diffractogram at R3 (dashed line)

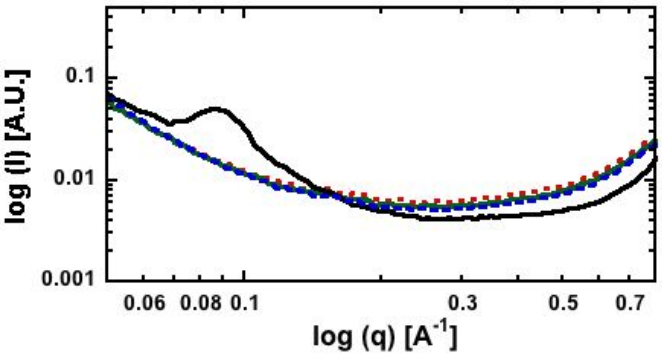

Figure 4.14: Small angle X-ray scattering diffractograms for ODMS-$COOCH_3$ co-oligomer sample at R3, R2 and R1

The results obtained on ODMS-$COOCH_3$ have evidence the utmost important role of hydrogen bonding on determining the low temperature structures of the ODMS-COOH co-oligomer. It seems that the supramolecular structures developed by cooling ODMS-COOH below 230 K is a key factor in preventing DMS crystallization and likely interfering in the aliphatic part ordering.

4.3.5 Broadband Dielectric Spectroscopy

Dielectric relaxation techniques allowed us to selectively study the relaxation phenomena related with the molecular mobility of the DMS segments and the carboxyl-terminated group forming part of the ODMS-COOH co-oligomer. The DMS component is majority within the co-oligomer sample, and it contributes by far more to the dielectric relaxation with negligible-contributions from the aliphatic part and weak-contributions from the terminal carboxyl group. We will star the description of the DS results with the segmental temperatures close to the glass transition where the motions of DMS are relevant, that is, the α-relaxation range.

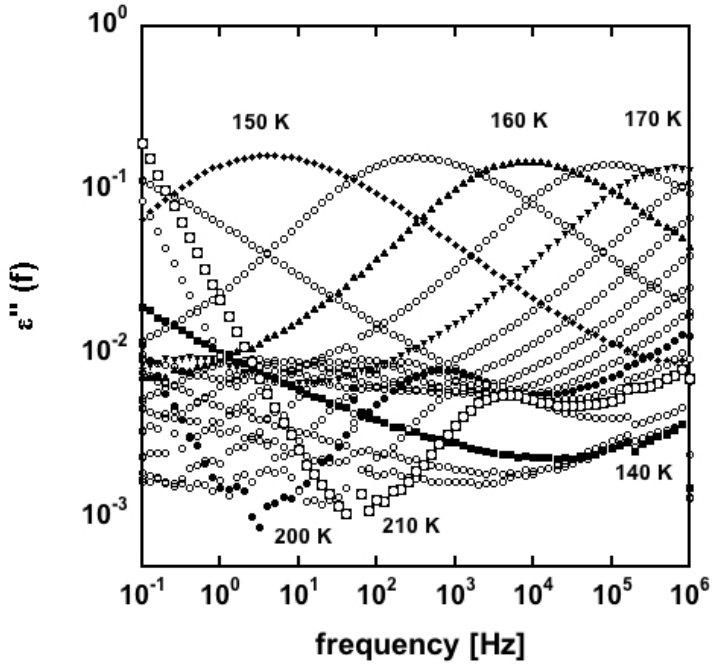

Figure 4.15: Dielectric losses as a function of frequency for the ODMS-COOH co-oligomer at different temperatures (130-210 K). Filled symbols corresponds to dielectric losses of the ODMS-COOH at specified different temperatures: 140 K (squares), 150 K (diamonds), 160 K (triangles), 170 K (up triangles) and 200 K (circles)

We can follow the evolution of the dielectric loss over frequency for different isothermal curves varying temperature from 130 K up to 210 K. Representative dielectric spectra (filled symbols) are presented in Figure 4.15. The dielectric losses on the ODMS-COOH co-oligomer were recorded isothermally after being cooled at a rate of 3 K/min in the dielectric cell. The dielectric experiments on the co-oligomer up to the lowest temperature showed time-independent results, i.e., the cooling rate do not modify the behaviour of the

co-oligomer relaxation in the temperature range of interest. The maxima of the dielectric loss peak give us the main relaxation time corresponding to the DMS segmental dynamics of the co-oligomer. The shape of the peak of the dielectric loss presents asymmetric features and a low frequency tail-like contribution, which at high temperatures develops as a distinct weak loss peak.

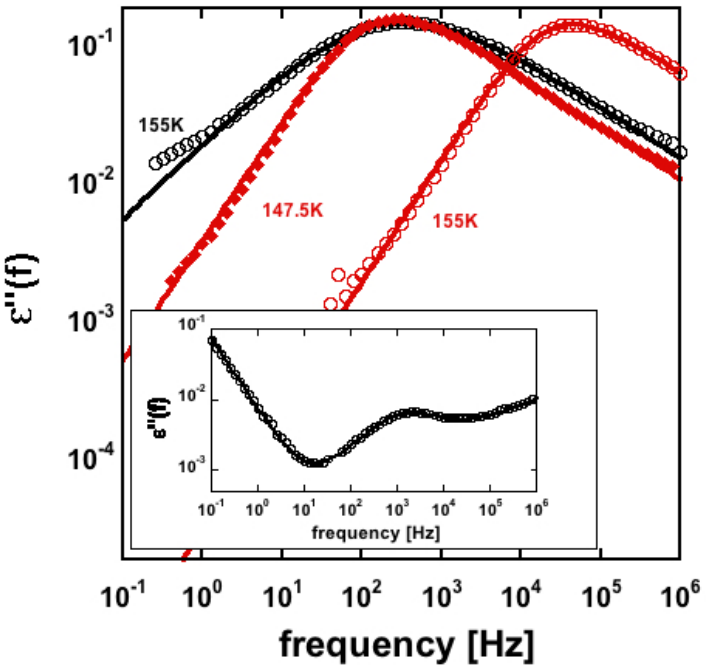

Figure 4.16: Dielectric losses as a function of frequency for ODMS-COOH co-oligomer at 155 K. Open black circles correspond to the data obtained for the ODMS-COOH co-oligomer, diamond and red open circles refer to experimental data of ODMS oligomer at two different temperatures 147.5 K and 155 K. Solid lines show the curve under the assumption of smoothness of the parameters obtained from the curve fitting by means of the HN equation. The inset shows the slower relaxation process occurring in the ODMS-COOH co-oligomer at 200 K, as before solid lines correspond to the fitting curves obtained as indicated in the text

Centering the attention at one specific temperature, Figure 4.16 illustrates a characteristic dielectric loss isothermal curve at 155 K (black open circles) for the ODMS-COOH co-oligomer. For comparative reasons two different dielectric loss data sets for the fully amorphous ODMS oligomer at 147.5 K (squares) and 155 K (red open circles) are also included with a suitable vertical scaling. From this comparison it is observed that a shift of about 7.5 K in temperature will make the ODMS oligomer have a similar dielec-

tric loss peak position to that obtained for the ODMS-COOH co-oligomer, whereas at the same temperature the dielectric relaxation in pure ODMS is about two orders of magnitude faster than in the co-oligomer. It is also observed that dielectric losses are in the co-oligomer broader than those observed in the pure ODMS, being the difference much more pronounced in the low frequency flank. The inset in Figure 4.16 is presented to highlight the slow dielectric loss part of the curve at 200 K where a weak but well resolved peak is detected superimposed in the "valley" formed by the low frequency flank of the main peak and the fast loss increasing at the lowest frequencies attributed to the d. c. conductivity of the sample. This finding is indicative of some slowly moving dipolar components that would be most probably related with the minority carboxyl group of the co-oligomer attached as an end group to the aliphatic part.

The BDS results have been further analysed quantitatively using a fitting procedure based on the Havriliak-Negami (HN) equation. According to equation 3.32, the dipolar contribution to the loss permittivity is given as:

$$\varepsilon^{''}(\omega) = \varepsilon_{\infty} + \frac{\Delta\varepsilon}{(1 + (i\omega\tau_{HN})^{\alpha})^{\gamma}} \tag{4.1}$$

In this equation, $\alpha - \gamma$ $(0 < \alpha, \alpha \cdot \gamma \leq 1)$ denotes the symmetric-asymmetric broadening of the relaxation peak, $\Delta\varepsilon$ corresponds to the relaxation strength, and τ_{HN} is the Havriliak-Negami relaxation time associated to the peak relaxation time τ by the equation:

$$\tau_{HN}\left[sin\left(\frac{\alpha\pi}{2\gamma+2}\right)\right]^{\frac{1}{\alpha}} = \tau\left[sin\left(\frac{\alpha\gamma\pi}{2\gamma+2}\right)\right]^{\frac{1}{\alpha}} \tag{4.2}$$

This empirical description also allows characterising the loss peak shape by the full width at half-maximum (FWHM) that can be approximately calculated from the shape fitting parameters α and γ by means of the empirical equation:

$$FWHM(\alpha,\gamma) = -0.516 + \frac{1.058}{\alpha} + \frac{0.039}{\gamma} + \frac{0.563}{\alpha\gamma} \tag{4.3}$$

In the analysis of the main peak the fitting has been restricted to loss values above 20% of the peak in order to avoid the influence on the obtained parameters of any weak contribution. However, when analysing the weak peak detected at high temperatures, the HN equation (with fixed $\gamma = 1$, i.e. symmetric shape) was combined with the previous HN equation plus a d.c. contribution to take into account for the faster relaxation process and the conductivity respectively. Solid lines in Figure 4.16 correspond to the so obtained fitting curves.

Regarding the characteristic relaxation times, Figure 4.17 shows the temperature dependence of the dielectric relaxation time as determined from the

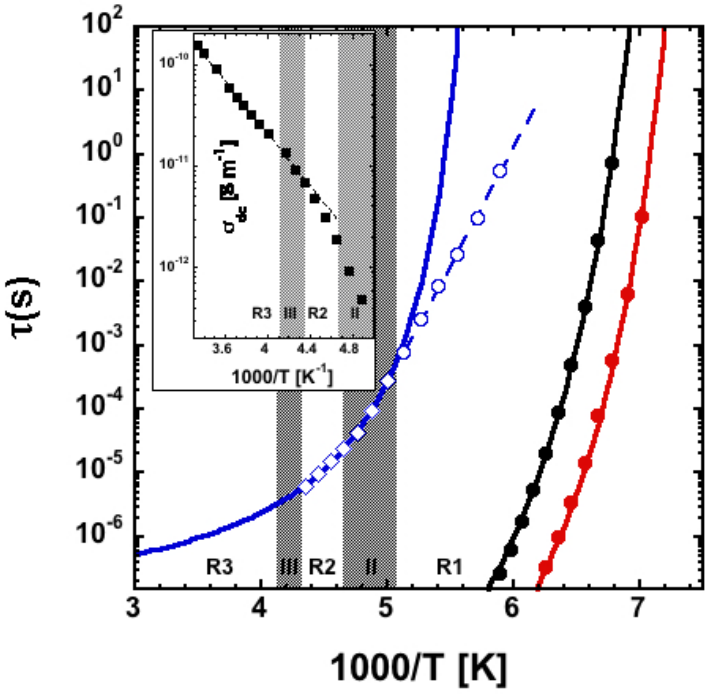

Figure 4.17: Characteristic relaxation time, deduced from the frequency of the dielectric loss maximum, as a function of 1000/T. Open circles and diamond symbols correspond to slow relaxation processes related to the carboxyl terminated aliphatic part in ODMS-COOH co-oligomer. Black filled circles correspond to the segmental relaxation of DMS part in the co-oligomer, while red filled circles correspond to the segmental relaxation of ODMS oligomer. Solid lines corresponds to fitting curves obtained by means of the Vogel-Fulcher-Tamman equation, dashed line correspond to the fitting to an exponential function. Inset in the figure show the conductivity as a function of the 1000/T

loss peak frequencies of the fitting curves. Black filled circles are data points corresponding to the main relaxation process of ODMS-COOH and are compared with those obtained on the pure ODMS oligomer (red filled circles). White-squares and circles correspond to the characteristic time of the weak dielectric relaxation detected at higher temperatures. It is confirmed that for the co-oligomer the segmental DMS dynamics is slowed down with respect to that in the pure ODMS oligomer with similar molecular weight, in both cases the non-Arrhenius behaviour characteristic of super-cooled liquids results evident. It is also shown that for the slow dielectric loss process an unusual behaviour is apparent around temperatures about 200 K where the temperature dependence seems to change. It is noteworthy that this temperature range coincides with that where ODMS-COOH showed a structural

transformation with some short range ordering reflected as a weak and broad feature in the WAXS diffractogram and as a crystallisation-like peak in DSC (see Figures 4.4b and 4.5). To analyse the temperature dependence of the relaxation times more quantitatively we have used the VFT equation.

$$\tau_\alpha = \tau_\infty exp\left(\frac{B}{T - T_0}\right) \tag{4.4}$$

Where T_0 is the characteristic Vogel temperature, τ_∞ is the high temperature asymptotic value of the relaxation time, and B-parameter is related to the so-called fragility parameter. The parameters obtained from the fittings are summarised in Table 4.1. The value of τ_∞ for ODMS and ODMS-COOH where fixed to that determined previously in Ref. [15] for fully amorphous PDMS.

Table 4.1: Characteristic Vogel temperature T_0, high temperature asymptotic value of the relaxation time τ_∞ and energetic contribution related to the fragility parameter B

Sample / relaxation process	$\tau_\infty\,[s]$	$T_0\,[K]$	$B\,[K]$
ODMS / segmental	5.5×10^{-13}	122	525
ODMS-COOH / main	5.5×10^{-13}	127.5	561
ODMS-COOH / slow (R1)	8×10^{-23}	0	8525
ODMS-COOH / slow (R2)	1.2×10^{-7}	168	504

The resulting lines from such fittings are shown in Figure 4.17 and the corresponding parameters are included in (Table 4.1). We can notice that for the slow process the fitting has been made independently above and below 200 K, where a change of behaviour was detected. When comparing the VFT parameters of the main relaxation in the co-oligomer with that of pure ODMS it is obvious that the Vogel temperature T_0 of the former is higher by 5.4 K as would be expected from the differences in peak position presented in Figure 4.17. However, the values of B are rather similar for both oligomers. Additionally, the VFT parameters for the slow process change dramatically around (grey area II in Figure 4.17) being particularly the low temperature range very close to an Arrhenius behaviour, which would correspond to $T_0 = 0$. As shown above the dielectric relaxation of ODMS-COOH is very fast in region R3 (i.e. above 230 K) and the possible effect of structure formation occurring at high temperature is hardly detectable. Nevertheless, the ODMS-COOH sample conductivity analysed above evidenced clear changes in the temperature dependence that can be associated to structure formation of the liquid ODMS-COOH giving rise to a lamella phase. The d.c. conductivity is contributing to the dielectric data at the lowest frequencies in the form of a f^{-1} increasing of the losses (see inset in Figure 4.16). Thus, d.c. conductivity of the co-oligomer was obtained by means of the following

equation.

$$\sigma_{d.c.} = \omega \varepsilon_o \varepsilon^{''}(\omega \to 0) \tag{4.5}$$

Where ω is the angular frequency, ε_0 is the vacuum permittivity and $\varepsilon^{''}$ is the dielectric losses for angular frequencies close to cero. The measured conductivity in the co-oligomer is mainly due to the diffusion of ionic impurities (unavoidable in the material synthesis). The ionic conductivity in viscous liquids generally presents a strong temperature dependence following a VFT-like equation. However, when plotting the conductivity of ODMS-COOH versus reciprocal temperature we found a nearly Arrhenius behaviour at high temperatures (see dashed line in the Figure 4.17) with a noticeable change in the temperature-dependence at about 230 K. Below this temperature the conductivity values lie below the extrapolated Arrhenius line. This means that as expected the structural development of the liquid interferes with the ionic diffusion. A second change should be expected at about 200 K related with the subsequent structural development and a small hint of it is observed.

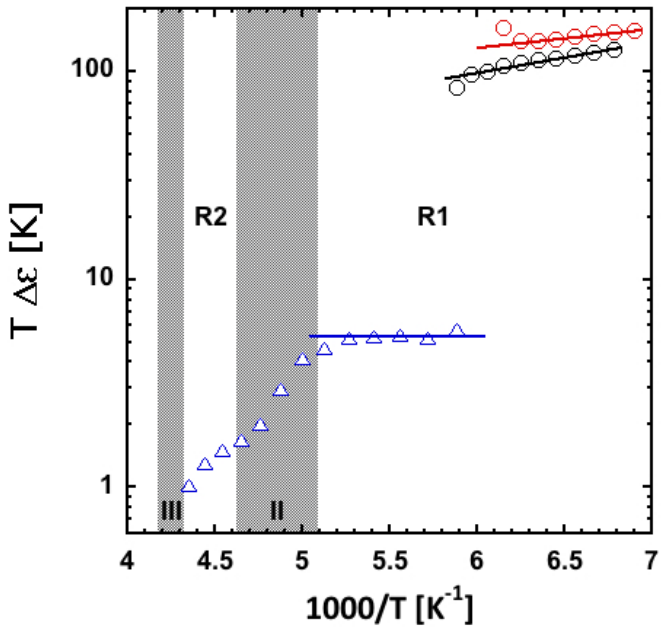

Figure 4.18: Dielectric relaxation strength as a function of 1000/T. Black open circles correspond to ODMS-COOH co-oligomer main relaxation and open triangles correspond to the slow aliphatic-carboxyl-terminated part. Red open circles correspond to the segmental relaxation of ODMS oligomer. Solid lines show the smooth linear behaviour of the dielectric strength for the temperature region of interest

In addition to the relaxation times and conductivity, the analysis of the dielectric data provides also the strength of the relaxation process, which is related with the amount of dipoles involved as well as with their ability to reorient. The dielectric strength obtained from the HN fits is represented in Figure 4.18 as a function of 1000/T For the DMS related relaxation in the co-oligomer (black open circles) large values are obtained, only slightly lower than those of the pure ODMS (triangles). The difference between them is about 10 %, which is not far from what could be expected by the "dilution effect" of DMS in the co-oligomer where DMS amount about 87 % weight fraction. For both ODMS and ODMS-COOH the relaxation strength decreases with temperature similarly, but more than expected from fully uncorrelated dipole reorientation ($\Delta\varepsilon \propto \mathrm{T}^{-1}$), which would mean that there exist temperature dependent orientation correlations between neighbouring dipole. The lines in the figure correspond to the following equations representing the temperature dependence of the relaxation strength:

$$\Delta\varepsilon_{ODMS}(T) = 370\ T^{-1} - 1.634 \tag{4.6}$$

$$\Delta\varepsilon_{ODMS-COOH}(T) = 332\ T^{-1} - 1.393 \tag{4.7}$$

On the other hand, for the slower weak-relaxation we can observe that the dielectric strength presents a non-monotonous temperature dependence changing from a moderate decreasing with temperature below 200 K (according to T^{-1}) towards a rather dramatic decreasing above 200 K which could suggest the lost of molecular dipoles involved in this relaxation process as far the structural features in the co-oligomer vanish.

The analysis of the dielectric loss also provided the shape of the corresponding relaxation components. In Figure 4.19 we present the Full Width at Half Maximum ($FWHM$) of the loss peak as a function of 1000/T for the different relaxation processes in ODMS-COOH, and the segmental relaxation in ODMS samples for comparison. We can observe that the $FWHM$ for the main relaxation of ODMS-COOH co-oligomer is at low temperatures significantly greater than the one observed for the ODMS oligomer. However both become closer as temperature increases, since whereas the former decreases with increasing temperature, the $FWHM$ of ODMS remains essentially T independent at around 2.25. As can be seen in Figure 4.19, the temperature dependent $FWHM$ of ODMS-COOH can be well described by:

$$FWHM(T) = 800\ T^{-1} - 2.23 \tag{4.8}$$

Comparing the $FWHM$ values for the slow weak relaxation in the co-oligomer we can see that in this case the relaxation is relatively narrow but still with a marked temperature dependence. Interestingly, the $FWHM$

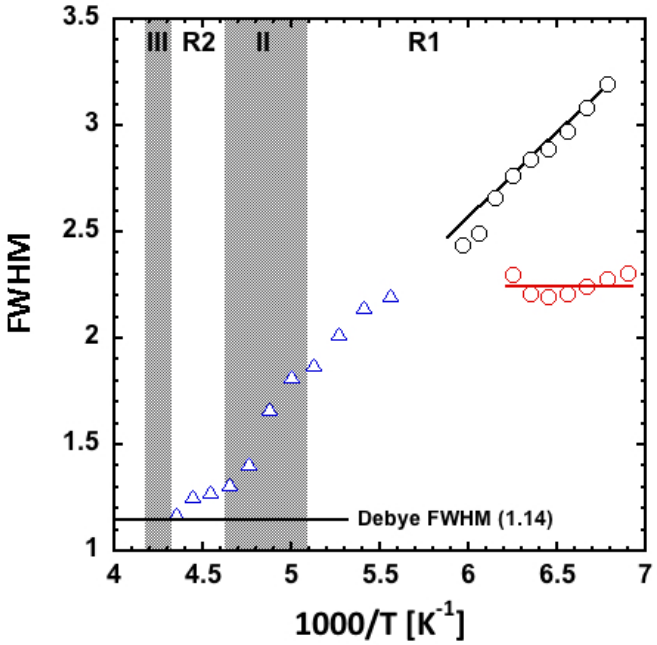

Figure 4.19: Full width at half maximum (FWHM) as a function of 1000/T. Black circles refer the $FWHM$ for the segmental DMS relaxation in the co-oligomer, triangles correspond to the $FWHM$ values of the weak slow aliphatic-relaxation process. Red circles show the $FWHM$ values for the ODMS oligomer. The straight lines sketch the linear behaviour of the data obtained

decreases very sharply when passing from R1 to R2 and at the highest temperatures the relaxation shape approach a Debye-like one. It should be noted that a Debye like relaxation is rarely found in polymeric materials or other molecular liquids. However, a Debye like relaxation is found in the dielectric relaxation of mono-alcohols (Ref. [74]) and it has been associated to the formation and breaking of H-bonds. This would suggest that the weak slow process in ODMS-COOH could be related with a similar phenomenon, at least in R2 The previous results evidence that the dielectric relaxation of ODMS-COOH is sensitive to the structural events occurring in this co-oligomer. However, this is not clear for the main relaxation process since the relaxation becomes to fast (already above 170 K) to be properly detected in the frequency range explored. Motivated by this, we performed DS experiments in a different setup covering higher frequencies, namely form 1 MHz to 1 GHz. Unfortunately, in this setup the signal-to-noise ratio is lower because instrumental limitations. Some representative results are presented in Figure 4.20. Here it is shown that the main relaxation loss peak of ODMS-COOH is located in the range 1 MHz-1 GHz when approaching R2

but is becomes again out of the accessible frequency range above 190 K. In agreement with the results obtained at lower frequencies, the DMS dynamics in ODMS-COOH is slower than that in pure ODMS as far as crystallisation of the later is not well developed. As can be seen in Figure 4.20 this is the case at 190 K but at lower temperatures there are new contributions to the dielectric relaxation in ODMS at low frequencies indicative of the onset of ODMS crystallisation (Ref. [17]).

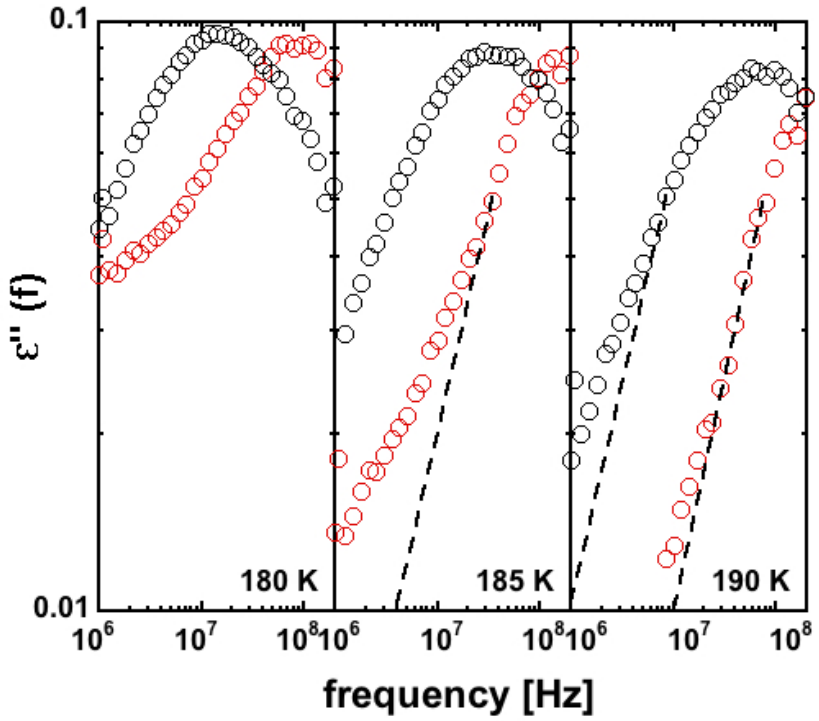

Figure 4.20: High-frequency dielectric spectroscopy measurements (1 MHz-1 GHz) for ODMS-COOH (black unfilled circles) and ODMS oligomer (unfilled red circles) at three different temperatures: 180 K, 185 K and 190 K. Dotted lines assume a smooth behaviour of the low-frequency losses without crystallisation of DMS

Despite these limitations, the high frequency experiments can be analysed in a different way trying to explore the possible changes in the characteristics of the main dielectric relaxation of ODMS-COOH in region R2. In particular, an isochronal representation of the data (in this kind of representation the systematic errors occurring at each frequency does not affect much the characteristic of the measured loss peaks) allows detecting the main dielectric

relaxation at temperatures above 200 K. This is not so clear at frequencies as low as 1 MHz as evidenced in Figure 4.20.

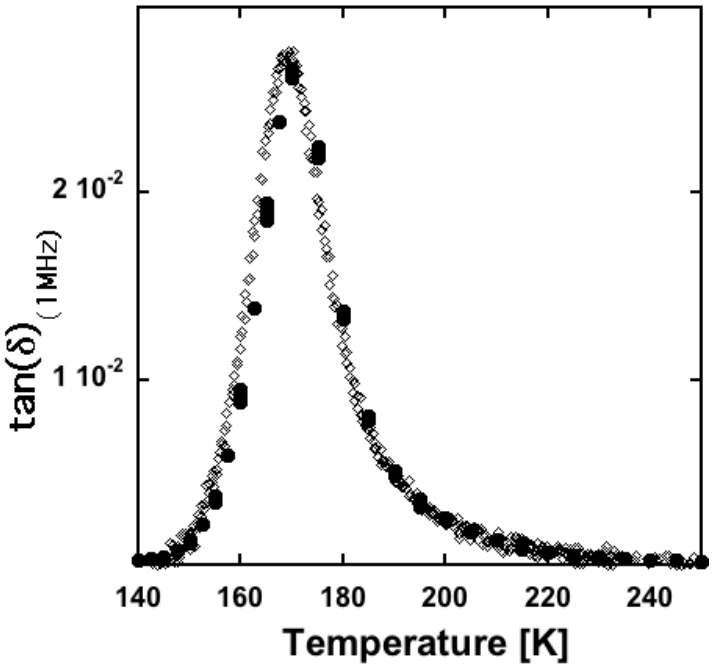

Figure 4.21: Isochronal representation (1 MHz) of $tan(\delta) = \left(\varepsilon''/\varepsilon'\right)$ as a function of temperatures. Dielectric spectroscopy measurements of ODMS-COOH co-oligomer were obtained with two different instrumental setups

In Figure 4.21 the data collected with the high frequency setup are compared with those (more accurate) obtained in the lower frequency setup showing the good compatibility of the two experiments. However, the measured losses are quite low above 200 K to be used for detecting possible changes associated to the structural transitions. Nevertheless, moving to higher frequencies the values of the dielectric losses in this range increase. In fact, at around 100 MHz the main loss peak of the isochronal representation occurs at around 200 K (see following figure).

In Figure 4.22 we show the dielectric losses as a function of temperature (isochronal representation) measured at three particular frequencies: 1×10^7 Hz, 1×10^8 Hz and 6.4×10^8 Hz. Data points of dielectric losses at the frequency of 1×10^7 Hz shows a well-defined and narrow peak centred at temperatures of at about 180 K. The next set of data points corresponds to measurements performed at the frequency of 1×10^8 Hz, the dielectric losses show a less intense peak at temperatures of about 190 K (in R1). Furthermore, as temperature increases a few degrees, the slope of the dielectric losses decreases as expected. However, for temperatures close to 200 K the dielec-

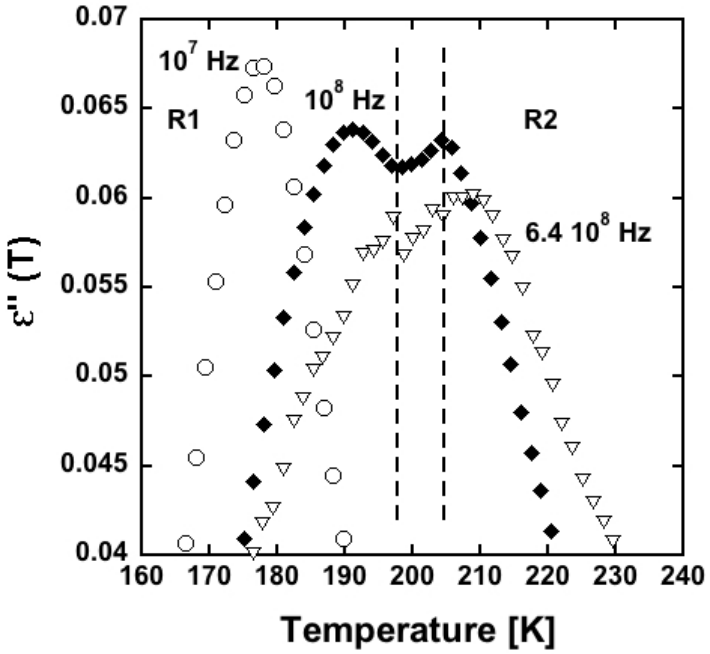

Figure 4.22: Dielectric losses as a function of temperature for the ODMS-COOH co-oligomer at three different frequencies: 1×10^7 Hz, 1×10^8 Hz, and 6.4×10^8 Hz

tric losses show a sudden increase that extends to temperatures about 205 K where only after this temperature they start to decrease monotonically. Additionally for measurements performed at a higher frequency 6.4×10^8 Hz, dielectric losses show a low-temperature wing that monotonically increase up to 198 K. After this temperature, losses exhibit a step-fall within the transition region (in-between R1 and R2) that increase to develop into a peak about 209 K (within R2) followed up by the monotonically decrease behaviour for higher temperatures. From these results it seems evident that above 200 K the DMS dynamics changes quite dramatically and becomes considerably slower (note that the peak at a fixed high frequency appears at a temperature of about 15 K higher than that detected below 200 K) when crossing from R1 to R2, in particular they reflect slower molecular movements. In order to quantify this effect Figure 4.23 shows the evolution of the dielectric peak maxima, obtained from the dielectric losses in the isochronal representation from two different measurements performed in the low-frequency instrumental setup (more accurate) and in the high-frequency instrumental setup.

It is observed that the only two data-points -that we were able to obtain- in region R2 are shifted with respect to the extrapolated curve of the dielectric losses peak maxima for the low-frequency (data-points within R1) by a

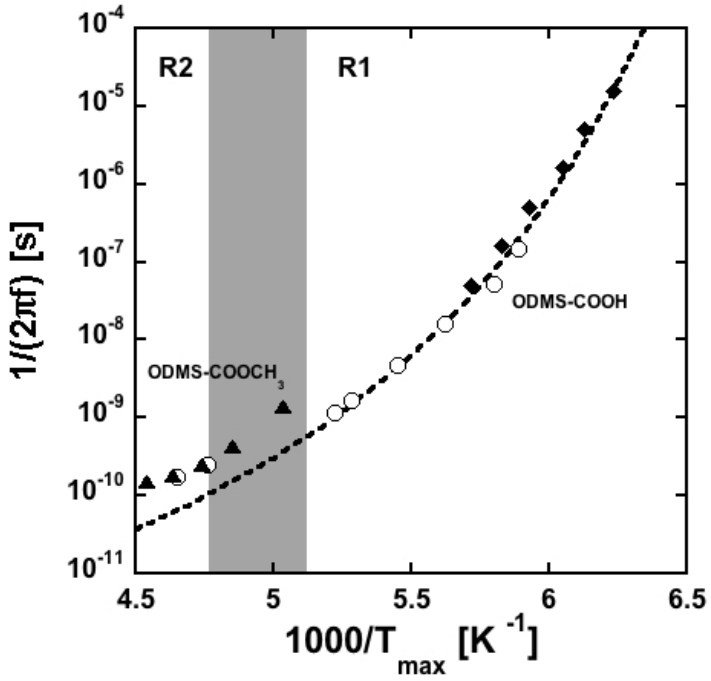

Figure 4.23: Dielectric losses peaks maxima ($1/2\pi f_{max}$) as a function of $1000/T_{max}$. Filled diamonds corresponds to measurements performed in the Low-frequency instrumental setup and unfilled circles correspond to measurements done in the High-frequency instrumental setup. Dashed line corresponds to the VFT curve obtained from the behaviour of the losses peaks maxima obtained with the low-frequency instrumental setup

factor close to two. A possible explanation for the origin of this shift could be the fact that ODMS-COOH co-oligomer within R1 presents a short-range structure that involves the aliphatic part of the co-oligomer and promotes the DMS segregation. Contrary, when considering the co-oligomer within R2, the short-range structure of the aliphatic part that was present is no longer existent. Moreover the DMS molecular movements will now include a rigid segment -corresponding to the aliphatic part- and will move in and environment that it is not the segregated environment from R1, therefore the molecular movements of DMS should be slower. A way to test this ideas is by comparing the dielectric relaxation due to DMS in ODMS-COOH with the corresponding one in ODMS-$COOCH_3$. This later co-oligomer can be maintained as an unstructured liquid during cooling until 190K. This allows us to characterise the peak temperature of the maximum dielectric losses in the isochronal representation. As can be seen in Figure 4.23 the obtained values for ODMS-$COOCH_3$ match very well with those determined in R2 for ODMS-COOH. This result has a two-fold consequence, on one hand con-

firms the DMS segregation occurring during cooling ODMS-COOH from R2 to R1, and on the other hand it evidences the fact that DSM dynamics in ODMS-COOH is not much affected thy the lamella structure that in this temperature range is present in this co-oligomer but not in ODMS-$COOCH_3$. Concerning other relaxation parameters, such as relaxation strength ($\Delta\varepsilon$) and full-with-half-maximum ($FWHM$), it is hard to reach any conclusion from the high frequency data.

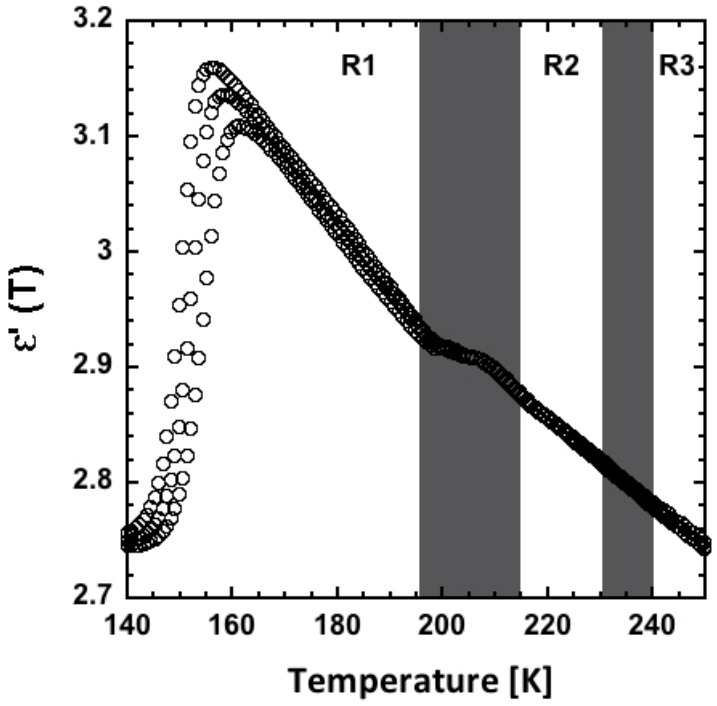

Figure 4.24: Dielectric dispersion as a function of Temperature for the ODMS-COOH co-oligomer at frequencies: 1, 10 and 100 Hz

Nevertheless, by analysing the temperature dependence of the static permittivity ($\varepsilon^{'}(\omega \to 0)$) of ODMS-COOH a clear increasing is observed when going from R1 to R2, as shown in Figure 4.24, indicating a corresponding increase of the relaxation strength. Such an increase would be expected if some DMS segments where partially blocked at (or near) the interphase with the structured aliphatic part in R1 and become unrestricted when the aliphatic structure is lost (in R2). Moreover, these same data indicate that not effect of the long-range lamella structure is evident on the ODMS-COOH dielectric relaxation strength when crossing from R2 to R3, i.e. when going from an structured liquid to a conventional melt. This later result is in line with the above commented matching in loss peak temperatures between structured ODMS-COOH and unstructured ODMS-$COOCH_3$

4.4 Conclusions

In the last section we have described the results for the obtained measurements of structure and dynamics for mainly ODMS-COOH carboxyl terminated co-oligomer. The results obtained by DSC show that conventional DMS crystallisation is inhibited in the ODMS-COOH co-oligomer, however different structural transitions take place. These arising structures are related to aliphatic block and carboxyl components. We can identify different temperature regions where the structural transitions take place; the glass transition at 150 K, the first structural transition happens at about 230 K, and the second structural transition is favoured by the carboxyl ending groups and takes place at 200 K. It has been noted that the end carboxyl functional group is essential at the moment of determining the structural properties of the material. In particular, it will give rise to the short-range lamellar structure. Additionally the influence of the carboxyl end-group partially limits the aliphatic ordering in the material. Furthermore, when characterising the molecular mobility of the material we have found out that the co-oligomer present two different relaxation phenomena in the range of study. The main relaxation has been attributed to the dynamics of the DMS part of the co-oligomer, while the secondary relaxation is most likely due to the carboxyl terminated end group. This molecular assignment has been proposed given the similarities that are present in the temperature dependence of the ODMS-COOH when compared with ODMS oligomer. Moreover, DMS part in the co-oligomer behaves in the same way as the amorphous DMS in the oligomer, nevertheless DMS dynamics in the co-oligomer appear to be slower due to the presence of the rigid aliphatic part which in turn also produces a greater dynamic heterogeneity.

The increase in dynamic heterogeneities is conditioned by the local structure of the aliphatic part that favours the segregation of the DMS. This effect becomes clear when we follow the dielectric relaxation times of DMS when crossing from region R1 to R2 and when the aliphatic structure is lost. Moreover, the fact of losing the aliphatic structure also leads to an increase of the dielectric relaxation intensity detected by the behaviour of the static permittivity as a function of temperature.

Regarding the confinement effects on the DMS dynamics, the obtained results show that when there exists only a lamella structure the DMS dynamics is not affected despite of the fact that the rather small structural length (about 6 nm periodicity). This is contrary to the conventional expectation that a pure geometrical confinement effect would give rise to a faster relaxation phenomenon if one consider the Adam-Gibbs picture of cooperative rearranging regions of increasing size on cooling. Most likely the reason is that in R2 the size of the cooperative rearranging regions is well below the structural length scale since DMS is moving very fast and is far above the

glass transition. The further structuration taking place in ODMS-COOH at lower temperature greatly affects the DMS dynamics and consequently the pure geometrical effects cannot be properly addressed. Nevertheless, no hint of a crossover in the temperature dependence of the DMS relaxation times is detectable when approaching Tg, a crossover that would be expected in the Adam-Gibbs framework.

The applied methodology, allowed us, to use different experimental techniques to elucidate and propose a molecular assignment that takes into account the dynamics and structure of the ODMS-COOH co-oligomer. Subsequent application of this methodology would permit a greater insight into the relation between mobility of the components and the structure of the system.

Chapter 5

Structure and dynamics of hybrid adhesives

"Hybrid materials represent one of the most growing new types of materials at the edge of technological innovations. Unique possibilities to create novel material properties, by synergically combining inorganic and organic components at the molecular scale, makes them interesting materials for application-oriented research."

Hybrid Materials - Past, Present and Future. Guido Kickelbick

Abstract: In this chapter we present the dielectric relaxation analysis of Acrylic-Polyurethane hybrid adhesives synthesized via mini-emulsion photopolymerization. As a starting point, we consider three different samples - both parts of the synthesized hybrid latex (Sol and Gel fractions)- and also a reference sample synthesized with the same protocol as the previous ones but with only acrylic groups as their constituents. Afterwards, the gel fraction of three distinct hybrid latex samples will be studied in connection with their synthesis conditions. The dielectric analysis of the distinct samples was carried out using Broadband Dielectric Spectroscopy (BDS). Additionally, Differential Scanning Calorimetry (DSC), Small Angle X-ray Scattering (SAXS) and ATR- FTIR measurements were performed in order to access their thermodynamical and structural properties. The analysis of these Acrylic-Polyurethane gels by BDS -in combination with SAXS- provides access to characteristics of the network structure that would ultimately influence the properties of these materials. We will start the chapter with a brief introduction on Acrylic-Polyurethane hybrid adhesives, and continue

with the description of the distinct samples and the experimental details. Then, we will present the results obtained by different experimental techniques, followed up by the discussion of important observations and summarizing it all in the conclusions.

5.1 Acrylic-Polyurethane hybrid adhesives

Self-adhesive materials, also called pressure-sensitive adhesives (PSA's), are special adhesive materials designed to stick on almost any surface by simple contact under light pressure [22]. This class of adhesives does not experience any physical transformation or chemical reaction during the bonding process. Commonly two different types of PSA's are produced depending on the components employed to produce them, these are, either "solvent-borne" or "water-borne" adhesives. Solvent-borne PSA's provide excellent moisture resistance and good wetting properties. However, due to environmental problems, a shift from solvent borne to water borne type has been taking place. One way to produce water-borne, environmentally friendly hybrid polymers that synergistically combine the positive properties of different materials is by means of the use of miniemulsion polymerization technique [19, 18, 75]. In particular, this technique has been employed to incorporate polyurethanes polymer chains into acrylic polymers in an attempt to improve the adhesive properties of the acrylic waterborne pressure-sensitive adhesives. The so obtained hybrid materials are found to have adhesive properties that are determined by the polymer architecture. Due to the interest of these hybrid materials, studying their structure, their chemistry and also their physical properties has been the main subject of several reports [76, 77, 78]. In this context, the hybrid Acrylic-Polyurethane (Acrylic/PU) polymers synthesized via miniemulsion photo-polymerization have been reported to be good candidates as pressure sensitive adhesives [79, 80]. With the acrylic part as the majority component and PU chains used to form a network, it has been reported that small changes in the formulation and synthesis conditions of these materials give rise to rather different adhesive properties [81]. However, the ultimate reasons for the observed differences remain unclear.

Moreover, in the adhesive industry the achievement of materials with good properties is a first prerequisite for further technological applications [21, 22, 23]. In order to obtain desired PU dispersions with improved properties, such as mechanical stability, toughness, solvent and chemical resistance, and to reduce costs, mixtures with poly-acrylic systems are used. Blending a poly-acrylic dispersion into a polyurethane dispersion often leads to final products with low quality, attributed to the poor compatibility between their components. However, the formation of hybrid particles where each particle contains both polymers and chemical linkages between them leads to a better compatibility of the components. Therefore, miniemulsion poly-

merization [18, 19, 20] is a suitable technique to synthesize complex materials that cannot be produced otherwise. Furthermore, miniemulsion photopolymerization technique allows obtaining different good quality materials by varying the initial synthesis conditions. In the literature we can find several comprehensive reports on the fabrication and chemical characterization of Acrylic-PU dispersions [19, 82, 83], in particular of pressure sensitive adhesives (PSA's). One of the main conclusions obtained from these reports is that the adhesive properties of PSA's materials are mostly determined by their polymer architecture [24]. Therefore, understanding the polymer architecture is of great importance for synthesizing optimal tailored adhesives. To begin with, we had focus our attention on the dielectric study of the components of a hybrid Acrylic/PU pressure sensitive adhesive latex. This latex is composed by a Gel fraction and a Sol fraction that coexist within each miniemulsion droplet. Moreover, a pure acrylic polymer synthesized in a similar way has been also investigated as a reference of the majority acrylic component ($\approx 90\%$) in the latex. Furthermore, by studying the structural and dynamical properties of the Gel fraction of three different latexes synthesized with the same components but with different synthesis conditions, we intend to get a deeper insight on the relation between the synthesis conditions and the corresponding material properties, for this a molecular description of the polymer architecture of the produced latexes is required. To conclude, the objective in this chapter is to show, compare and understand, different molecular characteristics of these Gel networks as inferred by BDS. The results are complemented with thermal characterization by MDSC and structural characterization of the distinct samples given by Small Angle X-ray Scattering and ATR-FTIR.

5.2 Samples and Experimental details

5.2.1 Samples

A complete description of the materials and the synthesis methods, employed in the production of the studied hybrid Acrylic-PU pressure sensitive adhesives (PSA's) is described elsewhere [19, 80, 81, 79]. In brief, first the organic phase was prepared by dissolving the Incorez 701 (10 weight based on organic phase %, 10 wbo%), Bisphenol A (BPA) chain extender and DBTDL catalyst (550 ppm based on the organic phase) in the monomer mixture (2-ethylhexylacrylate (2EHA)/n-octadecylacrylate (SA)/methyl methacrylate (MMA)/methacrylic Acid (MAA)/hydroxyethylmethacrylate (HEMA): 91.5 / 5.8 / 1.4 / 0.9 / 0.4 weight %). Then, the organic phase was mixed with an aqueous solution of the surfactant (Downfax 2A1, 2% wbo) and $NaHCO_3$ (0.02 M) under intensive stirring (15 min at 1000 rpm) to create an emulsion. The resulting coarse emulsion was sonicated for 15 min at 9 output control

and 80% duty cycle with a Branson 450 (Danbury, CT). Finally, in order to improve the miniemulsion stability, SDS was added (1% wbo).

The polymerizations were performed in two different ways, either by photo-polymerization or by thermal polymerization. In the case of the photopolymerization, the photoinitiator (non-bleaching oil soluble photo initiator 1-hydroxycyclohexyl phenyl ketone, I-184 or 1-[4-(2-Hydroxyethoxy)-phenyl]-2-hydroxy-2-methyl-1-propane-1-one, I-2959) were added to the organic phase before preparing the miniemulsion. The miniemulsion was then photopolimerized in a continuous quartz tubular reactor placed in a UV chamber (model BS 03, Dr. Gröbel UV-Elektronik GmbH) at 25°C with different incident light irradiances. For the sample prepared via thermal polymerization the miniemulsion was polymerized by a semi-continuous process in a 750 ml glass-jacketed reactor equipped with a reflux condenser, sampling device, N_2 inlet, two feeding inlets, and a stainless steel anchor-type stirrer rotating at 250 rpm. Initially, 20 wt% of the miniemulsion was placed into the reactor and allowed to polymerize over 1 hour by adding 0.48 wt% (weight based on monomer weight) initiator (Potassium persulfate, KPS). The rest of the miniemulsion and the initiator solution were then fed for 3 hours. After the end of the feeding period, polymerization was allowed to occur for 2 hours. The reaction temperature was 80°C. Table 5.1 summarizes relevant information on these materials such as: Gel percentage (Gel %) photo-initiator type (PI), photo initiator concentration (PI %) and incident light irradiance (ILI).

Table 5.1: Synthesis conditions for three Acrylic-Polyurethane latex, only Gel fraction is presented

Latex Samples	Gel %	Synthesis Conditions
A	73	0.75% PI (I-2959), 7 (mW/cm^2)
B	46	0.25% PI (I-184), 3.5 (mW/cm^2)
C	67	Thermal (80°)

Regardless which miniemulsion process is used as a synthesis method, the resulting products are always latexes composed by a Gel fraction and a Sol fraction that coexist within each miniemulsion droplet. In order to separate both parts of the latex we used Soxhlet extraction under THF reflux. The Gel fraction is composed of a network of linear acrylic chains with PU chains attached to the reactive sites of the main acrylic backbone through bifunctional HEMA monomer [24]. These PU chains link the acrylic backbones together to form the reticulated structure. The Sol fraction is made of acrylic polymer chains with polyurethane pendants attached to the main acrylic backbone. The Sol and the Gel part of the polymer were separated by Soxhlet extraction under THF reflux. A representative drawing of the Gel network and the Sol fraction is presented in Figure 5.1. A material

synthetized in similar conditions to obtain only acrylic chains, polyethylhexylacrylate (PEHA), without PU nor BPA, was used as reference and it is also schematized in the same figure. It was seen that both the only acrylic polymer and the Sol fraction of the composite polymer had a similar average molecular weight of about 3×10^6 g/mol.

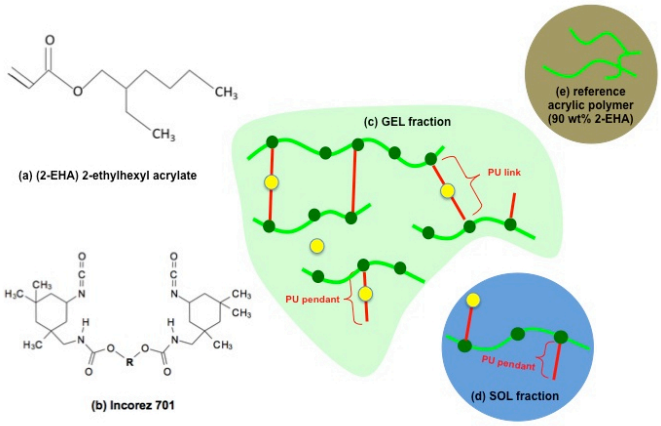

Figure 5.1: Chemical structural formula of (a) 2-ethylhexyl acrylate, (b) PU pre-polymer Incorez 701 and schematic representation of (c) Gel network, (d) Sol fraction and (e) acrylic reference polymer (PEHA). Green solid lines represent acrylic chain backbones, the green darker dots over the green lines correspond to junction points along the backbone, red lines represent PU chains and yellow circles correspond to BPA chain extenders

The concentration and type of photo initiator used, as well as the amount of incident light irradiance used in the fabrication of the studied samples have the optimum values for synthesizing hybrid PSAs with good standards for adhesive properties.

5.2.2 Experimental details

When preparing the samples for different experimental setups used in this work, all samples (Sol and Gel fractions, reference acrylic polymer and distinct protocol synthesized Gel fractions) were stored at 80°C in a vacuum oven for twelve hours. After this period of time the samples were allowed to cool down to room temperature in the vacuum oven before placing them into the corresponding sample holders. Before the experiments were performed, in situ heating up to 100°C of the samples was conducted to remove any trace of moisture.

5.2.2.1 Differential Scanning Calorimetry (DSC)

The experiments were carried out using the Q2000 set up from TA Instruments previously described. Temperature-modulated experiments were conducted using 60 s period and 0.5 K in amplitude, during cooling and heating at a mean rate of 3 K/min, in the temperatures range $150 - 420$ K. Samples for DSC experiments were prepared after the thermal treatment mentioned above, by encapsulating $5 - 10$ mg of sample in aluminium pans.

5.2.2.2 Broadband Dielectric Spectroscopy (BDS)

Measurements of the frequency dependent complex dielectric permittivity ($\epsilon^*(f) = \epsilon'(f) - i\epsilon''(f)$) were performed in the range $f : 10^{-1} - 10^6$ Hz, using the high-resolution dielectric analyser. The sample capacitor preparation for this setup consisted in an upper gold-coated electrode of 20 mm placed on a prepared film of the sample over a 30 mm gold-coated electrode. A separation of 100 μm between both electrodes was maintained by using a cross-shaped Teflon spacer of small area. The sample cell was set in a cryostat, and its temperature was controlled via nitrogen gas jet stream coupled with the Novocontrol quatro controller. The isothermal dielectric experiments were performed while cooling the sample from 420 to 150 K in steps of 10 K typically. The data reproducibility was checked during subsequent heating from 150 to 410 K. For the BDS analysis, the main part of the measured dielectric losses was fitted according to the empirical Havriliak-Negami (HN) equation 4.2.

5.2.2.3 Small Angle X-Ray Scattering (SAXS)

SAXS experiments were performed by means of the Rigaku PSAXS-L equipment previously described operating at 45 KV and 0.88 mA. The scattered intensities are presented as a function of the scattering vector q, $q = 4\pi(\lambda)^{-1}\sin(\theta)$, where θ is half the scattering angle. The sample to detector distance was set to 2 m & 50 cm & 20 cm, covering a q range from 0.008 to 1.7 $Å^{-1}$. In this way , the range usually considered as WAXS (local length scales) was also explored.

5.3 Results and Interpretation

As mentioned previously, to get a deeper insight into the relation between the synthesis conditions and the corresponding material properties, a molecular description of the polymer architecture of the produced latexes is required. Therefore, we will divide this section in two parts and start the first one with the results obtained for the structural and dynamical measurements for both parts (soluble and reticulated fractions) of an hybrid Acrylic-Polyurethane

latex synthesized via miniemulsion photopolymerization. Additionally, the obtained results are compared with those obtained for a reference acrylic latex synthesized with the same protocol as latex B (PEHA).

Analysing the structural and dynamical outputs allow us to obtain a molecular interpretation of the different dielectric relaxation observed, and related them to distinct entities of the material. This molecular interpretation give us a particular framework in which we are able to compare different molecular characteristics. We continue the second part of this section with the description, analysis and interpretation of the different structural and dynamical characteristics of the network relaxation of three distinct gel fractions and their relation with the synthetic conditions.

5.3.1 Molecular Interpretation of the dielectric relaxations in hybrid latexes

In this section we compared the results obtained in the Sol and Gel fraction of latex B (5.1) between them and with the reference PEHA. As a first result we show the Differential Scanning Calorimetric (DSC) measurements reflecting the thermal properties of the polymers under study. No signatures of crystallization and/or melting were detected in the explored temperature range (up to 470 K). Thus, in Figure 5.2 we present three different curves corresponding to the reversing heat capacity as a function of the temperature for all samples understudy, Gel, Sol and PEHA.

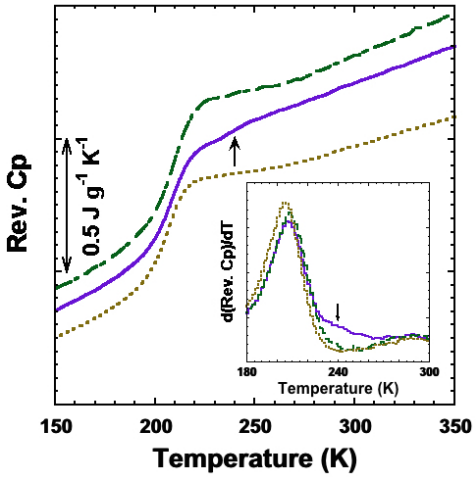

Figure 5.2: Differential Scanning Calorimetric scans for three different samples; Gel fraction of the obtained latex (solid line), soluble part of the latex, named Sol (dashed line), and the reference acrylic polymer, PEHA (dotted line). Inset in the figure corresponds to the derivative with respect to temperature of the reversible specific heat for the three samples

The data were obtained while cooling the material from 420 K at a rate of 3 K/min. The three samples explored by DSC exhibit similar thermal behaviour, particularly, at the glass transition where all of them exhibit a clear step like feature at about 210 K. It can be seen that the curve of the reference acrylic sample (PEHA) seems to exhibit a small but noticeable shift towards lower values of the glass transition temperature (measured as the temperature at the middle of the step) by about 2 K. In addition, we notice that Sol sample exhibits an additional small "step-like" change at about $240 - 250$ K, a feature that is absent in the other two samples. These differences are more evident in the inset of Figure 5.2 where the temperature derivative of the curves are depicted.

The main objective of this work was to investigate the dielectric relaxation on these hybrid polymers around and above the glass transition. Whereas the dielectric relaxation around the glass transition is known to be governed by the same molecular motions responsible of the thermal glass transition, large scale structures can be also detectable in the dielectric relaxation phenomena either by the existence of associated dipole moment fluctuations (normal mode dielectric relaxation originated by end-to-end vector fluctuations, mesogenic group reorientations in polymeric liquid crystals) and/or the effect of the interfaces on the charge transport (interfacial polarization phenomena) [12]. Figure 5.3 presents the real (a) and imaginary (b) part of the dielectric permittivity as a function of temperature (isochronal representation) at the frequency of 1 Hz for the three samples.

The first feature to notice in Figure 5.3 is that we can distinguish three different temperature regions where dielectric relaxation processes are detected. If we focus our attention at the imaginary part of the dielectric data, that is Figure 5.3 (b), we notice that the temperature region about $200 - 230$ K is where the three samples present a clear dielectric relaxation. This is a similar temperature region to that where the glass transition is observed in DSC experiments. Therefore this dielectric relaxation has to be related to the segmental dynamics dominated by the majority acrylic monomeric units. We will identify this relaxation as the so-called α-Relaxation (αR). The second temperature region where dielectric relaxation is detected is about $270 - 290$ K. Here Sol sample presents a prominent loss peak; without any signature of such relaxation in the reference acrylic sample. The major difference between Sol and PEHA samples is that the first contains PU chains attached to the main acrylic backbone by one side of the polyurethane chain (PU pendants), whereas the second one does not. Therefore this second relaxation process should be related to dipole moments given by the PU chains, and thus this relaxation will be referred as Dangling Chain Relaxation (DCR). Moving towards higher temperatures and examining the imaginary part of the dielectric data, Figure 5.3 (b), show that in that region the d.c. conductivity is dominant. However, when analyzing

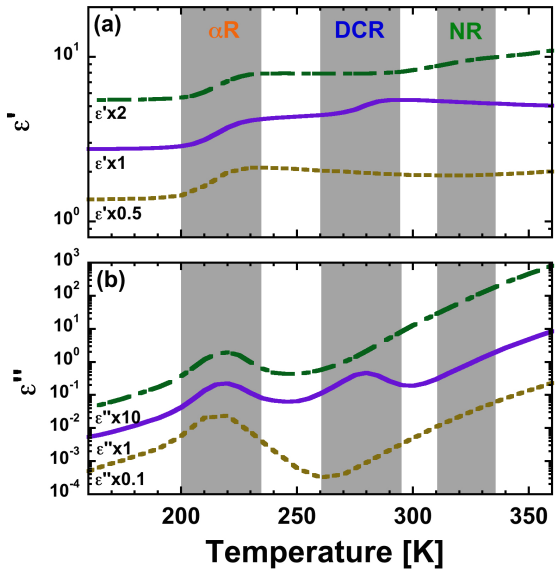

Figure 5.3: Real (a) and Imaginary (b) part of the dielectric permittivity as a function of temperature for Gel (dot-dash line), Sol (solid line), and the acrylic polymer, PEHA (dashed line), in the isochronal representation.The shadowed areas in the figure correspond to the three different temperature regions where the alpha relaxation (αR), dangling chain relaxation (DCR) and Network Relaxation (NR) are detected

the real part of the dielectric data in the same temperature region we notice that the Gel sample presents a step like feature about 320 K. This feature is not observed for Sol neither for PEHA samples. Thus, this third relaxation process would be linked to presence of a network structure in the Gel sample and so it will be called Network Relaxation (NR).

As we showed above, the αR process is observed in the three samples studied. In Figure 5.4 we present the imaginary part of the dielectric permittivity as a function of the frequency for the three different samples at a temperature of 240 K, where the α-relaxation process is clearly observed. As already commented, these loss peaks would be related to the segmental mobility involving polar groups of the acrylic chains explaining why the relaxation process exhibits similar characteristics, such as the intensity of the peak maxima and peak shape and position, for the three samples. One clear difference of the Gel and Sol samples with respect to the reference acrylic polymer, is that in the low frequency range the formers exhibit a plateau like behaviour with relatively high loss values, while the latest show a monotonous power-law like change of the losses. The higher intensity in Gel and Sol samples is indicative of the existence of slower contributions likely

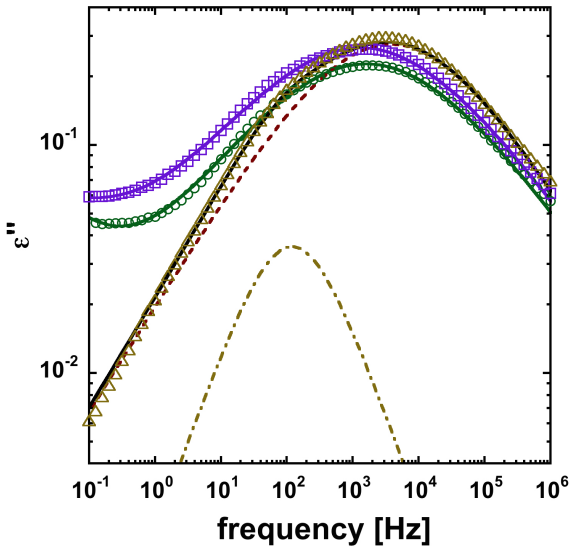

Figure 5.4: Frequency dependent Imaginary part of the dielectric permittivity at 240 K of Gel (circles), Sol (squares) and reference acrylic polymer (PEHA) (triangles). Lines correspond to the fitting of the reference acrylic data to the sum of two Cole-Cole functions, dotted and dash dotted lines representing the components and solid line the sum

due to motions involving the PU chains segments. As the reference acrylic sample does not contain such PU chains, in order to obtain an accurate description of the α-relaxation process we preferred starting our analysis with the dielectric data obtained for the reference acrylic sample (PEHA). The α-relaxation process was modelled by the sum of two Cole-Cole [84] functions (Eq. 4.2, with $\beta = 1$) to take into account not only the main relaxation, but also a slower and weak contribution detectable as a shoulder that could be related to the presence of a minor amount of hydroxyl groups as part of the acrylic chains. It is important to clarify that due to the weakness of this relaxation, in the final fitting (see Figure 5.4) at all temperatures, both the shape parameter and relaxation strength of the weak relaxation component were fixed to the average parameter values obtained in a preliminary unrestricted fitting. Figure 5.4 shows that fitting in this way the loss data of the reference acrylic polymer are very well described.

When fitting the dielectric α-relaxation of the Sol and Gel samples we used an approach similar to that used for the reference sample but with further constrains. Namely, these two samples evidence the presence of extra contributions at lower frequencies that would be related with the presence of the PU chains. This prevents an accurate characterization of the weak component of the α-relaxation in these two samples and consequently we have restricted the fitting by imposing constrains to the three parameters

describing the weak component. Namely, the ratios between both the relaxation times and relaxation strengths of these two components as well as the shape parameter of the weaker were fixed to those describing the reference polymer. This is justified by the assignment of this weaker component to minor molecular groups that would be in any case related with the acrylic main chain and consequently both components are expected to change in a similar way when incorporating the PU branching chains. Furthermore, a power law tail-like contribution was added to account for the mentioned extra low frequency losses, with a fix exponent value -0.15, which was found adequate for describing the data of Sol sample at 300 K in this intermediate range (see below). As can be seen in Figure 5.5, in this way a very good fitting is obtained by allowing only four parameters to vary, namely the relaxation time, shape and strength of the main component of the α-relaxation and the amplitude factor of the power law contribution.

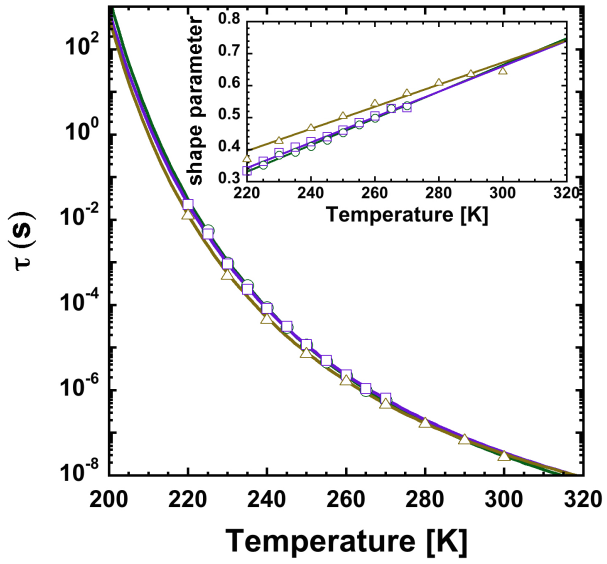

Figure 5.5: Characteristic relaxation times for Gel (open circles), Sol (open squares), and the reference acrylic polymer (PEHA) (open triangles). The lines in the figure correspond to VFT fitting

The similarities in the α-relaxation range for the three samples observed in Figure 5.5 are confirmed in a more quantitative way by comparing the temperature dependence of the main relaxation parameters so obtained. Particularly, the characteristic relaxation times (τ_{max}) for the three samples, Gel, Sol and PEHA, (see Figure 5.5) exhibit typical super-Arrhenius behaviour with minor differences that could be straightforwardly associated to the small changes in the glass transition temperatures as detected by DSC. For a quantitative probe of that, we have fitted the data by using the Vogel-Fulcher-Tammann (VFT) equation [85, 86, 87]. The VFT equation reads

as:

$$\tau = \tau_\infty exp\left(\frac{DT_0}{T - T_0}\right) \tag{5.1}$$

where the value of τ_∞ has been fixed to one ps., which is in the range of the time corresponding to the molecular vibrations, T_0 is the so-called Vogel temperature, and D is a dimension-less parameter often related to the so called kinetic fragility index. Solid lines in Figure 5.5 correspond to the main relaxation process of the three samples, the lines fitting the data of the main relaxation component correspond in the three samples to VFT equations with fixed values of $D = 9.4$ and T_0 values changing only slightly from sample to sample. Particularly we obtain: $T_{0Gel} = 158.3$ K, $T_{0Sol} = 158.1$ K and $T_{0PEHA} = 156.9$ K. On the other hand, when comparing the VFT parameters of the weak component with those of the main one, it is found that the parameter D is much higher ($D = 18$), and conversely, the value of T_0 resulted significantly lower ($T_0 = 129$ K). Noteworthy, both time scales nearly match each other at T_g. The inset in Figure 5.5 shows the shape parameters of the main relaxation component as a function of temperature for the three samples. It is found that in the reference polymer this parameter is systematically higher (a slightly narrower peak) than in the Sol and Gel samples. However, in all cases the shape parameter increases with the temperature and the values at the highest temperatures become indistinguishable. For the relaxation strength we obtain also slightly higher values for the reference acrylic polymer, which could be expected because the ≈ 10 % reduction in the acrylate group density due to the incorporation of the PU chains. Nevertheless, the differences among samples are close to the typical uncertainties of this parameter (≈ 10 %) originated by the difficulties in the determining accurately the actual sample capacitor geometry. Namely we found: $T * \Delta\epsilon_{Gel} = 280$ K, $T * \Delta\epsilon_{Sol} = 320$ K and $T * \Delta\epsilon_{PEHA} = 360$ K.

Summarizing the relaxation results, the analysis done shows that the segmental relaxation process is made by sum of two detectable relaxation processes; one weak component and a major one that exhibit similar dielectric properties for the three samples under study.

Next, we consider the second relaxation process (DCR) that it is very pronounced in the Sol sample, i.e., the soluble part of the latex obtained, where most of the PU chains are attached to the acrylic polymeric backbone by a single end, as side chains. Figure 5.6 shows the imaginary part of the dielectric data as a function of the frequency at a temperature of 300 K, where a well-defined and asymmetric loss peak is observed. At first, these data were fitted with a Havriliak-Negami equation as the main component (short-dash line in Figure 5.6). However, in the fitting routine we also included two additional contributions. The low frequency tail increase was modelled as due to the d.c. conductivity (dotted line), i.e.,$\epsilon_0\epsilon'' = \sigma_{dc}/\omega$.

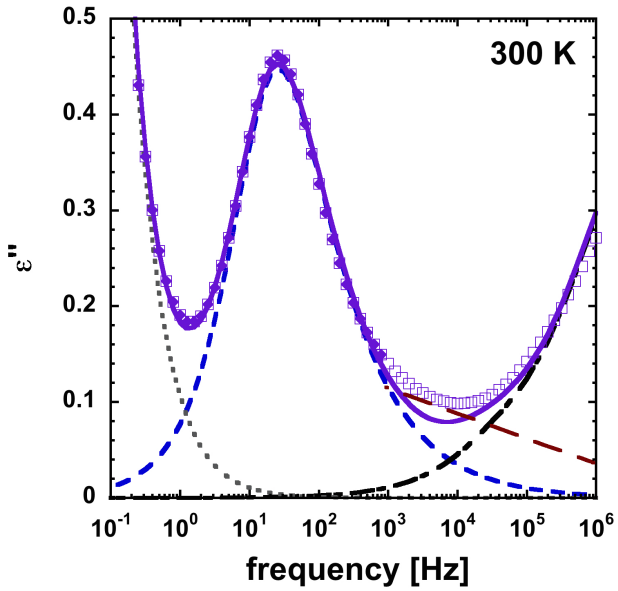

Figure 5.6: Imaginary part of dielectric permittivity as a function of frequency for Sol (squares) sample. In the figure dotted line corresponds to the conductivity, the short-dash and dot-dash lines correspond to the fitting of the data to a Havriliak-Negami and the extrapolated model for αR respectively. Solid line corresponds to the whole losses description including also the conductivity contribution. Long-dashed line corresponds to a power law description with exponent -0.15 of the intermediate range (see the text)

The high frequency range still exhibits the contributions corresponding to the α-relaxation that was modelled extrapolating the parameters obtained for this sample at lower temperatures (dot-dash line). Nevertheless, when using this procedure, there was a mismatching of the fitting function (solid line) and the data at frequencies of about $10^3 - 10^4$ Hz. This is indicative of some extra minor contribution that make the measured losses in this range to behave as a power law tail (see long-dashed line), which was used above in describing the lower temperature data at low frequencies. Because of that, the fitting parameters reported below were obtained by considering only the loss data points fulfilling the condition $0.1 < \epsilon''(\omega)/\epsilon''_{max} \leq 1$, where ϵ''_{max} refers to the loss value at the peak frequency. In fitting these data we used the sum of two contributions, a HN relaxation function and a dc-conductivity component.

Figure 5.7 show the so obtained values of the loss peak relaxation time as a function of the temperature. The inset in the figure shows the corresponding relaxation shape parameter values. When the VFT equation is used to fit the data it is found that, on one hand the pre-exponential factor of the DCR times is quite large (≈ 1.5 ns) suggesting that the molecular unit responsible

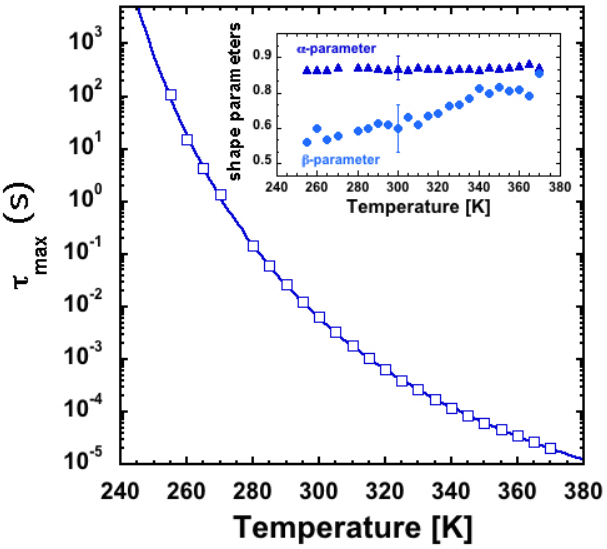

Figure 5.7: Loss peak relaxation times for the dangling chain relaxation. The line in the figure represents the VFT fit to the relaxation times. Inset shows the shape parameters of this relaxation process with representative error bars

for this relaxation is also large. On the other hand, the value of T_0 (184 K) is much higher than that of the α-relaxation. Noteworthy, the obtained value of D is 9.56, that is, nearly indistinguishable from that of the α-relaxation. Concerning the shape of the DCR, inset in Figure 5.7 shows that the loss peak is less asymmetric as temperature increases becoming relatively narrow at the highest temperatures. Finally, we found that the relaxation strength can be well approximated as: $T * \Delta\epsilon_{DCR}^{Sol} = 420$ K. i.e. about 15% larger than that of the α-relaxation at a similar temperature.

The third dielectric relaxation process (NR) is detectable only in the Gel sample at higher temperatures. This strongly suggests that it is related with the network structure, but its actual molecular origin is unclear. A detail analysis of this NR should help to this end.

Figure 5.8 shows the real part of the dielectric permittivity of the Gel sample as a function of frequency at two temperatures. Here, we can clearly identify a step like feature corresponding to the network relaxation process. However, the direct evaluation of the low frequency plateau determining the static permittivity value is prevented by an upward of the measured values, most likely due to the onset of interfacial polarization effects. Interfacial polarization arises when the conductivity of the material filling the sample capacitor increases so much that significant accumulation of ions occurs in internal sample interfaces (commonly known as Maxwell-Wagner-Sillars relaxation) [84] and/or in the contact between the sample and the electrodes.

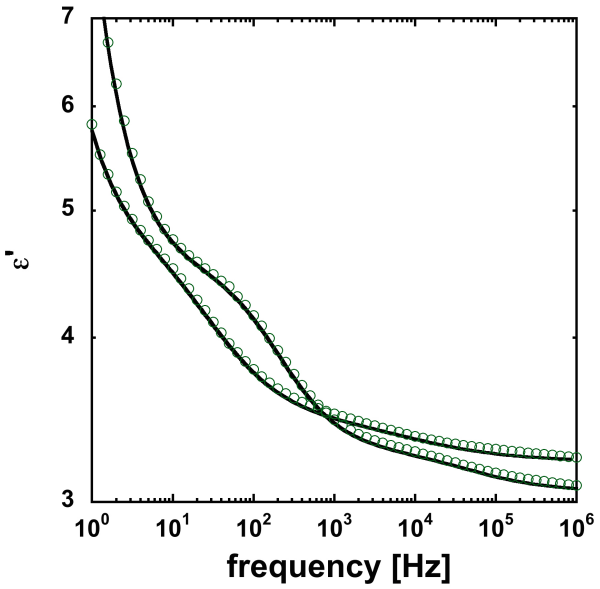

Figure 5.8: Real part of the dielectric function for Gel sample at 370 K and 410 K. Solid lines correspond to the fitting model

It is clear that at these high temperatures (more than 150 K above T_g) the conductivity of the samples is relatively high.

In order to gain more information on the NR we will also analyse the imaginary part of the dielectric data of Gel at this temperature, circles in Figure 5.9, despite the fact that the conductivity contribution is by far dominating the low frequency range (see line in Figure 5.9). The network relaxation phenomenon in this representation is not easily detectable, as the data do not exhibit any visible feature in the corresponding frequency range since the signal is dominated by the dc conductivity contribution. However, we can clearly distinguish a small shoulder appearing at higher frequencies, of about 10^5 Hz at 410 K. Thus, to identify more clearly the relaxation processes detectable in the Gel sample at this temperature, we have made use of one-dimensional derivative techniques [84, 88], namely we have calculated numerically the first derivative of the real part of the dielectric permittivity with respect to the logarithm of the frequency (squares in Figure 5.9). In this derivative representation both relaxation features become evident, a rather prominent peak is detected around 300 Hz and a weaker but well resolved one at about 400 kHz. Moreover, by comparing these data with those obtained at the same temperature for the Sol sample it seems that the weak relaxation detected in the Gel can be related with the DCR identified above (see vertical arrow in Figure 5.9).

The quantitative analysis of the Gel sample data was made by fitting both the real and imaginary parts of the dielectric data to the superposition

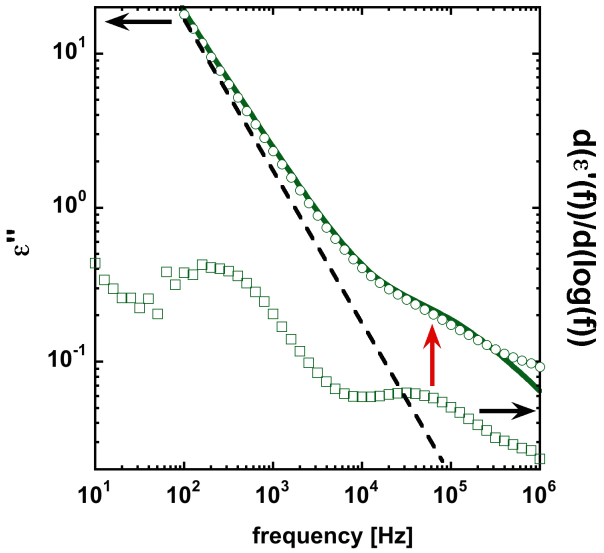

Figure 5.9: Imaginary part of the dielectric function as a function of frequency for Gel at 410 K. Solid points correspond to the measured loss data and open squares correspond to the derivative of the real part with respect to the logarithm of frequency. The arrow exhibits the peak position of the Sol sample at the same temperature. The dashed line corresponds to the dc conductivity contribution

of two symmetric Cole-Cole equations plus a d.c. conductivity contribution and an additional low frequency power law increasing of the real part. The peak time of the weak DCR component in the Gel sample was fixed to that obtained in the Sol one. This method was applied to temperatures where the NR component is still well resolved from the low frequency increase in the real part, i.e. for $T > 350$ K. Lines in Figure 5.8 and 5.9 show representative examples of this approach, evidencing that in this way we obtained a high quality fitting, maintaining a moderate uncertainty in the parameters characterizing the NR of the Gel sample. The results so obtained for the NR time of the Gel sample are presented in Figure 5.10. The lower inset in Figure 5.10 shows that the NR relaxation narrows gradually by increasing temperature. By analysing the temperature dependence of the NR times we have found that a VFT equation with either $T_0 = 184$ K (that found for DCR) or $T_0 = 158$ K (that found for αR) describe equally well the data. The corresponding values of D and τ_∞ are 11 and 90 ns, and 16 and 25 ns, respectively. Even if the uncertainty is large, the values of the pre-exponential factors are in the range of tens nanosecond, i.e. motions much slower than those of the DCR suggesting molecular entities considerably larger than those responsible of the DCR. On the other hand, it is found

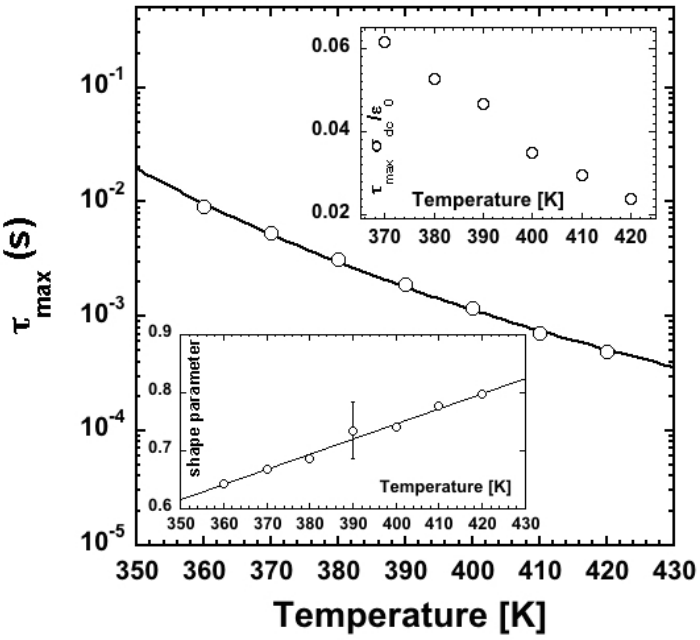

Figure 5.10: Characteristic relaxation times for the network relaxation process. The line in the main frame represents the VFT fit to the relaxation times. Lower inset shows the shape parameter of the network relaxation described by a linear temperature variation (line) with a representative error bar. Upper inset evidences the distinct temperature dependence of the relaxation time and the sample dc conductivity

that the relaxation strength of the NR is given in good approximation by $T * \Delta\epsilon_{NR} = 555$ K, which again is quite large taking into account the relatively low amount of PU chains.

The results presented above evidence that despite the similar thermal behaviour exhibit by the three acrylic based polymers investigated, they present strong differences in the dielectric relaxation around and above room temperature. Particularly, the Sol and Gel fractions of the hybrid Acrylic/PU material obtained by incorporating about 10% PU pre-polymer to the polymerization reaction of the acrylic units present prominent characteristic relaxations in addition to the more conventional relaxation connected with the glass transition phenomenon. The Sol sample shows a well-resolved loss peak, with a maximum frequency at about 100 Hz at room temperature, and the Gel sample presents a distinguishable slower relaxation reaching the same peak frequency of 100 Hz at about 100°C. The fact that in these two samples there are additional PU chains either as side chains of the main acrylic ones or as bridges forming a network (in the Gel sample only) naturally leads to relate this new relaxation processes with the presence of the

PU chains and look for the molecular origin of the resolved dielectric relaxation in connection with the distinct polymer architectures. Contrary the α-relaxation associated to the glass transition is quite similar in all the samples, which clearly indicates that it is mainly determined by the segmental mobility of the acrylic units. These results opens the possibility of using the dielectric relaxation as a tool for characterization of this kind of hybrid Acrylic/PU materials provided the molecular origin of the relaxation processes is properly addressed.

In this context, the result obtained on the Sol sample seems to unambiguously evidence that the slower relaxation detected cannot be originated by interfacial polarization phenomena, but must be attributed to the dynamics of the PU chains attached to the main acrylic ones. The reason is that the low conductivity of the sample in the relevant temperature range ensures that the dielectric relaxation detected is due to some molecular dipole fluctuation. Furthermore, it is expected that the presence of PU chains in this sample should necessarily result in higher values of the static permittivity because the incorporation of quite strong molecular dipoles. Since there is no hint of contribution of such additional dipoles to the dielectric α-relaxation (the α-relaxation strength decreases a bit with respect to the reference only acrylic sample) the one detected at higher temperatures/lower frequencies must be originated by these PU chains. When considering the specific characteristics of this relaxation process it is very significant the fact that the relaxation time changes with temperature according with a VFT equation with a pre-exponential factor much higher than the reciprocal of the typical vibrational frequencies. This implies that the molecular dipole would involve a relatively large molecular entity. For instance, this is the case of the terminal relaxation in polymers that in some cases is also detectable dielectrically as the so-called normal mode relaxation. This dielectric relaxation is the result of the fact that in these polymers (1,4 cis-polyisoprene as a prototype) [89] there is a dipole moment proportional to the end-to-end chain vector and therefore a detectable dielectric relaxation reflecting these fluctuations. However, there is not evidence of the presence of an end-to-end dipole moment in PU polymers. Moreover, if any, the strong dielectric strength and quite narrow loss peak DCR would be hardly compatible with this origin. Note particularly that the time scales of a normal mode depends as a power of the chain mass with the exponent 3 for untangled chains, and 3.4 for larger chains, so only for very monodisperse polymers a narrow dielectric loss peak can be found.

On the other hand, it has already been widely reported [90, 91, 92, 93] that the so called segmented polyurethanes are typical block copolymers with a block consisting of a relatively flexible soft segment (SS) and the other block forming a highly polar hard segment (HS). This structure usually leads to microphase separation (MS) at mesoscopic length scales, resulting

in a morphology consisting of microdomains rich in each of the blocks. The DSC results of the Sol fraction (see Figure 5.2) had evidenced the presence of a weak jump of the heat capacity at around 240 K (30 K above the main glass transition) that could be indicative of the occurrence of some PU segregation in this sample. This opens the possibility to associate the observed dielectric relaxation to this segregated phase. Taking into account the temperature where the DCR is detectable ($\tau_{DCR} = 1$ s at $T \approx 270$ K as seen in Figure 5.5), it cannot be directly associated to the glass transition phenomenon within this phase. Contrary, as aforementioned, the properties of the DCR point to a bigger scale motion.

It is well known that PU segments have a strong tendency to crystallize [94]. The investigated samples show no signature of crystallization, but this circumstance can favour the development of some orientational correlation [95]. So, a suitable origin of the DCR could be the presence of certain kind of mesogenic order in the segregated phase, which would be compatible with the relatively large molecular entity responsible for the DCR. Moreover, the existence of mesogenic-like entities with relatively strong dipole moment can result in a significant dipole orientation correlation. This scenario could explain the quite strong DCR strength observed experimentally that arises due to just 10% of PU pre-polymer, which was added in the synthesis formulation. However, one question that remains to be clarified in this picture is whether a dielectric signature of the glass transition in the segregated phase exists. To answer this, we performed Thermally Stimulated Depolarization Current (TSDC) experiments [84, 96] which confirmed the presence of a distinguishable peak in the depolarization current at around 235 K just in between the two main peaks related respectively with the main α-relaxation at 208 K and the DCR at 255 K. Such a weak additional dielectric relaxation component will also be the responsible of the miss fitting of the Sol sample loss data shown in Figure 5.6 in the valley (at around 10^4 Hz) in between the two main loss peaks. In this framework, the observation of a DCR component also in the Gel sample would be due to the existence of residual PU chains attached by a single end to the acrylic main chain without being involved in the network formation

The assignment of the slowest relaxation detected in the Gel sample is less straightforward. A main reason is that in the relevant temperature range the sample conductivity is relatively large, which can give rise to relaxation processes reflecting charge trapping at interfaces. Trying to test this possibility we have analysed the temperature dependence of the dc conductivity and compared it with that of the NR time. The upper inset in Figure 5.10 shows that the quantity $\tau_{NR}\sigma_{dc}/\epsilon_0$ changes markedly with temperature, opposite to the expectation of simple models of dielectric relaxation associated to charge trapping [84]. On the other hand, the shape of the relaxation associated to charge trapping would be determined by the spatial distribution of

the trapping interfaces and it would not be expected to change significantly with temperature. However, our finding is a marked decrease of the NR when increasing temperature. Overall, these results point to the fact that the NR is not originated in a charge trapping process but it would reflect the fluctuations of some molecular dipolar entity. Since the α-relaxation in the Gel is also quite similar to that of the pure acrylic polymer, these molecular entities should involve the PU chains that in the Gel are cross-linking chains responsible for the network formation.

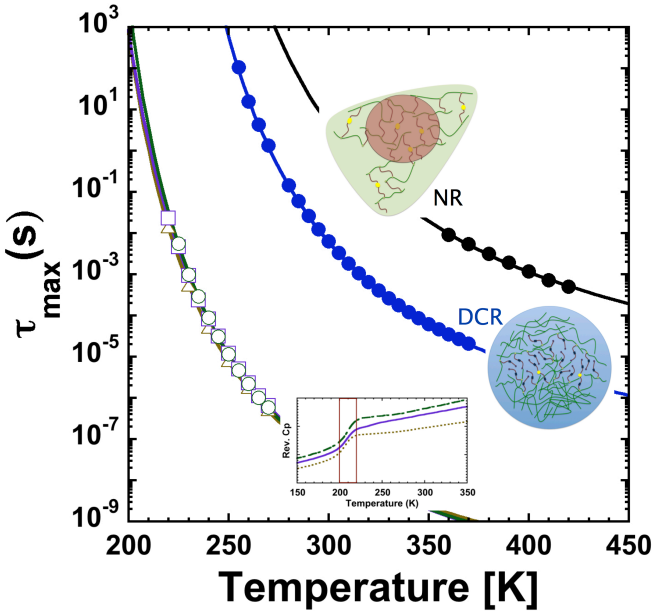

Figure 5.11: Characteristic relaxation times as a function of temperature for the three different relaxation processes (αR, DCR, NR) studied in these Acrylic/PU polymers. Correspondingly a schematic representation of entities responsible for the relaxation processes is depicted

The differences respect to the DCR would be related with the fact that both PU chain ends are attached to the main acrylic backbone. This network structure would, on one hand, restrict the possibility of the PU units to form a well-segregated phase and on the other hand it would slow down the corresponding dipole moment fluctuations. Moreover, it is known that most of the PU chains forming the network have been extended during the synthesis process [9] (see scheme c in Figure 5.1). This together with the required fluctuations of the network junction points would results in a large size of the molecular entities involved in the dipole moment fluctuations responsible of the NR. These could be bundles of PU hard segments forming part of the crosslinking chains with some degree of orientational order that would require the fluctuation of the network structure for a full decorrelation

of the resulting dipole moments. A schematic representation of these bundles is depicted in NR-drawing of Figure 5.11. In this drawing we also included some of the remaining PU chains attached by a single end that would be responsible for the weak DCR component in the Gel. Additionally, Figure 5.11 shows a quantitative and qualitative summary of the three different dielectric processes studied in the Acrylic/PU samples together with schematic representations of the entities responsible for these relaxation processes.

This molecular framework allow us the possibility to study the network relaxation characteristics for different Gel fractions of hybrid materials synthesized via miniemulsion photopolimerization with distinct protocols and also to compare it with a sample synthesized via thermal miniemulsion polymerization. In the following subsection we will describe the structural and dynamical results for the three different gel fractions investigated.

5.3.2 Effects of the synthetic conditions in the network structure of hybrid Gels

We will start with the results obtained by DSC for the three different Gel fractions of latex A, B and C (5.1) named, Gel A, Gel B and Gel C respectively. Figure 5.12 shows the reversing heat capacity as a function of the temperature for the three Gel samples under study, the data were obtained while cooling the materials from 420 K at a rate of 3 K/min. The DSC data showed no signatures of crystallization and/or melting processes in the explored temperature range (up to 470 K). Moreover, the three samples exhibit similar thermal behavior, particularly in the glass transition region, where all present a clear step like feature at a temperature of about 210 K. In order to highlight possible differences (if present) we also used the derivative of the reversible heat capacity as a more sensitive representation (depicted as inset in Figure 5.12). In the inset, we can notice a distinguishable peak centered around 210 K that corresponds to the glass transition which is similar for the three samples. Furthermore, the thermodynamic curves present similar behavior up to temperatures of about 420 K, within the statistical errors. Thus, even though DSC is a useful technique and help us to identify the glass transition temperature for these particular Acrylic-Polyurethane samples (at about 210 K), it does not reveal any clear difference related with the synthesis conditions.

Broadband Dielectric Spectroscopy measurements provides us a suitable method for characterizing this complex Acrylic-Polyurethane hybrid materials. We will start this subsection with results and comparison for the three samples under investigation. Figure 5.13a presents the real part of the dielectric permittivity as a function of the temperature at a frequency of 1 Hz (isochronal representation). This way of presenting the data allow us to visually identify the relaxation phenomena occurring in different temperature regions. Here we can clearly distinguish three different regions where dielec-

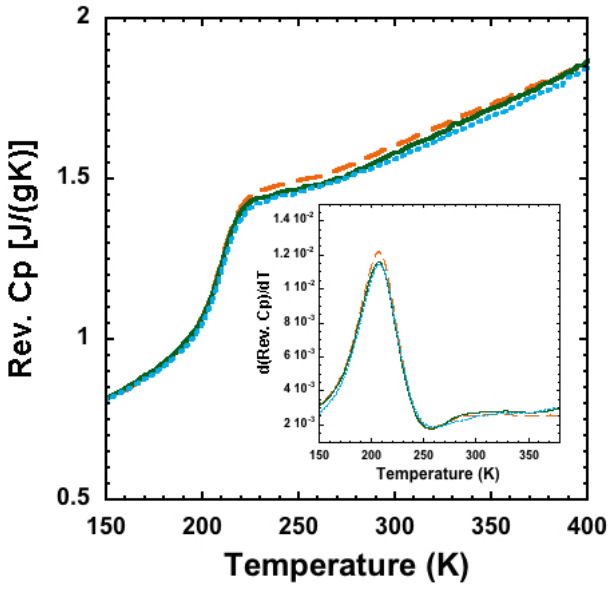

Figure 5.12: Differential Scanning Calorimetry curves for samples Gel A (dashed line), Gel B (solid line) and Gel C (dotted line). The inset shows the reversible heat capacity derivative with respect to temperature for all samples

tric processes occur. In a previous publication, the dielectric relaxation of the Gel B sample in comparison to both, that of the sol fraction and that of a purely acrylic sample, was reported. In this way, we were able to identify three different molecular entities responsible for the dielectric relaxation phenomena observed in the Gel fraction. The dielectric relaxation phenomenon present at low temperatures (about 210 K) was related to the segmental motion of dipole groups corresponding to the acrylic backbone, that is the α-relaxation (αR). The relaxation process observed at about 280 K was related to motions involving Polyurethane (PU) chains attached to polymer acrylic backbones by only one end, since it was the most prominent in the sol fraction. This relaxation was referred to as dangling chain relaxation (DCR). The relaxation process observed at temperatures above 320 K was only present in the Gel fraction of the previously studied latex and therefore it is closely related to the network structure. This relaxation phenomenon was attributed to dipolar entities formed by aggregation into bundles of PU chains which are responsible for the reticulated structure of the Gel and for this reason named network relaxation (NR).

When comparing the real part of the dielectric data of different Gel samples (see Figure 5.13a), we notice that in the lowest temperature region (about 210 K) the real part of the dielectric permittivity exhibits a similar well-defined step present in the three samples, this similarity is in accordance

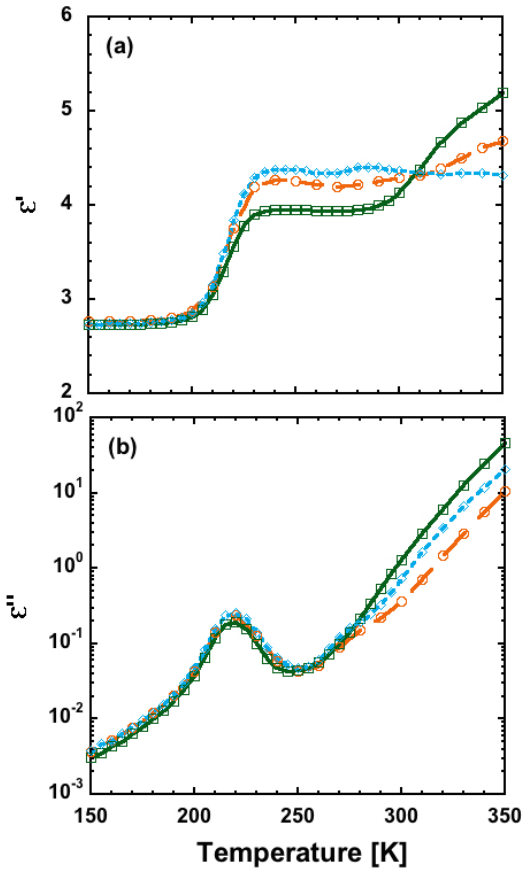

Figure 5.13: Real (a) and Imaginary (b) parts of the dielectric permittivity as a function of temperature for Gel A (circles), Gel B (squares), and Gel C (diamonds), in the isochronal representation at 1 Hz. Lines in the figure are used as guides for the eye

with the coincident glass transition observed by means of DSC on the samples. Figure 5.13b presents the imaginary part of the dielectric permittivity in the isochronal representation at the frequency of 1 Hz. The dielectric data in the first temperature region also confirm these results. Consequently, as this relaxation is attributed to the movement of dipolar segments of the polymeric acrylic backbones and it is not affected by the synthesis method the α-relaxation will not be the further discussed in this work.

Looking at higher temperatures of about $240-300$ K, in Figure 5.13a we can notice a second relaxation process visible for Gel A and Gel C samples and hardly identifiable in this representation for Gel B. As above commented, this relaxation process was related to the dangling chain dynamics of the PU polymers attached to the acrylic backbone. In this high temperature range the dc conductivity contributions to the dielectric losses strongly overlap

the dipolar relaxation (see Figure 5.13b). Nevertheless, between 240 K and 300 K, in the loss permittivity we can still detect the presence of the DCR relaxation process, namely for Gel A and Gel C, and not so obvious for Gel B. At temperature above 320 K, in Figure 5.13a we detect a third relaxation process visible in the three Gel samples, that would be the most relevant in connection with the network characteristics. Observing the dielectric data in this temperature range we notice that the jump of the permittivity in this relaxation is quite small in the case of Gel C. This relaxation is completely hindered in the dielectric loss data.

In order to extract more information about the network-related phenomena a quantitative evaluation is required. Hence we analyzed the data in the isothermal representation. Due to the strong conductivity contributions at high temperatures, the analysis of the dielectric relaxation behavior was performed using the first derivative of the real part of the dielectric permittivity [88, 84].

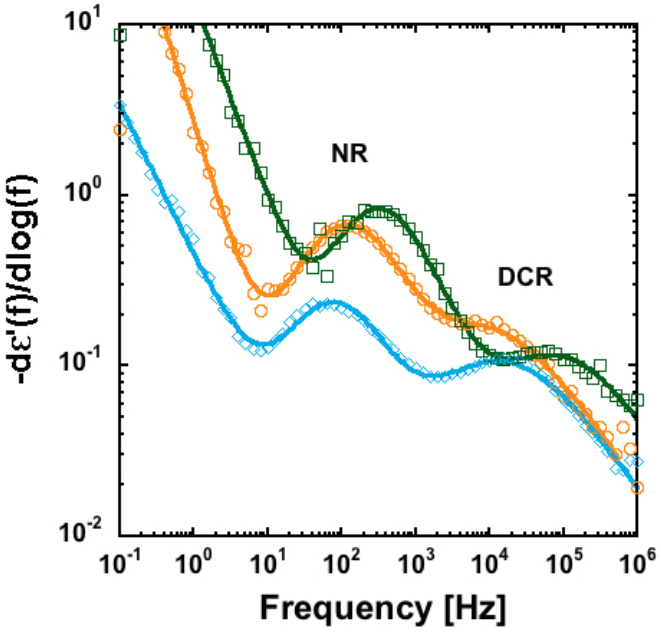

Figure 5.14: Derivative of the real part of the dielectric function with respect to the logarithm of frequency for the three samples Gel A (circles), Gel B (squares) and Gel C (diamonds), solid lines correspond to the fit of the curve (see description)

Figure 5.14 presents the dielectric data in the derivative representation at a temperature of 420 K for the three Gels. In this representation, a step-like feature in the real part of the dielectric permittivity is transformed into a peak (narrower than the one present in the imaginary part of the dielectric permittivity and without the influence of the dc conductivity). In the figure

the two relaxation processes NR (leading to the peak about 10^2 Hz) and DCR (responsible for the peak at 10^4 Hz) are clearly evident for the three samples. In this kind of representation we can follow both relaxation processes down to temperatures of about 350 K. It is quite obvious that the two relaxation processes are faster for Gel B sample. As we are interested in quantifying the differences between the network-related relaxations of the three Gels, the analysis of the relaxation characteristics was performed by fitting the derivative data at relatively high temperatures where the α-relaxation is out of the window. Thus, the superposition of two symmetric Cole-Cole equations [84] (to take into account DCR and NR processes) plus an extra power law contribution to account for the electrode and/or interfacial polarization phenomena was used,

$$\epsilon^{'}(\omega) = \epsilon_{\infty} + Re\left(\frac{\Delta\epsilon_1}{1+(i\omega\tau_1)^{\alpha_1}} + \frac{\Delta\epsilon_2}{1+(i\omega\tau_2)^{\alpha_2}}\right) + \left(\frac{A}{\omega}\right)^{\kappa}. \tag{5.2}$$

Here, $\omega = 2\pi$f, ϵ_{∞} is the high frequency limiting permittivity, A and κ are the parameters used to take into account the electrode and/or interfacial polarization contributions, α_i denotes the symmetric broadening of the relaxation component i $(= 1, 2)$, $\Delta\epsilon_i$ corresponds to its relaxation strength and τ_i refers to its characteristic relaxation time.

Figure 5.15 shows the so obtained characteristic times τ of both relaxation process (DCR as solid symbols and NR as empty symbols) for the three samples. Both relaxation processes exhibit typical super-Arrhenius temperature dependence. We can notice that in the network relaxation process (empty symbols) Gel A and Gel C exhibit similar characteristic relaxation times around 400 K, however the temperature dependencies are different. Comparing the samples Gel A and Gel B, the opposite situation is found, that is, the temperature dependences are rather similar but the characteristic relaxation times are quite different. In an analogous way, in the case of the dangling chain relaxation process, when comparing the temperature dependence we see that it is quite similar between Gel A and Gel B samples but clearly different for Gel C. Furthermore, the relaxation times of the DCR process are quite different for the three samples. Gel B gives the smallest values of the relaxation times, i.e., the fastest relaxation process, followed by Gel C that gives intermediate values, and Gel A that corresponds to the slowest DCR process.The data in Figure 5.15 have been described by using a Vogel-Fulcher-Tamman (VFT) equation [85, 86, 87],

$$\tau = \tau_{\infty} exp\left(\frac{B}{T - T_0}\right), \tag{5.3}$$

where τ_{∞} is the high temperature limiting relaxation time, B is an energetic constant and T_0 is the so called Vogel temperature. Due to the relative

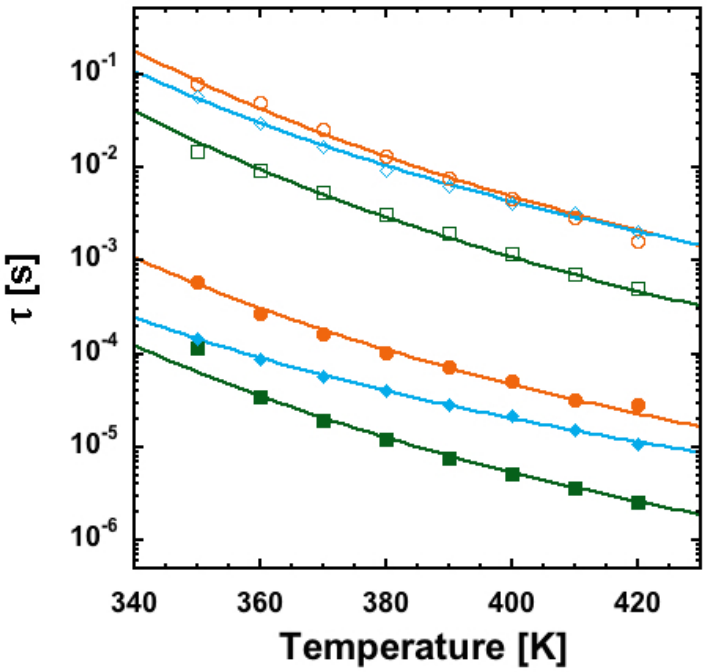

Figure 5.15: Characteristic relaxation times of the network relaxation (unfilled) and dangling chain relaxation (filled) processes for Gel A (circles), Gel B (squares) and Gel C (diamonds) samples. Lines in the figure correspond to VFT fits.

narrow range of time scales available for each relaxation process, the accurate determination of the three parameters of the VFT by a free fitting is not feasible. Thus, we fixed the value of T_0 to that determined previously for the α-relaxation time of Gel B ($T_0 = 158$ K) [97]. Since, as commented above, the segmental dynamics is not sensitive to the distinct network characteristics of our samples, using the same value of T_0 for all samples is well justified. Moreover, due to the aforementioned similarities in the temperature dependence between Gel B and Gel A samples we looked for a common B parameter value, on the contrary a different B value was necessary for describing data of Gel C. The so obtained fitting curves are shown as solid lines in Figure 5.15, being the parameters τ_∞ and B reported in Table 5.2.

Table 5.2: Characteristic dielectric relaxation parameters for the Gels.

Samples	$\tau_{\infty DCR}$[ns]	B_{DCR}[K]	$\Delta\epsilon_{DCR}$	$\tau_{\infty NR}$[ns]	B_{NR}[K]	$\Delta\epsilon_{NR}$
Gel A	3.5	2300	0.83	85	2650	2.34
Gel B	0.4	2300	0.58	19	2650	2.86*
Gel C	10.5	1830	0.65	250	2360	0.88

Now, centering our attention in the relaxation strength (see Figure 5.16) we notice that the behavior of the three Gels is also quite different. The network relaxation process of Gel B presents the largest relaxation strength, decreasing smoothly as the temperature increases. The temperature-dependance for the other two samples is similar, yet the relaxation strength of Gel A is much larger than that of Gel C but still smaller than the value of Gel B. For the case of the dangling chain relaxation, the relaxation strengths of Gel A, B and C are quite low. The average relaxation strength values for both relaxation processes at temperatures of around 390 K are given in Table 5.2.

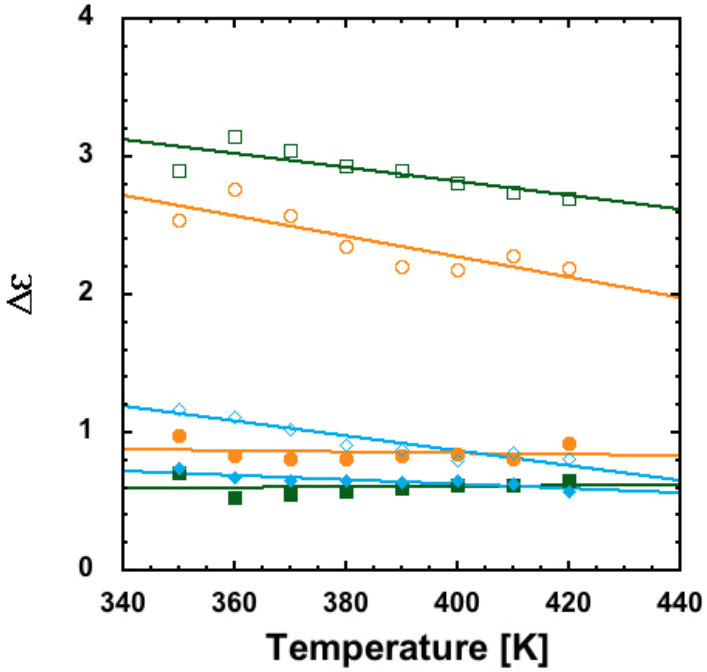

Figure 5.16: Relaxation strengths of the network relaxation (unfilled) and dangling chain relaxation (filled) processes for Gel A (circles), Gel B (squares) and Gel C (diamonds) samples. Lines in the figure correspond to the linear fit

In order to get insight into the structural features of these materials, we performed X-Ray diffraction experiments covering the SAXS and WAXS regions. The diffractograms for the three Gel samples are shown in Figure 5.17. All Gels exhibit two broad but well resolved peaks for high values of the scattering vector, namely, centered around $q_1 \approx 0.41\text{Å}^{-1}$ and $q_2 \approx 1.57\text{Å}^{-1}$. From these peak positions, periodicity lengths of about 1.5 and 0.4 nm respectively can be deduced in the Bragg approximation ($d = 2\pi/q_{max}$). These peaks are also present in the reference acrylic sample, as can be seen in Figure 5.17. A number of structural investigations on polymers with long

or bulky side groups [98, 99, 100, 101, 102, 103, 104] –like those considered in this work– including e. g. the family of poly(n-alkyl acrylates) [98] have established a scenario of nano-phase segregation between main chains and side groups to explain the origin of these peaks in the diffraction patterns [98, 105, 106]. All these systems display a 'pre-peak' in the region where we find q_1, that has been attributed to the existence of nano-domains rich in each of the polymeric subspecies (main chains or side groups). Such hypothesis was supported by coarse-grained simulations on generic comb-like polymers [107]. Peak at q_1 would be related to inter-domain correlations [107]. Within this context, peak at q_2 is assigned to correlations between atoms belonging to side groups of different monomers within a nano-domain.

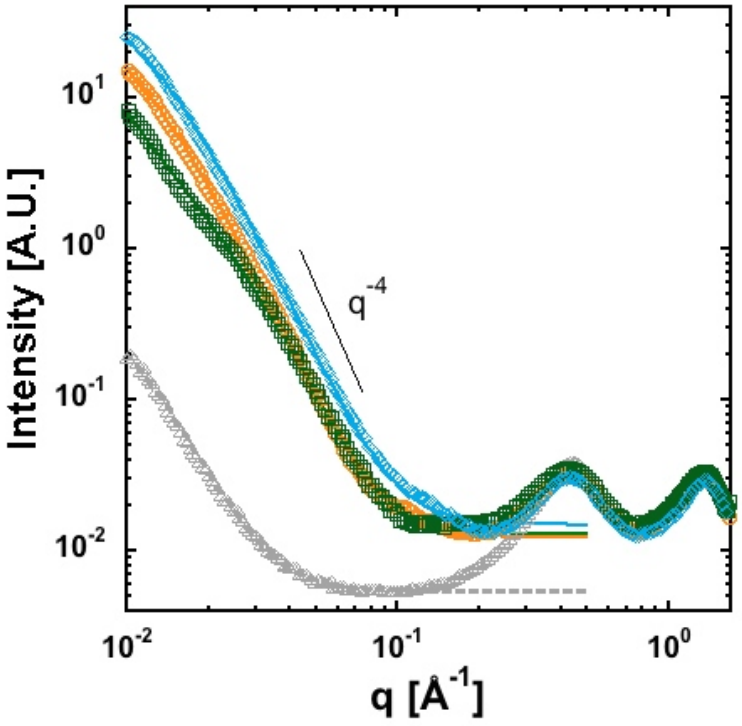

Figure 5.17: X-Ray diffractograms for Gel A (circles), Gel B (squares) and Gel C (diamonds) at room temperature. Data obtained for the acrylic polymer (triangles) is also shown for comparison. The Lines correspond to different fittings (see the text).

For q-values within the range $\approx 0.1 - 0.2$ Å^{-1}, extra intensity contributions are observed for samples that have PU chains incorporated within the synthesis method, i.e., the Gel fraction of the Acrylic-PU latex but not the reference linear Acrylic polymer. This extra intensity has to be related with contributions that arise from the contrast given by the presence of PU chains. Further decreasing the q-value, the scattered intensity rapidly increases for

the three Gel samples. Gels A and C display a slight convexity, while for Gel B a broad shoulder is readily resolved. However, the reference linear acrylic polymer also presents a low-q increase of intensity. This behavior can be attributed to the microstructure generated by miniemulsion polymerization, with typical sizes of $100 - 200$ nm [24]. We have found that this low-q scattered intensity can be well described by a power law with exponent value of -3.6 (see dashed line in Figure 5.17). Such a scattered intensity is expected to be present in the Gel samples also prepared by miniemulsion polymerization but the increasing at low q in the Gel samples is more pronounced. The extra low-q intensity in the Gel samples at $q \leq 0.2$ Å^{-1} can be described by the Debye-Bueche function [108],

$$I_{DB} = \frac{I_o}{[1 + (\Xi q)^2]^2}. \tag{5.4}$$

Where I_o is an amplitude factor that depends on the correlation length Ξ and the scattering contrast between the phases leading to the observed inhomogeneities. This function is usually used for neutral Gels, to describe the large-scale inhomogeneities produced by concentration fluctuations of the network that are influenced by the physical constraints imposed by the cross-links [109, 110]. In the present hybrid Gels the origin could also be related with the presence of clusters formed by the urethane groups. The fit of the low-q data using Eq. 5.4 plus a constant background and an additional $q^{-3.6}$ contribution -reflecting the latex structure- is shown by solid lines in Figure 5.17. The fitting of Gels A and C delivers very similar values for the correlation length ($\Xi = 96$ and 88 Å for Gel A and Gel C, respectively). The intensity I_o is somewhat larger for Gel C than for Gel A. We note the markedly different behavior of Gel B, with a well distinguishable shoulder in the region of about ≈ 0.02 Å^{-1}. The value of the correlation length, Ξ, obtained for Gel B was 52 Å, i.e., it is about half of those observed for Gels A and C.

Our results evidence that the distinct network characteristics of the three Gel samples investigated manifest in the dielectric relaxation behavior at frequencies/temperatures lower/higher than that characteristic of the segmental relaxation. However, the segmental dynamics, and the related thermal glass-transition as well, is rather insensitive to the network characteristics. In agreement with these results the X-ray diffraction features of the three samples differ mainly at low q values (correlation lengths larger than few nm). In the following we discuss the connection of the analysis of the dielectric relaxation data at relatively high temperatures with the structural features determined by SAXS.

In order to understand the differences exhibited by the network relaxation it is useful to recall the molecular interpretation described previously, recall that Acrylic-PU samples present mainly three different dielectric relaxations,

the α-relaxation, the dangling chain relaxation and the network relaxation. The dipolar entities responsible for the α-relaxation were attributed to segments of the acrylic main chains. In the case of the dangling chain relaxation, the entities were related to PU chains attached by only one end to the acrylic main chain, without being involved in the network formation. Finally, the network relaxation process was reported to be originated by the presence of orientationally correlated urethane-segment bundles belonging to PU chains linked by both ends to the acrylic main chain and forming the Gel network. The presence of such large molecular entities responsible for the relaxation phenomena was inferred by the high values of both the dielectric strength and the limiting high temperature relaxation time [97].

Now, when comparing the values of τ_{max} obtained for the network relaxation in the three Gel samples at 400 K, we see that Gel A and Gel C show both values close to 5 ms and that τ_{max} is nearly a factor of 5 smaller for Gel B (see Figure 5.15). Thus one would infer that the size of the bundles in Gel B is smaller than that in the other Gel samples. This result is well correlated with the SAXS diffraction patterns, where relatively large correlation lengths were inferred for Gel A and Gel C but the correlation length in Gel B was clearly smaller. This direct correspondence between dielectric relaxation results and SAXS can be rationalized considering that the identified SAXS features correspond to the typical distance among bundles. In this case the bigger bundles of Gels A and C will be, in average, apart from each other more than the smaller bundles in Gel B, since the PU-Acrylic ratio is quite similar in the three Gel samples, being however the value of Gel B slightly lower than those of Gel C and Gel A - the differences of the PU-Acrylic ratio for different samples were estimated using ATR-FTIR measurements, by calculating the ratio of the intensities of two specific PU (1115 cm^{-1}) and Acrylic (1160 cm^{-1}) bands identified in the IR spectra of each Gel sample.

Regarding the dielectric strength of the network relaxation, we know that this parameter is not only determined by the amount of molecular dipoles participating in the relaxation process but also by any orientational correlation between urethane dipoles constituting these dipolar entities (bundles). Particularly, the larger the orientational correlation between urethane dipoles is, the higher the resulting dipole moment of the bundle entity would be. Since there are no significant differences among the Gels in the amount of urethane units, the results obtained for the network relaxation strengths of the different Gels (see Table 5.2) suggest that the correlation between neighboring urethane dipoles forming the bundles is strong in Gel B, not so much in Gel A, and clearly less important in Gel C. The lesser dipolar correlations in Gel C may be related with the fact that this Gel was synthesized by thermal polymerization, whereas Gel B and Gel A both showing significant PU dipole correlation were obtained via photo-polymerization. The different polymerization methods used in the synthesis of the Gel samples could also

explain the different temperature dependence of the relaxation times manifested in the distinct values of the energetic parameter B obtained by the VFT fitting of both NR and DCR relaxation times (see Table 5.2). Now the question is what are the reasons for the differences observed between Gel A and Gel B samples, particularly the quite different bundle sizes.

A way of rationalizing the large differences in size and mobility between both Gels could be related with constrains imposed by the anchorage of the PU chains to the acrylic-backbone. The shorter the linkage between the bundles and the acrylic backbone is the slower the relaxation is expected to be. Both samples were prepared with the same molecular weight PU-prepolymer and with similar concentration of their components (in particular PU 10% wbo). However, in the synthesis formulation there was also a small fraction of Bisphenol A that promotes the chain extension of the PU chains forming the network by connecting two or more PU pre-polymer chains. Therefore, the present results can be indicative that chain extension occurred more efficiently in Gel B than in Gel A.

To understand how this can occur let us recall some ideas underlying the polymerization process of the produced latexes. Miniemulsion polymerization is one of the most useful techniques for producing waterborne nanocomposites; it allows the possibility of working with pre-formed hydrophobic polymers, plus the advantage that step-growth and free radical polymerization can be carried out within the miniemulsion droplet. In order to obtain hybrid latex products, the polymerization of the acrylic components is driven by the free radical polymerization mechanism. On the other hand, the polymerization of the urethane/urea components is activated by step-growth polymerization. Moreover, in the case of miniemulsion photo-polymerization the Gels are formed only by reaction of OH groups of the HEMA units of the acrylic polymer chains (free radical polymerization) with the NCO groups of the PU (step-growth polymerization). The free PU can be incorporated into the acrylic network in one of several distinct ways [111]; 1) by direct reaction with pendant hydroxyl groups in the acrylate chain, 2) chain extension by Diol's and subsequent reaction with pendant NCO groups from the acrylic chain, or 3) by addition of water to NCO groups and subsequent rapid urea forming with the pendant NCO groups in the acrylic chain. In the polymerization conditions used for our samples, PU extension seems to be more favorable by reaction with water [111].

The effect of having extended PU chains would be two-fold. On one hand, a larger linkage to the acrylic backbones would reduce the restriction in movement of the bundles related with the proximity of the anchorage site, thus explaining a faster relaxation in Gel B sample. On the other hand, larger linkages would allow a better dispersion of the urethane groups in Gel B sample, which would result in smaller bundles. If this interpretation is correct one should expect a significant amount of chain extender entities in

the network of Gel B. Looking for a signature of such extender entities we performed FTIR experiments on Gel A and Gel B samples.

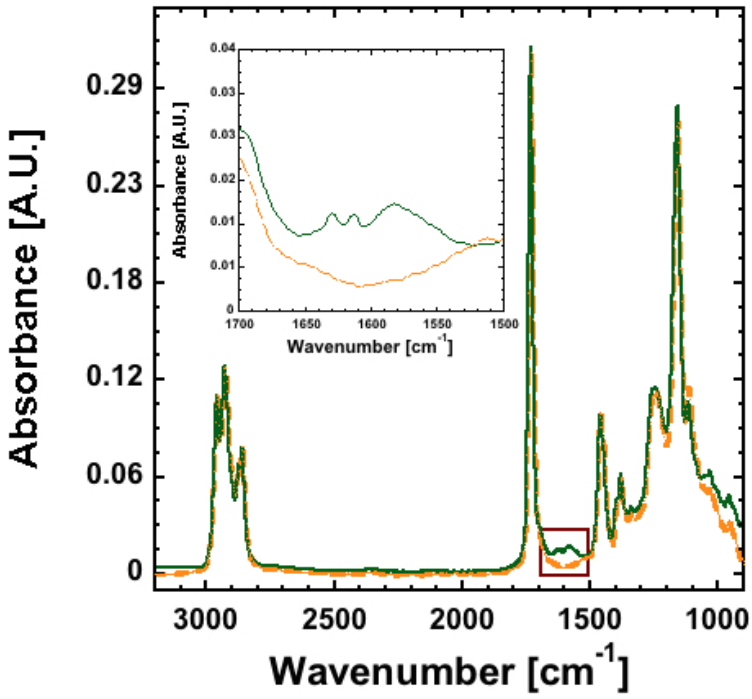

Figure 5.18: Fourier transform infrared spectrum (FTIR) for Gel A (dashed line) and Gel B (solid line). Inset in the spectrum highlights the differences exhibited by relevant bands in the corresponding range for both samples

By analyzing both Gel samples by FTIR experiments we detected (see Figure 5.18) extra weak absorption bands for Gel B in the range of $1700 - 1500$ cm^{-1} that could be attributed to the presence of these extender entities. When the same comparison is made in samples not previously subjected to a careful drying, also extra absorption bands for Gel B arise in the range of $3300 - 3500$ cm^{-1} were the OH related contributions usually appear [112, 113, 114]. A termogravimetric analysis of the two Gels showed that both also differ in the water-vapor uptake ability, up to 3 % for Gel B and less than 0.1 % for Gel A (see the following Figure). The greater water-vapour uptake of Gel B sample could be also rationalized as the effect of the efficient incorporation of chain extenders that would promote the formation of hydrophilic sites.

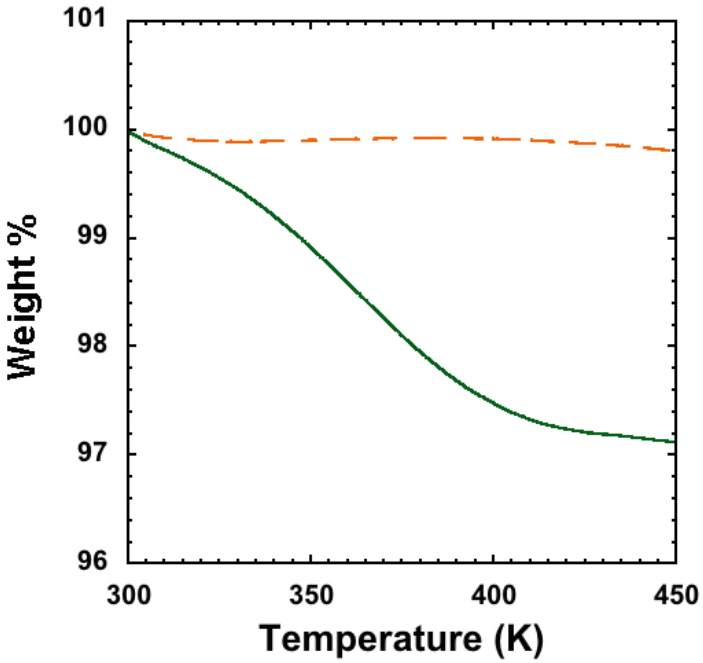

Figure 5.19: Termogravimetric scans for Gel A (dashed line) and Gel B (solid line) samples.

5.4 Conclusions

In this chapter we showed that Broadband Dielectric Spectroscopy (BDS) technique provide a suitable method for characterizing complex hybrid Acrylic / PU pressure sensitive adhesive materials. Despite the similar thermal behaviour of the three materials investigated, BDS results show up quite clear differences. We have been able to identify and establish the reason for these differences on the basis of a molecular assignment of three main different relaxation processes. Particularly, the fastest of these relaxation processes is attributed to the segmental motion of the main acrylic chains (αR) and thus it exists in all samples. The analysis of the second fastest relaxation process that it is completely absent in the reference pure acrylic polymer and very prominent on the Sol sample it is attributed to the presence of some orientational correlations in the segregated PU phase. In this framework, the observation of a DCR component also in the Gel sample is attributed to the existence of residual PU chains attached by a single end to the acrylic main chain without being involved in the network formation. Concerning the slowest relaxation process (NR) that it is only present in the Gel sample, it has been attributed to the presence of orientationally correlated PU hard segment bundles of the PU chains forming the Gel network. A step forward in this direction lead us to the comparison (in particularly of the

NR) between different Gel materials obtained by using the same chemical ingredients but varying synthetic conditions. Despite of the similar thermal behavior of the three samples, BDS results show up important differences of the characteristic dielectric parameters for two of the relaxation processes detected at frequencies lower than those of the segmental dynamics. Particularly, the network dielectric relaxation process shows differences in the dielectric parameters that have been rationalized in connection with the corresponding synthesis method used. In this way, we show that the Gel produced via thermal polymerization presents larger bundles but with poorer orientational correlation among the constituting PU dipoles. Contrary the Gel samples obtained via photo-polymerization (Gel A and Gel B) present similar characteristics concerning both, the temperature dependence of the characteristic relaxation times, and the orientational correlation of the constituting PU dipoles. However, the network relaxation rate of Gel B is about three times faster than that of Gel A, which has been attributed to the significant incorporation of PU chain extenders in Gel B. This finding was supported by FTIR analysis and it can also be the reason for the higher water-uptake tendency of Gel B.

Chapter 6

Concluding remarks

"An investigator starts research in a new field with faith, a foggy idea, and a few wild experiments. Eventually the interplay of negative and positive results guides the work. By the time the research is completed, he or she knows how it should have been started and conducted."

Donald J. Cram, 1994

In the previous chapters we have described the results obtained for the dielectric relaxation phenomena and structure of two different polymeric complex materials; named ODMS-COOH carboxyl terminated co-oligomer and Acrylic-Polyurethane latexes. Additionally an interpretation of the molecular dipole assignments and the dynamic behaviour in different structured and unstructured environments has been given.

In particular and for the ODMS-COOH carboxyl terminated co-oligomer, DSC results show that conventional DMS crystallisation is inhibited in the co-oligomer, however different structural transitions take place. These arising structures are related to aliphatic block and carboxyl components. Moreover, we were able to identify different temperature regions where characteristic structural transitions take place. From the results it has been noted that the end carboxyl functional group is essential in determining the structural properties of the material. In particular, it gives rise to the short-range lamellar structure while cooling the material. Additionally the influence of the carboxyl end-group partially limits the aliphatic ordering and also completely prevents DMS crystallisation. Furthermore, when characterising the molecular mobility of the material we found that the co-oligomer present two particular and different relaxation phenomena. The main dielectric relaxation has been attributed to the dynamics of the DMS part of the co-oligomer, while a weak and slower relaxation is most likely due to the car-

boxyl terminated end group. This molecular assignment has been proposed given the similarities that are present in the temperature dependence of the ODMS-COOH when compared with ODMS oligomer. Moreover, DMS part in the co-oligomer behaves similarly as the amorphous DMS in the oligomer, nevertheless DMS dynamics in the co-oligomer appear to be slower due to the presence of the rigid aliphatic part which in turn also produces a greater dynamic heterogeneity than in the ODMS reference. The DMS dynamics in the co-oligomer is conditioned by the local structure of the aliphatic part that favours the segregation of the DMS.

Regarding the confinement effects on the DMS dynamics, the obtained results show that when there exists only a lamella structure the DMS dynamics is not affected despite of the fact that the rather small structural length (about 6 nm periodicity). This is contrary to the conventional expectation that a pure geometrical confinement effect would give rise to a faster relaxation phenomenon if one considers the Adam-Gibbs picture of cooperative rearranging regions of increasing size on cooling. The further structuration taking place in ODMS-COOH at lower temperature noticeably affects the DMS dynamics and consequently the pure geometrical effects cannot be properly addressed. Nevertheless, no hint of a crossover in the temperature dependence of the DMS relaxation times is detectable when approaching the glass transition temperature, a crossover that would be expected in the Adam-Gibbs framework.

Concerning Acrylic-Polyurethane hybrids produced by different synthetic conditions, and in order to understand fundamental structure-adhesive properties of these materials we made use of distinct thermal, structural and dynamic characterization techniques to establish qualitative and quantitative structure-property relationships. Thermodynamic characterization results evidence very similar characteristics among the investigated components of the produced Acrylic-Polyurethane latexes. In agreement with this, the structures as determined by means of wide angle X-ray scattering (WAXS) measurements are also quite similar. Conventional structural characterization is not sufficient to get insight into the complex structure of these materials. However, larger scale structural differences can be detected by small angle X-ray scattering (SAXS) experiments. To get insight on the dielectric phenomena related to the distinct components of the complex materials we carried out broadband dielectric spectroscopy (BDS) measurements. We have been able to identify and establish differences, interpreted thanks to the molecular assignment of three main different relaxation processes. Particularly, the fastest of these relaxation processes is attributed to the segmental motion of the main acrylic chains (αR) and thus it exists in all samples with significant differences. The analysis of the second fastest relaxation process that it is completely absent in the reference pure acrylic polymer and very prominent on the soluble fraction of the latex sample it is attributed to

the presence of some orientational correlations in the segregated PU phase, which leads us to identify this a dangling chain relaxation (DCR). In this framework the observation of a DRC component also in the Gel fraction of the latex is attributed to the existence of residual PU chains attached by a single end to the acrylic main chain without being involved in the network formation. Concerning the slowest relaxation process identified as network relaxation (NR) because it is only present in the Gel, it has been attributed to the presence of orientationally correlated PU hard segment bundles of the PU chains forming the Gel network. A step forward in this direction, lead us to the comparison (in particularly of the NR) between different Gel materials obtained by using the same chemical ingredients but varying synthetic conditions. In such case broadband dielectric spectroscopy results shows differences in the dielectric parameters that have been rationalized in connection with the corresponding synthesis method used. In this way, we show that the gel produced via thermal polymerization presents larger bundles but with poorer orientational correlation among the constituting PU dipoles. Contrary the gel samples obtained via photo-polymerization (Gel A and Gel B) present similar characteristics concerning both, the temperature dependence of the characteristic relaxation times, and the orientational correlation of the constituting PU dipoles. However, the network relaxation rate of Gel B is about three times faster than that of Gel A, which has been attributed to the significant incorporation of PU chain extenders in Gel B. This finding was supported by FTIR analysis and it can also be the reason for the higher water-uptake tendency of Gel B.

Sumarizing, the applied methodology, allowed us, to use different experimental techniques to elucidate and propose a molecular assignment that takes into account the dynamics and structure of the ODMS-COOH co-oligomer and the Acrylic-Polyurethane hybrid adhesives. Subsequent application of this methodology to investigation of other complex materials would permit a greater insight into the relation between mobility of the components and the structure of the system.

Bibliography

Y así, del mucho leer y del poco dormir,
se le secó el cerebro de manera que vino
a perder el juicio.

Miguel de Cervantes Saavedra

[1] H-A Klok and Sébastien Lecommandoux. Supramolecular materials via block copolymer self-assembly. *Advanced Materials*, 13(16):1217–1229, 2001.

[2] Thomas H Epps III and Rachel K O'Reilly. Block copolymers: controlling nanostructure to generate functional materials–synthesis, characterization, and engineering. *Chemical Science*, 7(3):1674–1689, 2016.

[3] Allen Noshay and James E McGrath. *Block copolymers: overview and critical survey*. Elsevier, 2013.

[4] Jean MJ Frechet et al. Functional polymers and dendrimers: reactivity, molecular architecture, and interfacial energy. *Science-AAAS-Weekly Paper Edition-including Guide to Scientific Information*, 263(5154):1710–1714, 1994.

[5] Paschalis Alexandridis and Bjoern Lindman. *Amphiphilic block copolymers: self-assembly and applications*. Elsevier, 2000.

[6] Mark W Matsen and Frank S Bates. Origins of complex self-assembly in block copolymers. *Macromolecules*, 29(23):7641–7644, 1996.

[7] Ludwik Leibler. Theory of microphase separation in block copolymers. *Macromolecules*, 13(6):1602–1617, 1980.

[8] M Muthukumar, CK Ober, and EL Thomas. Competing interactions and levels of ordering in self-organizing polymeric materials. *Science*, 277(5330):1225–1232, 1997.

[9] L Brunsveld, BJB Folmer, EW Meijer, and RP Sijbesma. Supramolecular polymers. *Chemical Reviews*, 101(12):4071–4098, 2001.

[10] Roland Böhmer, Catalin Gainaru, and Ranko Richert. Structure and dynamics of monohydroxy alcohols?milestones towards their microscopic understanding, 100 years after debye. *Physics Reports*, 545(4):125–195, 2014.

[11] AN Semenov, J-F Joanny, and AR Khokhlov. Associating polymers: equilibrium and linear viscoelasticity. *Macromolecules*, 28(4):1066–1075, 1995.

[12] Tom FA De Greef, Maarten MJ Smulders, Martin Wolffs, Albert PHJ Schenning, Rint P Sijbesma, and EW Meijer. Supramolecular polymerization. *Chemical Reviews*, 109(11):5687–5754, 2009.

[13] Shao-Lu Li, Tangxin Xiao, Chen Lin, and Leyong Wang. Advanced supramolecular polymers constructed by orthogonal self-assembly. *Chemical Society Reviews*, 41(18):5950–5968, 2012.

[14] Liulin Yang, Xinxin Tan, Zhiqiang Wang, and Xi Zhang. Supramolecular polymers: historical development, preparation, characterization, and functions. *Chemical reviews*, 115(15):7196–7239, 2015.

[15] C Lorthioir, A Alegria, J Colmenero, and B Deloche. Heterogeneity of the segmental dynamics of poly (dimethylsiloxane) in a diblock lamellar mesophase: dielectric relaxation investigations. *Macromolecules*, 37(20):7808–7817, 2004.

[16] Andreas Schönhals, Harald Goering, Ch Schick, B Frick, and R Zorn. Glassy dynamics of polymers confined to nanoporous glasses revealed by relaxational and scattering experiments. *The European Physical Journal E*, 12(1):173–178, 2003.

[17] Lourdes del Valle-Carrandi, Angel Alegría, Arantxa Arbe, and Juan Colmenero. Unexpected pdms behavior in segregated cylindrical and spherical nanophases of ps–pdms asymmetric diblock copolymers. *Macromolecules*, 45(1):491–502, 2011.

[18] Ravindra Udagama, Elise Degrandi-Contraires, Costantino Creton, Christian Graillat, Timothy FL McKenna, and Elodie Bourgeat-Lami. Synthesis of acrylic- polyurethane hybrid latexes by miniemulsion polymerization and their pressure-sensitive adhesive applications. *Macromolecules*, 44(8):2632–2642, 2011.

[19] Aitziber Lopez, Elise Degrandi-Contraires, Elisabetta Canetta, Costantino Creton, Joseph L Keddie, and José M Asua. Waterborne polyurethane- acrylic hybrid nanoparticles by miniemulsion polymerization: Applications in pressure-sensitive adhesives. *Langmuir*, 27(7):3878–3888, 2011.

[20] José M Asua. Miniemulsion polymerization. *Progress in polymer science*, 27(7):1283–1346, 2002.

[21] Istvan Benedek. *Pressure-sensitive adhesives and applications*. CRC Press, 2004.

[22] Costantino Creton. Pressure-sensitive adhesives: an introductory course. *MRS bulletin*, 28(06):434–439, 2003.

[23] Antonio Pizzi and Kashmiri L Mittal. *Handbook of adhesive technology, revised and expanded*. CRC press, 2003.

[24] Yuri Reyes, Aitziber Lopez, and José M Asua. Modeling the microstructure of acrylic-polyurethane hybrid polymers synthesized by miniemulsion polymerization. *Macromolecular Reaction Engineering*, 5(9-10):352–360, 2011.

[25] Richard AL Jones. *Soft condensed matter*, volume 6. Oxford University Press, 2002.

[26] IW Hamley. Introduction to soft matter: Polymers, colloids, amphiphiles and liquid crystals. 2000.

[27] Ian W Hamley. *Introduction to soft matter: synthetic and biological self-assembling materials*. John Wiley & Sons, 2013.

[28] Gregg Jaeger. The ehrenfest classification of phase transitions: introduction and evolution. *Archive for history of exact sciences*, 53(1):51–81, 1998.

[29] Pablo G Debenedetti and Frank H Stillinger. Supercooled liquids and the glass transition. *Nature*, 410(6825):259–267, 2001.

[30] Frank S Bates and GH Fredrickson. Block copolymers-designer soft materials. *Physics today*, 2000.

[31] Arthur E Woodward. *Atlas of polymer morphology*. Hanser Publishers. Distributed in the USA by Oxford University Press, 1988.

[32] Paul J Flory. *Principles of polymer chemistry*. Cornell University Press, 1953.

[33] Nikos Hadjichristidis, Stergios Pispas, and George Floudas. *Block copolymers: synthetic strategies, physical properties, and applications*. John Wiley & Sons, 2003.

[34] Ian W Hamley et al. *Developments in block copolymer science and technology*. Wiley Online Library, 2004.

[35] Mark W Matsen and Michael Schick. Stable and unstable phases of a diblock copolymer melt. *Physical Review Letters*, 72(16):2660, 1994.

[36] Lev Davidovich Landau and Evgenii Mikhailovich Lifshitz. *Course of theoretical physics*. Elsevier, 2013.

[37] Boris Vladimirovich Gnedenko. *The Theory of Probability and the Elements of Statistics*, volume 132. American Mathematical Soc., 2005.

[38] Herbert B Callen and Theodore A Welton. Irreversibility and generalized noise. *Physical Review*, 83(1):34, 1951.

[39] Angel Alegria and Juan Colmenero. Dielectric relaxation of polymers: segmental dynamics under structural constraints. *Soft Matter*, 2016.

[40] F Kremer and A Schönhals. *2 Broadband Dielectric Measurement Techniques (10–6 Hz to 1012 Hz)*. Springer, 2012.

[41] Arthur K Doolittle. Studies in newtonian flow. ii. the dependence of the viscosity of liquids on free-space. *Journal of Applied Physics*, 22(12):1471–1475, 1951.

[42] Morrel H Cohen and David Turnbull. Molecular transport in liquids and glasses. *The Journal of Chemical Physics*, 31(5):1164–1169, 1959.

[43] Morrel H Cohen and GS Grest. Liquid-glass transition, a free-volume approach. *Physical Review B*, 20(3):1077, 1979.

[44] Gerold Adam and Julian H Gibbs. On the temperature dependence of cooperative relaxation properties in glass-forming liquids. *The journal of chemical physics*, 43(1):139–146, 1965.

[45] C Austen Angell. Formation of glasses from liquids and biopolymers. *Science*, 267(5206):1924, 1995.

[46] Dieter Richter, Michael Monkenbusch, Arantxa Arbe, and Juan Colmenero. Neutron spin echo in polymer systems. *Neutron Spin Echo in Polymer Systems*, pages 1–221, 2005.

[47] Wolfgang Götze. Aspects of structural glass transitions. *Liquids, freezing and the glass transition*, 1, 1991.

[48] W Gotze and L Sjogren. Relaxation processes in supercooled liquids. *Reports on progress in Physics*, 55(3):241, 1992.

[49] Wolfgang Götze. Recent tests of the mode-coupling theory for glassy dynamics. *Journal of Physics: condensed matter*, 11(10A):A1, 1999.

[50] Shankar P Das. Mode-coupling theory and the glass transition in supercooled liquids. *Reviews of modern physics*, 76(3):785, 2004.

[51] David R Reichman and Patrick Charbonneau. Mode-coupling theory. *Journal of Statistical Mechanics: Theory and Experiment*, 2005(05):P05013, 2005.

[52] KL Ngai and M Paluch. Classification of secondary relaxation in glass-formers based on dynamic properties. *The Journal of chemical physics*, 120(2):857–873, 2004.

[53] Gyan P Johari and Martin Goldstein. Viscous liquids and the glass transition. ii. secondary relaxations in glasses of rigid molecules. *The Journal of chemical physics*, 53(6):2372–2388, 1970.

[54] David Hoagland. The physics of polymers: Concepts for understanding their structures and behavior, by gert r. strobl, springer-verlag, new york, 1996. isbn 3-540-60768-4. *Journal of Polymer Science Part A: Polymer Chemistry*, 35(7):1337–1338, 1997.

[55] Barbara Stuart. *Infrared spectroscopy*. Wiley Online Library, 2005.

[56] Peter J Haines. *Thermal methods of analysis: principles, applications and problems*. Springer Science & Business Media, 2012.

[57] George Odian. *Principles of polymerization*. John Wiley & Sons, 2004.

[58] Els Verdonck, Ko Schaap, and Leonard C Thomas. A discussion of the principles and applications of modulated temperature dsc (mtdsc). *International journal of pharmaceutics*, 192(1):3–20, 1999.

[59] Ho-Cheol Kim, Sang-Min Park, and William D Hinsberg. Block copolymer based nanostructures: materials, processes, and applications to electronics. *Chemical reviews*, 110(1):146–177, 2009.

[60] Jin Kon Kim, Seung Yun Yang, Youngmin Lee, and Youngsuk Kim. Functional nanomaterials based on block copolymer self-assembly. *Progress in Polymer Science*, 35(11):1325–1349, 2010.

[61] Ian W Hamley. *Block copolymers in solution: fundamentals and applications*. John Wiley & Sons, 2005.

[62] Massimo Lazzari, Carlos Rodríguez-Abreu, José Rivas, and M Arturo López-Quintela. Self-assembly: a minimalist route to the fabrication of nanomaterials. *Journal of nanoscience and nanotechnology*, 6(4):892–905, 2006.

[63] Kunyue Xing, Sabornie Chatterjee, Tomonori Saito, Catalin Gainaru, and Alexei P Sokolov. Impact of hydrogen bonding on dynamics of hydroxyl-terminated polydimethylsiloxane. *Macromolecules*, 49(8):3138–3147, 2016.

[64] Yiannis N Kaznessis, Davide A Hill, and Edward J Maginn. A molecular dynamics study of macromolecules in good solvents: Comparison with dielectric spectroscopy experiments. *The Journal of chemical physics*, 109(12):5078–5088, 1998.

[65] Keiichiro Adachi and Tadao Kotaka. Dielectric normal mode relaxation of tethered polyisoprene chains in styrene-isoprene block copolymers. *Pure and applied chemistry*, 69(1):125–130, 1997.

[66] Wilfred H Tang. Confinement of symmetric diblock copolymer thin films. *Macromolecules*, 33(4):1370–1384, 2000.

[67] E Laredo, MC Hernández, A Bello, M Grimau, AJ Müller, and V Balsamo. Local and segmental dynamics in homopolymer and triblock copolymers with one semicrystalline block. *Physical Review E*, 65(2):021807, 2002.

[68] Sergei Zhukov, Steffen Geppert, Bernd Stühn, Rosina Staneva, and Wolfram Gronski. Dielectric relaxation in isotropic/liquid crystalline block copolymers: Effect of nanoscale confinement on the local β and γ dynamics. *Macromolecules*, 36(16):6166–6170, 2003.

[69] Mohammed Zakaria Slimani, Angel J Moreno, and Juan Colmenero. Heterogeneity of the segmental dynamics in lamellar phases of diblock copolymers. *Macromolecules*, 44(17):6952–6961, 2011.

[70] Connie B Roth and John M Torkelson. Selectively probing the glass transition temperature in multilayer polymer films: Equivalence of block copolymers and multilayer films of different homopolymers. *Macromolecules*, 40(9):3328–3336, 2007.

[71] Erik Kühnel, David DP Laffan, Guy C Lloyd-Jones, Teresa Martínez del Campo, Ian R Shepperson, and Jennifer L Slaughter. Mechanism of methyl esterification of carboxylic acids by trimethylsilyldiazomethane. *Angewandte Chemie International Edition*, 46(37):7075–7078, 2007.

[72] S Förster, L Apostol, and W Bras. Scatter: software for the analysis of nano-and mesoscale small-angle scattering. *Journal of Applied Crystallography*, 43(3):639–646, 2010.

[73] A Lee Smith and Dennis R Anderson. Vibrational spectra of me2sicl2,me3sicl,me3siosime3,(me2sio)4,(me2sio)x, and their deuterated analogs. *Applied spectroscopy*, 38(6):822–834, 1984.

[74] Ranko Richert. Supercooled liquids and glasses by dielectric relaxation spectroscopy. *Advances in Chemical Physics*, 156:101, 2014.

[75] C Wang, F Chu, C Graillat, A Guyot, C Gauthier, and JP Chapel. Hybrid polymer latexes: acrylics–polyurethane from miniemulsion polymerization: properties of hybrid latexes versus blends. *Polymer*, 46(4):1113–1124, 2005.

[76] A Kyritsis, K Raftopoulos, M Abdel Rehim, Sh Said Shabaan, A Ghoneim, and G Turky. Structure and molecular dynamics of hyperbranched polymeric systems with urethane and urea linkages. *Polymer*, 50(16):4039–4047, 2009.

[77] E Kontou, G Spathis, M Niaounakis, and V Kefalas. Physical and chemical cross-linking effects in polyurethane elastomers. *Colloid and Polymer Science*, 268(7):636–644, 1990.

[78] AJ Bur and LJ Fetters. The chain structure, polymerization, and conformation of polyisocyanates. *Chemical Reviews*, 76(6):727–746, 1976.

[79] Vesna Daniloska, Paula Carretero, Radmila Tomovska, Maria Paulis, and José M Asua. High-performance adhesives resulting from spontaneous formation of nanogels within miniemulsion particles. *ACS applied materials & interfaces*, 6(5):3559–3567, 2014.

[80] Vesna Daniloska, Radmila Tomovska, and Jose M Asua. Hybrid miniemulsion photopolymerization in a continuous tubular reactor?a way to expand the characteristics of polyurethane/acrylics. *Chemical Engineering Journal*, 184:308–314, 2012.

[81] Vesna Daniloska, Paula Carretero, Radmila Tomovska, and José M Asua. High performance pressure sensitive adhesives by miniemulsion photopolymerization in a continuous tubular reactor. *Polymer*, 55(20):5050–5056, 2014.

[82] Elise Degrandi-Contraires, Ravindra Udagama, Elodie Bourgeat-Lami, Timothy McKenna, Keltoum Ouzineb, and Costantino Creton. Mechanical properties of adhesive films obtained from pu- acrylic hybrid particles. *Macromolecules*, 44(8):2643–2652, 2011.

[83] Sultan Misbah. *Synthesis and Characterization of Polyurethane Acrylate Copolymers*. PhD thesis, University of Agriculture, Faisalabad, 2012.

[84] Andreas Schönhals and F Kremer. Analysis of dielectric spectra. In *Broadband dielectric spectroscopy*, pages 59–98. Springer, 2003.

[85] Hans Vogel. The law of the relation between the viscosity of liquids and the temperature. *Phys. Z*, 22:645–646, 1921.

[86] Gordon S Fulcher. Analysis of recent measurements of the viscosity of glasses. *Journal of the American Ceramic Society*, 8(6):339–355, 1925.

[87] Gf Tammann and W Hesse. Die abhängigkeit der viscosität von der temperatur bie unterkühlten flüssigkeiten. *Zeitschrift für anorganische und allgemeine Chemie*, 156(1):245–257, 1926.

[88] Michael Wübbenhorst and Jan van Turnhout. Analysis of complex dielectric spectra. i. one-dimensional derivative techniques and three-dimensional modelling. *Journal of non-crystalline solids*, 305(1):40–49, 2002.

[89] Reidar Lund, Fabienne Barroso-Bujans, Mohammed Zakaria Slimani, Angel J Moreno, Lutz Willner, Dieter Richter, Angel Alegría, and Juan Colmenero. End-to-end vector dynamics of nonentangled polymers in lamellar block copolymer melts: the role of junction point motion. *Macromolecules*, 46(18):7477–7487, 2013.

[90] A Kanapitsas and P Pissis. Dielectric relaxation spectroscopy in crosslinked polyurethanes based on polymer polyols. *European polymer journal*, 36(6):1241–1250, 2000.

[91] ZORAN S Petrovic, Ivan Javni, and Vladimir Divjakovic. Structure and physical properties of segmented polyurethane elastomers containing chemical crosslinks in the hard segment. *Journal of Polymer Science Part B Polymer Physics*, 36(2):221–235, 1998.

[92] Helena Valentová, Jan Nedbal, Michal Ilavskỳ, and Polycarpos Pissis. Dsc, dielectric and dynamic mechanical behavior of two-and three-component ordered polyurethanes. *Polymer*, 46(12):4175–4182, 2005.

[93] P Pissis, A Kanapitsas, Yu V Savelyev, ER Akhranovich, EG Privalko, and VP Privalko. Influence of chain extenders and chain end groups on properties of segmented polyurethanes. ii. dielectric study. *Polymer*, 39(15):3431–3435, 1998.

[94] MH Jomaa, L Seveyrat, L Lebrun, K Masenelli-Varlot, and JY Cavaille. Dielectric properties of segmented polyurethanes for electromechanical applications. *Polymer*, 63:214–221, 2015.

[95] Domenico Acierno, Eugenio Amendola, Cosimo Carfagna, Simona Concilio, Pio Iannelli, Loredana Incarnato, and Paola Scarfato. Synthesis and characterisation of a nematic homo-polyurethane. *Polymer*, 44(17):4949–4958, 2003.

[96] A Alegria, L Goitiandia, and J Colmenero. Interpretation of the tsdc fractional polarization experiments on the α-relaxation of polymers.

Journal of Polymer Science Part B: Polymer Physics, 38(16):2105–2113, 2000.

[97] G Martínez-Rugerio, Angel Alegría, Vesna Daniloska, Radmila Tomovska, M Paulis, and Juan Colmenero. Dielectric relaxations of acrylic-polyurethane hybrid materials. *Polymer*, 74:21–29, 2015.

[98] Mario Beiner and Heiko Huth. Nanophase separation and hindered glass transition in side-chain polymers. *Nature materials*, 2(9):595–599, 2003.

[99] A-C Genix and F Lauprêtre. Subglass and glass transitions of poly (di-n-alkylitaconate) s with various side-chain lengths: dielectric relaxation investigation. *Macromolecules*, 38(7):2786–2794, 2005.

[100] I Iradi, F Alvarez, J Colmenero, and A Arbe. Structure factors in polystyrene: a neutron scattering and md-simulation study. *Physica B: Condensed Matter*, 350(1):E881–E884, 2004.

[101] A Arbe, A-C Genix, J Colmenero, D Richter, and P Fouquet. Anomalous relaxation of self-assembled alkyl nanodomains in high-order poly (n-alkyl methacrylates). *Soft Matter*, 4(9):1792–1795, 2008.

[102] Christine Gerstl, Martin Brodeck, GJ Schneider, Y Su, J Allgaier, A Arbe, J Colmenero, and D Richter. Short and intermediate range order in poly (alkylene oxide) s. a neutron diffraction and molecular dynamics simulation study. *Macromolecules*, 45(17):7293–7303, 2012.

[103] Rémi Busselez, Arantxa Arbe, Fernando Alvarez, Juan Colmenero, and Bernhard Frick. Study of the structure and dynamics of poly (vinyl pyrrolidone) by molecular dynamics simulations validated by quasielastic neutron scattering and x-ray diffraction experiments. *The Journal of chemical physics*, 134(5), 2011.

[104] Rubén Tejero, Arantxa Arbe, Marta Fernández-García, and Daniel López. Nanostructuration by self-assembly in n-alkyl thiazolium and triazolium side-chain polymethacrylates. *Macromolecules*, 48(19):7180–7193, 2015.

[105] M Wind, Robert Graf, S Renker, Hans Wolfgang Spiess, and W Steffen. Structure of amorphous poly-(ethylmethacrylate): A wide-angle x-ray scattering study. *The Journal of chemical physics*, 122(1), 2005.

[106] S Hiller, O Pascui, H Budde, O Kabisch, D Reichert, and M Beiner. Nanophase separation in side chain polymers: new evidence from structure and dynamics. *New Journal of Physics*, 6(1):10, 2004.

[107] Angel J Moreno, Arantxa Arbe, and Juan Colmenero. Structure and dynamics of self-assembled comb copolymers: comparison between simulations of a generic model and neutron scattering experiments. *Macromolecules*, 44(6):1695–1706, 2011.

[108] Peter Debye and AM Bueche. Scattering by an inhomogeneous solid. *Journal of Applied Physics*, 20(6):518–525, 1949.

[109] Erik Geissler, Ferenc Horkay, and Anne-Marie Hecht. Scattering from network polydispersity in polymer gels. *Physical review letters*, 71(4):645, 1993.

[110] Ferenc Horkay, Peter J Basser, Anne-Marie Hecht, and Erik Geissler. Structural investigations of a neutralized polyelectrolyte gel and an associating neutral hydrogel. *Polymer*, 46(12):4242–4247, 2005.

[111] Nicholas Ballard, Paula Carretero, and José M Asua. Effect of reaction temperature on adhesive properties of waterborne polyurethane/acrylic hybrids synthesized by semicontinuous miniemulsion polymerization. *Macromolecular Reaction Engineering*, 7(10):504–514, 2013.

[112] Marcia C Delpech and Gisele S Miranda. Waterborne polyurethanes: influence of chain extender in ftir spectra profiles. *Central European Journal of Engineering*, 2(2):231–238, 2012.

[113] Pablo J Peruzzo, Pablo S Anbinder, Oscar R Pardini, Carlos A Costa, Carlos A Leite, Fernando Galembeck, and Javier I Amalvy. Polyurethane/acrylate hybrids: effects of the acrylic content and thermal treatment on the polymer properties. *Journal of applied polymer science*, 116(5):2694–2705, 2010.

[114] Pablo J Peruzzo, Pablo S Anbinder, Oscar R Pardini, Jorge R Vega, and Javier I Amalvy. Influence of diisocyanate structure on the morphology and properties of waterborne polyurethane-acrylates. *Polymer journal*, 44(3):232–239, 2012.

–¿Qué te parece desto, Sancho? – Dijo Don Quijote –
Bien podrán los encantadores quitarme la ventura,
pero el esfuerzo y el ánimo, será imposible.

Segunda parte del Ingenioso Caballero
Don Quijote de la Mancha
Miguel de Cervantes